PONTIFICIA UNIVERSIDAD CATÓLICA DEL PERÚ

Escuela de Posgrado

TESTING NEW PHYSICS IN LONG BASELINE NEUTRINO OSCILLATION EXPERIMENTS

Tesis para obtener el grado académico de Doctor en Física que presenta:

Félix Napoleón Díaz Desposorio

Asesor:

Dr. Alberto Martín Gago Medina

Lima, 2022

Informe de Similitud

Yo, Alberto Martin Gago Medina, docente de la Escuela de Posgrado de la Pontificia Universidad Católica del Perú, asesor(a) de la tesis/el trabajo de investigación titulado *Testing new pyshics in long baseline neutrino oscillation experiments* del autor Félix Díaz Desposorio,

dejo constancia de lo siguiente:

- El mencionado documento tiene un índice de puntuación de similitud de 56%, pero el alumno toma como referencias sus propios trabajos (las referencias 1,2,3,4,5,6,11,14 y 93 de la tesis) disminuyendo a un 12%, lo que está dentro del límite establecido. Así lo consigna el reporte de similitud emitido por el software *Turnitin* el 11/11/2022.
- He revisado con detalle dicho reporte y la Tesis o Trabajo de Suficiencia Profesional, y no se advierte indicios de plagio.
- Las citas a otros autores y sus respectivas referencias cumplen con las pautas académicas.

Lugar y fecha:
Lima, 13 de diciembre de 2022

Apellidos y nombres del asesor / de la asesora: Gago Medina, Alberto Martín	
DNI: 07835422	Firma:
ORCID: 0000-0002-0019-9692	

Félix Napoleón Díaz Desposorio
ORCID: 0000-0002-8232-058X

ACKNOWLEDGEMENTS

First, I want to thank my father, Napoleón, and my grandfather Félix who are still alive in my memory. I also want to express my special thanks to my mother, Adelaida; my sisters, Melissa, Dyanira, and Mariangela; and my brother Daniel for their unconditional support throughout this adventure.

I also want to thank my advisor, Dr. Alberto Gago, for his wise guidance, motivation, and friendship. Furthermore, I thank Juan Carlos and Jaime Hoefken for their invaluable contribution to this project. Additionally, I thank Dr. Jose Bazo and Dr. Joel Jones for their vital work in the HEP group.

I want to thank my friends, colleagues, and all those people who in some way contributed to this trip: Karen, Jhonny, Milagros, Edwin, José M., Segundo, María, Marvin, Nhell, Álvaro, Sandro, Omar S., Dante, Jairo, Carlos S., Javier, Edgar, Luis C., Sebastián, Rodrigo H., Carlos A, Domingo, Anthony, Ernesto, Ronald, Deyssi, Bertín, Rafael, Omar V., Víctor, Francis, Cesar G., Erick, Carlos y Karla S., Alex T., Belinda, Mónica, Marilyn, Marcelo, Deepak T., Mabel, Luis V., Junior, Miguel, Julio, Juan, Jony, Jes-

sica L., Ivette, Carlos T., Cinthia V., José C., Cieza M., Antonio R., Juan Z., Maritza D., and others.

Finally, I would like to thank CienciActiva-CONCYTEC for financing this work under the Grant No.000236-2015-FONDECYT-DE.

ABSTRACT

In this thesis, we focus on analyzing the different ways in which new physics scenarios, such as Violation of the Equivalence Principle (VEP) and Quantum Decoherence, can manifest themselves in the context of the neutrino oscillation phenomenon. Within the framework of the DUNE experiment, we examine several effects of the VEP, such as the possibility of getting a misconstructed neutrino oscillation parameter region provoked by our ignorance of VEP in nature, as well as the impact on the DUNE sensitivity for CPV and mass hierarchy. Additionally, we set limits for the different textures of the gravitational matrix and the diverse scenarios of energy dependencies associated with the Lorentz Violation. On the other hand, we demonstrate that the quantum decoherence phenomenon applied to the neutrino system leads us to fascinating phenomenological scenarios. One of the scenarios analyzed, within the context of quantum decoherence, is the one that breaks the fundamental CPT symmetry. For the latter, we identify what textures that include certain non-diagonal elements of the decoherence matrix are necessary. In this line, we propose a way to measure the CPT violation in the DUNE experiment using the muon neutrino and antineutrino channels for different energy dependen-

cies. Another intriguing effect of considering the neutrino as an open quantum system is the possibility of discovering the neutrino nature by measuring the Majorana phase at the DUNE experiment achieving a competitive precision. As a consequence of the latter, we find that the crucial measurement of the CP violation phase ($\delta_{\rm CP}$), planned to be performed at the DUNE experiment, can be spoiled by the introduction of the decoherence and the Majorana phases in nature. Thus, a signature of a non-null Majorana phase is a sizable distortion in the measurement of the Dirac CP violation phase $\delta_{\rm CP}$ at DUNE when compared with T2HK measurement. Subsequently, via simulation, we measured the Majorana phase for values of $\phi_1/\pi = \pm 0.5$ and decoherence parameter $\Gamma = 4.5(5.5) \times 10^{-24}$GeV, reaching a precision of 23 (21) %. This precision is consistent with the corresponding to the Dirac CP phase at T2K experiment.

RESUMEN

En la presente tesis, nos enfocamos en analizar las diferentes formas en que los escenarios de física nueva, como la Violación del Principio de Equivalencia (VEP) y la Decoherencia Cuántica, pueden manifestarse en el contexto del fenómeno de oscilación de neutrinos. En el marco del experimento DUNE, examinamos distintos efectos de VEP, como la posibilidad de obtener una región de parámetros de oscilación de neutrinos mal construida debido a no considerar VEP en la naturaleza, el impacto en la sensitividad del experimento DUNE para CPV y la determinación de la jerarquía de masas. Adicionalmente, establecemos límites para las diferentes texturas de la matriz gravitacional y los diversos escenarios con distintas dependencias energéticas asociadas a la Violación de Lorentz. Por otro lado, demostramos que el fenómeno de la decoherencia cuántica aplicado al sistema de neutrinos nos conduce a fascinantes escenarios fenomenológicos. Uno de los escenarios analizados, dentro del contexto de la decoherencia cuántica, es el de la ruptura de la simetría fundamental CPT. Para esto último, identificamos que son necesarias texturas que incluyan ciertos elementos no diagonales de la matriz de decoherencia. En esta línea, proponemos una forma de medir la violación de CPT en el experimento DUNE

utilizando los canales de neutrinos y antineutrinos muónicos para diferentes dependencias energéticas. Otro efecto interesante de considerar al neutrino como un sistema cuántico abierto es la posibilidad de descubrir la naturaleza del neutrino midiendo la fase de Majorana en el experimento DUNE con una precisión competitiva. Como consecuencia de lo último, encontramos que la medición de la fase de violación de CP (δ_{CP}), planificada para realizarse en el experimento DUNE, puede verse afectada por la introducción de la decoherencia y las fases de Majorana en la naturaleza. Por lo tanto, en el marco de la decoherencia, mostramos que una señal de una fase de Majorana no nula, es la observación de una distorsión considerable en la medición de la fase de violación CP δ_{CP} en DUNE en comparación con la medición realizada por T2HK. Posteriormente, mediante simulación, medimos la fase Majorana para valores de $\phi_1/\pi = \pm 0.5$ y el parámetro de decoherencia $\Gamma = 4.5(5.5) \times 10^{-24}\mathrm{GeV}$, alcanzando una precisión de 23 (21) %. Esta precisión es consistente con la medida correspondiente a la fase CP de Dirac en el experimento T2K.

PUBLISHED CONTENT AND CONTRIBUTIONS

[1] J. C. Carrasco-Martínez, F. N. Díaz, and A. M. Gago, "Uncovering the Majorana nature through a precision measurement of the CP phase," *Phys. Rev. D*, vol. 105, no. 3, p. 035 010, 2022. DOI: 10.1103/PhysRevD.105.035010. arXiv: 2011.01254 [hep-ph].

[2] F. N. Díaz, J. Hoefken, and A. M. Gago, "Effects of the Violation of the Equivalence Principle at DUNE," *Phys. Rev. D*, vol. 102, no. 5, p. 055 020, 2020. DOI: 10.1103/PhysRevD.102.055020. arXiv: 2003.13712 [hep-ph].

[3] J. C. Carrasco, F. N. Díaz, and A. M. Gago, "Probing CPT breaking induced by quantum decoherence at DUNE," *Phys. Rev. D*, vol. 99, no. 7, p. 075 022, 2019. DOI: 10.1103/PhysRevD.99.075022. arXiv: 1811.04982 [hep-ph].

Table of Contents

List of Illustrations

List of Tables

INTRODUCTION

0.1 New physics through neutrino oscillation

Neutrino oscillation is the large-scale manifestation of a quantum interference phenomenon that is caused by the existence of non-zero neutrino masses and the misalignment between mass eigenstates and flavor eigenstates. Currently, overwhelming experimental evidence supports the neutrino oscillation phenomenon induced by mass. [1–10].

Even though the non-zero (non-equal) neutrino masses are the well-established responsible for having neutrino oscillation, the co-existence of a sub-leading mechanism originated by new physics is not forbidden. The sub-leading effects can be produced by a miscellany of physics scenarios beyond the standard oscillation such as nonstandard interactions [11–15], neutrino decay [16–25], quantum decoherence [26–32], violation of the equivalence principle (VEP) [33–37], among others [38–40]. It is important to note that on some occasions, these new physics scenarios bring about the option of breaking fundamental laws of nature, for instance, the equivalence principle or Lorentz invariance [41–43]. Additionally, neutrino oscillation physics is moving toward a precision era, implying that the sensitivity for performing searches for signa-

tures from nonstandard physics would also improve. In the present thesis, we focus on two beyond standard physics hypotheses: the violation of the equivalence principle and quantum decoherence. We study the sensitivity for both of them in future Long-Baseline neutrino oscillation experiments.

Firstly, the equivalence principle is one of the pillars on which the theory of gravitation is based. In particular, the weak equivalence principle establishes that in vacuum, bodies fall in the same way within a gravitational field; this means that the trajectory followed by the body is independent of its mass. This is an indication of the equivalency between gravitational and inertial mass. The VEP in neutrino physics was initially considered to explain the solar neutrino problem [44–51]. Nevertheless, once the oscillation induced by mass was established as the solution of the neutrino data, studies about VEP scenarios focused on looking for constraints on its parameters [33–37]. In this context, we analyze the possibility of the Deep Underground Neutrino Experiment (DUNE) [52, 53] for setting constraints on VEP parameters. Also, we assess how subleading VEP effects could influence the projected precision measurements of neutrino oscillation parameters in DUNE. Furthermore, we reinterpret our results beyond the context of VEP, converting its linear energy dependency into a quadratic, cubic, etc. Consequently, we make a correspondence of terms between the kind mentioned above with the Lorentz violating (LV) interaction terms that arises in the Standard Model extension (SME) [41, 54]. The SME is a low-energy effective field theory containing all possible LV operators, constituted of ones originating from spontaneous Lorentz symmetry violation [55] and others explicitly constructed. We must point out that astrophysical neutrinos should provide the most significant sensitivity for these effects [56–58], nevertheless, if we consider a manufactured neutrino source, the DUNE experiment will be the most sensitive tool at our disposal.

Secondly, the Lagrangian of the Standard Model Extension (SME) shows terms that explicitly violate the combined action of the charge conju-

gation (C), the parity inversion (P), and the time inversion (T), symmetries, usually known as CPT symmetry [54]. There have been many types of research on testing CPT violation (CPTV) in the context of the SME [38–40, 59]. It is important to note that, because of the unequal number of particles and antiparticles in nature, there is CPTV in the neutrino oscillation phenomenon through matter [60]. Furthermore, hidden behind a pervasive environment that can weakly interact with neutrinos [60, 61] are the effects of a variety of theoretical hypotheses, for instance string and branes [62–64], and quantum gravity [65–68]. We refer to this environment as pervasive because our physical system is inherently open to inescapable and decoherent interactions with the Planck-scale space-time dynamics. In its simplest version, this type of interaction is usually described by the decoherence damping factor $\exp^{-\Gamma t}$ in the context of the neutrino oscillation probabilities [26, 29, 69–74]. In a model-independent way for an open system approach, the effects of the pervasive environment (the space–time and its Planck-scale dynamics) are contained by the parameters of the decoherence matrix, also called the dissipative matrix. In this Thesis, we study another CPT violation scenario that arises from the latter and the impossibility of defining a CPT operator due to the fact that quantum decoherence causes transitions from pure states to mixed states [75, 76]. Consequently, we will focus on investigating different non-diagonals textures of the dissipative matrix paying particular attention to those which can produce an observable non-zero CPTV. One of our working hypotheses is to consider that the environment affects neutrinos and antineutrinos similarly. Additionally, we evaluate the possibility that the parameters of the dissipative matrix can be energy-dependent [77–79]. Eventually, in the context of the DUNE experiment [52, 53], we estimate how significant the CPTV signal caused by quantum decoherence would be.

Thirdly, one of the essential questions in particle physics is the origin of the neutrino masses. [80, 81]. Assuming the Dirac nature of neutrinos within

the framework of the standard model of particle physics, neutrino masses arise via the Brout–Englert–Higgs mechanism [82, 83]. However, the latter cannot explain why the mass of a neutrino is one-millionth of the mass of the lightest charged lepton, the electron. One of the most promising solutions to this question is the Seesaw mechanism, where one of its most straightforward variants considers neutrinos as Majorana particles [84–96]. A Majorana particle is a fermion that is its own antiparticle; therefore, considering neutrinos as Majorana particles implies a violation of Lepton number conservation [97, 98]. Thus, to verify the Majorana nature of neutrinos, processes that violates the lepton number conservation, such as neutrinoless double-beta decay, are sought [99–102]. It is important to note that, to date, there is no evidence for neutrinoless double-beta decay [103–106] or any other method of searching for Majorana neutrinos [107–110].

On the other hand, the nature of the neutrinos does not affect the standard oscillation phenomenon; i.e., the oscillation probabilities are the same for Dirac or Majorana neutrinos. The latter is because the Majorana CP phases are cancelled, leaving just the Dirac CP phase as the only observable one [111]. Nevertheless, this Thesis also analyzes scenarios where the Majorana phases can appear in the neutrino oscillation probability in the context of quantum decoherence. In other words, the present work raises the possibility that the neutrinos Majorana nature can manifest itself in the oscillation phenomenon. One of our working hypotheses is to consider the Dirac CP phase value measured by the T2K experiment as the true value [112]. The latter is because the characteristic baseline of the T2K experiment allows us to assume that its detection is not affected by the quantum decoherence phenomenon. In contrast, the DUNE experiment may enable observations of quantum decoherence effects and a non-zero Majorana CP phase on the oscillation phenomenon. Therefore, part of the present investigation focuses on analyzing the effects of the Majorana nature on the neutrino oscillation in the context of the DUNE

experiment. The first part of this analysis estimates how much the Dirac CP phase measurement by the DUNE experiment can deviate from its true value (measured by T2K). For this, we compare the CP phase measured by DUNE with the projection of the CP phase estimated by the natural extension of T2K, T2HK experiment [113]. The second part of this study consists of testing the accuracy of DUNE to measure the Majorana CP phase and the decoherence parameter.

Consequently, we present this thesis as follows:

- Chapters I and II: Theoretical background; general introduction to neutrino oscillation, Majorana neutrino, CP and CPT symmetry. Experimental Context; open questions in neutrino oscillation phenomenon, future neutrino oscillation experiments, DUNE and T2HK experiments.
- Chapter III: We present the effects of the different VEP scenarios on the probability of oscillation, the impact of VEP on the measurement of standard oscillation parameters, the sensitivity of DUNE to observe VEP parameters, findings, and conclusions.
- Chapter IV: We introduce the quantum decoherence theoretical framework, the dissipative matrix's effects according to its texture, and the decoherence parameters that cause CP and CPT violation. We also present the quantum decoherence scenarios that make the Majorana phases emerge in the oscillation probability formula, the proposal to observe CPTV, and the possibility of manifestation of the neutrino Majorana nature in the context of the DUNE experiment and conclusions.
- Chapter V: Ultimately, we present our conclusions and comments.

CHAPTER 1

GENERAL THEORETICAL BACKGROUND

The neutrinos are fundamental particles with no electrical charge and a very tiny mass. These particles are the second most abundant particle in the universe, and they are tremendously challenging to detect. The latter is because they interact very little with the matter. This interaction is performed only via weak interaction and gravity.

Neutrino physics begins hand in hand with the discovery and study of radioactivity. In 1899 Ernest Rutherford discovered alpha and beta radiation, which were identified as helium nuclei and electrons, respectively. In that context, beta radiation was assumed to be the emission of a single particle, the electron. Therefore, the electron from beta radiation was expected to have a well-defined energy. However, James Chadwick observed that this spectrum

was continuous [114]. The problem was of such magnitude that abandoning the principle of conservation of energy was considered. It was not until 1930 when W. Pauli, as a desperate measure, proposed the existence of a neutral particle, with spin 1/2 and very light, the neutrino. Subsequently, in 1956 Clyde L. Cowan and Frederick Reines were able to verify the existence of this new particle [115].

In 1962 a second type of neutrino was discovered, the muon neutrino (ν_μ) [116]. After the existence of a third family of quarks was proposed to explain CP violation [117], it was suggested that something analogous should happen with neutrinos. The third type of neutrino, the tau neutrino (ν_τ), was discovered in 2000 by the DONUT experiment at Fermilab [118].

As far as we know, in the standard model (SM) of particle physics, there are three types of neutrinos (flavors), associated with the charged leptons, i.e. $\nu_e \rightarrow$ Electron (e), $\nu_\mu \rightarrow$ Muon (μ) and $\nu_\tau \rightarrow$ Tau (τ). Furthermore, in the SM context, the neutrino mass was assumed to be zero for a long time. Notwithstanding, the discovery of the neutrino oscillation phenomenon implies neutrinos with non-zero mass.

1.1 Neutrino Oscillation

The neutrino oscillation is caused by slight differences between neutrino masses (squared masses), which are already small in themselves, and the lack of coincidence between neutrino mass eigenstates (ν_1, ν_2, ν_3) and flavor eigenstates (ν_e, ν_μ, ν_τ) [1, 4–10, 119].

The coherent interference of massive neutrinos is the mechanism behind neutrino oscillation. The mass and flavor eigenstates are two orthonormal bases that are connected by a mixing matrix U (unitary linear transformation). Therefore, the flavor eigenstates are a superposition of different mass eigenstates. The mixing matrix is analogous to the CKM matrix (for quarks) and is known as the PMNS (Pontecorvo - Maki - Nakagawa - Sakata) or MNS (Maki -

Nakagawa - Sakata) mixing matrix [120]. The mass eigenstates and the flavor eigenstates of neutrinos are related as follows:

$$|\nu_k\rangle = \sum_{\alpha=e,\mu,\tau} U_{\alpha k} |\nu_\alpha\rangle \tag{1.1}$$

$$|\nu_\alpha\rangle = \sum_{k=1}^{3} U^*_{\alpha k} |\nu_k\rangle \tag{1.2}$$

Considering the three types of neutrinos (flavors), the PMNS matrix can be expressed as follows

$$U = U_{\text{PMNS}} = \begin{pmatrix} c_{12}c_{13} & s_{12}c_{13} & s_{13}e^{-i\delta_{\text{CP}}} \\ -s_{12}c_{23} - c_{12}s_{23}s_{13}e^{i\delta_{\text{CP}}} & c_{12}c_{23} - s_{12}s_{23}s_{13}e^{i\delta_{\text{CP}}} & s_{23}c_{13} \\ s_{12}s_{23} - c_{12}c_{23}s_{13}e^{i\delta_{\text{CP}}} & -c_{12}s_{23} - s_{12}c_{23}s_{13}e^{i\delta_{\text{CP}}} & c_{23}c_{13} \end{pmatrix} \tag{1.3}$$

where s_{ij} and c_{ij} are $\sin\theta_{ij}$ and $\cos\theta ij$, respectively. The parameter θ_{ij} represent the mixing angle between the mass and flavor eigenstates. The phase δ_{CP} is related to the diferrence between the neutrino and antineutrino ($U_{\text{PMNS}} \to U^*_{\text{PMNS}}$) nature, and the CP (charge-parity) violation [121–123].

The Hamiltonian on the flavor basis for oscillation in vacuum is as follows:

$$\text{H}^{\text{f}}_{\text{osc}} = U \frac{\mathbf{H}_{\text{osc}}}{2E} U^\dagger \tag{1.4}$$

where $\mathbf{H}_{\text{osc}} = \text{diag}(0, \Delta m^2_{21}, \Delta m^2_{31})$.

The mass eigenstates are eigenstates of the Hamiltonian $\text{H}|\nu_k\rangle = E_k|\nu_k\rangle$ with the eigenvalue $E_k = \sqrt{\vec{p}^{\,2} + m_k^2}$. The mass states of neutrinos

evolve in time as a plane wave; therefore, the time evolution of a flavor eigenstate is as follows.

$$|\nu_\alpha(t)\rangle = \sum_{k=1}^{3} U^*_{\alpha k} e^{-iE_k t} |\nu_k\rangle \tag{1.5}$$

Considering the Eq. (1.1), we obtain an expression that relates a flavor state to another.

$$|\nu_\alpha(t)\rangle = \sum_{\beta=e,\mu,\tau} \left(\sum_{k=1}^{3} U^*_{\alpha k} e^{-iE_k t} U_{\beta k} \right) |\nu_\beta\rangle \tag{1.6}$$

Assessing neutrinos as ultrarelativistic particles, we can estimate the neutrino oscillation probability from one flavor state to another. We must remark that for the antineutrino case, we consider $\delta_{CP} \to -\delta_{CP}$ and obtain the same formula.

$$\begin{aligned} P_{\nu_\alpha \to \nu_\beta} = \delta_{\alpha\beta} - 4 \sum_{k>j} Re\left[U^*_{\alpha k} U_{\beta k} U_{\alpha j} U^*_{\beta j}\right] \sin^2\left(\frac{\Delta m^2_{kj} L}{4E}\right) \\ +2 \sum_{k>j} Im\left[U^*_{\alpha k} U_{\beta k} U_{\alpha j} U^*_{\beta j}\right] \sin\left(\frac{\Delta m^2_{kj} L}{2E}\right) \end{aligned} \tag{1.7}$$

On the other hand, to consider the matter effects on the neutrino oscillation, we have the following Hamiltonian on the flavor basis.

$$\mathbf{H}^{\mathrm{f}}_{\mathrm{osc}} = \frac{1}{2E}\left[U \mathbf{H}_{\mathrm{osc}} U^\dagger + \mathbf{A}_{\mathrm{matt}}\right] \tag{1.8}$$

with

$$\mathbf{A}_{\mathrm{matt}} = \mathrm{diag}(A_{CC}, 0, 0) \tag{1.9}$$

where $A_{CC} = 2\sqrt{2} G_F N_e E$, and N_e represents the electron density. For antineutrinos must change $A_{CC} \to -A_{CC}$ ($\mathbf{A}_{\mathrm{matt}} \to -\mathbf{A}_{\mathrm{matt}}$).

Analogously to Eq. (1.4), the formal way of diagonalization in matter is as follows.

$$\mathbf{H}^{\mathrm{f}}_{\mathrm{osc}} = \frac{1}{2E}\left[U\mathbf{H}_{\mathrm{osc}}U^{\dagger} + \mathbf{A}_{\mathrm{matt}}\right] \overset{\mathrm{def}}{=\!=} \frac{1}{2E}\left[\tilde{U}\tilde{\mathbf{H}}_{\mathrm{osc}}\tilde{U}^{\dagger}\right] \tag{1.10}$$

where $\tilde{U}$ is the mixing matrix in matter, and $\tilde{\mathbf{H}}_{\mathrm{osc}} = \mathrm{diag}(0, \Delta\tilde{m}^2_{21}, \Delta\tilde{m}^2_{31})$ is the effective squared mass in matter.

It is important to note that the parameterization of the mixing matrix depends on whether the neutrinos are Dirac or Majorana particles. However, in the context of the standard oscillations, it is not possible to distinguish between the two. The latter is because the Majorana phases are global and do not intervene in the standard neutrino oscillation phenomenon. The mixing matrix, considering the Majorana phases, can be obtained by redefining the Eq. (1.3) as follows:

$$U_{Majorana} = U_{\mathrm{PMNS}} \begin{pmatrix} 1 & 0 & 0 \\ 0 & e^{-i\phi_1} & 0 \\ 0 & 0 & e^{-i\phi_2} \end{pmatrix} \tag{1.11}$$

where ϕ_1 and ϕ_2 are the two Majorana CP violation phases [120].

Although both natures (Dirac and Majorana) imply a different mixing matrix (Eq. (1.3) and Eq.(1.11)), the oscillation probability (Eq. (1.7)) is the same, making it impossible to distinguish the nature of neutrinos in oscillation experiments, within the context of the standard oscillation. However, part of this analysis is to consider a scenario beyond the standard oscillation in which the nature of the neutrino can be manifested through the oscillation probability. Furthermore, within this new scenario, we are going to study the effects that the Majorana nature can have on the measurement of the standard oscillation parameters, as well as on the violation of the CP symmetry.

1.2 Neutrino Nature

The Dirac and Majorana theories are equivalent in the case of massless neutrinos. However, their theoretical simplicity makes Majorana massive neutrinos more plausible than Dirac massive neutrinos. Furthermore, in the framework of the standard oscillation, we must take into account that the kinematic effects of the mass of the Dirac or Majorana neutrino are identical.

Dirac Neutrino

A Dirac particle is a fermion that differs from its antiparticle. Considering the Dirac nature of the neutrino, the Brout-Englert-Higgs mechanism will generate its mass, the same mechanism responsible for giving masses to charged quarks and leptons in the standard model of particle physics. To generate mass to Dirac neutrinos by the Brout-Englert-Higgs mechanism, the Standard Model requires considering the existence of right-handed neutrinos. Nevertheless, right-handed neutrino fields are expressed by singlets, which do not transform under $SU(2)_L \bigotimes U_Y(1)$ and therefore do not participate in weak, strong, or electromagnetic interactions. The latter makes it impossible to detect right-handed neutrinos, which is why they are considered sterile. On the other hand, left-handed neutrinos are called active neutrinos.

In the Minimally Extended Standard Model with three right-handed neutrino fields, the Yukawa Lagrangian for leptons is as follows:

$$\mathscr{L}_{Leptons} = -\sum_{\alpha,\beta=e,\mu,\tau} Y'^{\ell}_{\alpha\beta}\overline{L_{\alpha L}}\Phi\ell'_{\beta R} - \sum_{\alpha,\beta=e,\mu,\tau} Y'^{\nu}_{\alpha\beta}\overline{L_{\alpha L}}\widetilde{\Phi}\nu'_{\beta R} + \text{H.c.} \qquad (1.12)$$

where $L_{\alpha L}$ are the three generations of left-handed weak isospin doublets, $\ell'_{\beta R}$ and $\nu'_{\beta R}$ the right-handed singlets, Φ the Higgs doublet, $Y'^{\ell}_{\alpha\beta}$ and $Y'^{\nu}_{\alpha\beta}$ are the Yukawa coupling matrix for charged leptons and neutrinos, respectively.

As a consequence of symmetry breaking, the diagonalization of the Yukawa matrices, and focusing only on the neutrino terms, the previous equa-

tion takes the following form:

$$\mathscr{L}^{D}_{mass} = -\sum_{k=1}^{3} \frac{y^{\nu}_{k} v}{\sqrt{2}} \overline{\nu_k} \nu_k - ... \tag{1.13}$$

where y^{ν}_{k} are real and positive eigenvalues of the Yukawa matrix, v is the vacuum expectation value (VEV) of Φ, and $\nu_k = \nu_{kL} + \nu_{kR}$ is the Dirac field of the neutrinos.

Therefore, the mass term for Dirac neutrinos is given by:

$$m_k = \frac{y^{\nu}_{k} v}{\sqrt{2}} \qquad (k = 1, 2, 3) \tag{1.14}$$

The neutrinos masses acquired with this mechanism are proportional to v (VEV), similar to the masses of quarks and charged leptons. However, there is no justification for why the Yukawa constants y^{ν}_{k} should take tiny values to explain the neutrino masses.

Majorana neutrino

As is known, neutrinos are massive, so it is natural to assume that they are like other fermions (quarks and charged leptons) and, therefore, should be Dirac spinors. However, there is an essential difference between neutrinos and the remainder of fundamental fermions; neutrinos do not have an electric charge. The latter leads us to assess the possibility that neutrinos are Majorana spinors. In contrast to a Dirac fermion, a Majorana fermion is a fermion that is its own antiparticle.

Without introducing any new particles, the Lagrangian with the least dimension that could generate a Majorana mass term respecting the symmetries of the standard model except for the conservation of the lepton number is $d = 5$:

$$\mathscr{L}^{M}_{mass} = \frac{\Upsilon}{\mathrm{M}}(L_L^T \sigma_2 \Phi) C^{\dagger} (\Phi^T \sigma_2 L_L) + \mathrm{H.c.} \tag{1.15}$$

where Υ is a symmetric matrix of coupling constants, σ is the Pauli matrix, and M can be interpreted as a typical symmetry-breaking mass at high energies. After electroweak symmetry breaking, and focusing on the neutrino terms, we get the following

$$\mathscr{L}^{M}_{mass} = \frac{1}{2}\frac{\Upsilon v^2}{\mathrm{M}} \nu_L^T C^{\dagger} \nu_L + \mathrm{H.c.} \tag{1.16}$$

In this context, the mass of the active neutrinos are proportional to v^2/M resulting in a tiny value for their masses due to the suppression provoked by the huge value of M.

1.3 CP and CPT Violation

In the 1950 decade, it appeared to be a rational inference that laws of physics respected the P symmetry, which implied that nature should not care if our system was right or left-handed. However, in 1957, the weak interaction that violates parity [124, 125] was uncovered. Thus, the subsequent proper assumption was preserving CP symmetry [126]. Nevertheless, in 1964 an experiment discovered evidence of CP violation in the decay of neutral K-mesons. The latter led us to infer that matter and antimatter behave differently [127]. This would help explain the prevalence of matter over antimatter in the universe, even though the Big Bang theory predicts a similar production of matter and antimatter [128–133]. The explanation of this imbalance is rooted in the Sakharov conditions, one of them being the violation of the CP symmetry [134]. In this context, the magnitude of the CP violation measured in the quark sector is not high enough to produce the matter-antimatter asymmetry. [120, 127, 135]. Nevertheless, in the leptonic sector, another potential source of CP violation could help unravel this mystery via the Leptogenesis process

[136–140]. The T2K experiment has been able to measure a CP violation phase in the neutrino oscillation phenomenon [112] giving an additional boost to the underway efforts for building experiments [53, 113] with the capabilities for enhancing the accuracy of its measurement and also to cross-check it.

After verifying the P violation, it is assumed that this happened because P symmetry was part of a more extensive symmetry called CP, which had to be preserved by nature. Similarly, knowing the CP violation, it is assumed that CP is part of a larger symmetry that includes time-reversal (T), the CPT symmetry [41, 141, 142]. The CPT invariance comes from a theorem of the quantum field theory set in a flat space, the so-called CPT theorem [141]. However, although there is no evidence for the violation of this symmetry, many theoretical hypotheses consider the CPTV, including quantum decoherence.

In the neutrino oscillation phenomenon and within the framework of quantum decoherence, we study scenarios where a CPT symmetry violation (CPTV) occurs. Furthermore, we propose a way to measure the CPTV in the DUNE experiment.

CHAPTER 2

EXPERIMENTAL CONTEXT

The neutrino oscillation phenomenon is governed by the PMNS matrix, shown in the equation (1.11), that contains different oscillation parameters, such as the mixing angles θ_{12}, θ_{13} and θ_{23}, as well as the CP-violating phases δ_{CP}, ϕ_1 and ϕ_2. In the context of the standard neutrino oscillation, it is impossible to measure the Majorana phases ϕ_1 and ϕ_2; moreover, there are three main open questions. First, is the measure of the CP-violating phase $\delta_{\text{CP}} \neq 0$? The $\delta_{\text{CP}} \neq 0$ tells us that the oscillation probability $\nu_\mu \to \nu_e$ is different from the oscillation probability $\bar{\nu}_\mu \to \bar{\nu}_e$; additionally, a measure of $\delta_{\text{CP}} \neq 0$ would help to understand the asymmetry between matter and antimatter in the universe. The second open question concerns the neutrino mass hierarchy, is the normal hierarchy (where ν_1 is the lightest) or the inverted hierarchy (where ν_3 is the lightest) the predominant one?. Finally, the octant problem of the neutrino mixing angle θ_{23}, is the mixing angle value θ_{23} maximal ($\theta_{23} = \pi/4$) or is it below (above) $\theta_{23} < \pi/4$ ($\theta_{23} > \pi/4$)? [143–146]

On the other hand, neutrino oscillation is an open window for the manifestation of physics beyond the standard model, which can manifest as subleading effects in the oscillation phenomenon. Aimed at solving the main open questions of the standard neutrino oscillation, and studying the possible manifestations of new physics, have been proposed long and medium baseline experiments, such as DUNE (Deep Underground Neutrino Experiment) and T2HK (Tokai to Hyper Kamiokande).[13, 15, 147–151]

2.1 Deep Underground Neutrino Experiment - DUNE

The DUNE experiment is one of the most powerful tool designed for studying fundamental and unknown aspects of neutrino physics. The experiment will produce a muon neutrino (antineutrino) beam in the Fermilab Main Injector by accelerating and colliding a proton beam against a graphite target. At Fermilab, 62 m depth and 574 m from the neutrino source will be the near detector (ND); while located in the Sanford Underground Research Facility (SURF) will be based the far detector (FD) [53]. The FD will consist of an approximately 40 kt liquid argon time projection chamber (LArTPC) [152]. In contrast, the ND will consist of a magnetized gaseous argon time projection chamber (TPC), a magnetized beam monitor, and a LArTPC [153]. After being produced, the neutrino beam will travel through the Earth, with an average matter density of $\rho = 2.96$ g/cm^3, a distance of approximately 1300 km from ND to FD, as shown in Fig. 2.1.

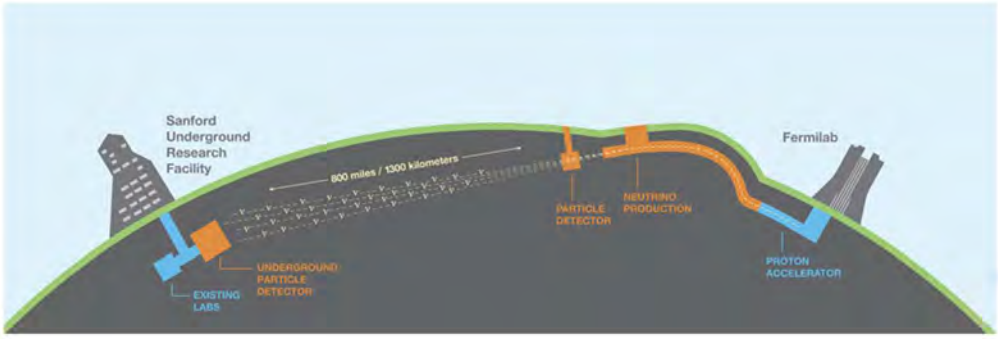

Figure 2.1: DUNE experiment design. Figure taken from [154]

To simulate the DUNE data sample, we use the information of the cross-section, neutrino fluxes, resolution function, efficiency and systematic uncertainties from [52] with the GLoBES package [155, 156]. Additionally, the configuration of 80 GeV energy with 1.07 MW power in the primary proton beam from the Main Injector is assumed. On the other hand, in the context of quantum decoherence, we use nuSQuIDS to calculate the matter neutrino oscillation probabilities [157].

2.2 Tokai to Hyper Kamiokande - T2HK

The Tokai to Kamioka (T2K) experiment consists of the generation of a muon neutrino (antineutrino) beam in the Japan Proton Accelerator Research Complex (J-PARC) located on the East coast of Japan. Consequently, the neutrino beam travels 295 km to the mountains of western Japan, where the Super-Kamiokande (SK) neutrino detector will observe it [158]. The most recent and relevant contribution of the T2K experiment is the most robust constraint for matter-antimatter asymmetry in neutrino physics [112].

With similar objectives and complementing the DUNE experiment, it is proposed to enhance SK, thus giving rise to Hyper-Kamiokande (HK), increasing the fiducial mass of the detector approximately 20 times. The Tokai to Hyper-Kamiokande (T2HK) experiment will use the identical neutrino experimental facility that T2K, with upgraded beam power, and its detector HK will be 2.5° off-axis from the J-PARC beam. [113, 159, 160]

Analogously to DUNE, T2HK simulated data samples and the oscillation probabilities are generated with GLoBES [155, 156] and nuSQuIDS [157], respectively. Likewise, we use the configuration and inputs from [113, 161] considering a 258-kt detector, as well as 3 and 9 years for neutrino and antineutrino mode, respectively.

CHAPTER 3

VIOLATION OF THE EQUIVALENCE PRINCIPLE

3.1 Hamiltonian and oscillation probabilities

In this chapter, we study the Violation of the Equivalence Principle (VEP) as a second-order correction in the neutrino oscillation phenomenon.

We break the universality of Newton's gravitational constant (G_N) by introducing the γ_i parameter to introduce the VEP in the neutrino oscillation phenomenon. Thus, we define a gravitational constant and, consequently, the gravitational potential as follows,

$$G'_N = \gamma_i G_N \tag{3.1}$$

This implies

$$\Phi' = \gamma_i \Phi \tag{3.2}$$

where Φ is the mass-dependent gravitational potential, and i runs over the three gravity eigenstates.

On the other hand, the space-time metric in the weak field approximation is given by:

$$g_{\mu\nu}(x) = \eta_{\mu\nu} + h_{\mu\nu}(x) \tag{3.3}$$

where $h_{\mu\nu}(x) = -2\gamma_i \Phi(x)\delta_{\mu\nu}$ and $\eta_{\mu\nu} = diag(1, -1, -1, -1)$ is the Minkowski metric. Substituting Eq. (3.3) in the relativistic invariant $g_{\mu\nu}p^\mu p^\nu = m^2$ and considering that $|\vec{p}| = p$, we get the following energy-momentum relation [35]:

$$E^2(1 - 2\gamma_i\Phi) = p^2(1 + 2\gamma_i\Phi) + m^2 \tag{3.4}$$

Considering $p^2 \gg m^2$ and ignoring terms $\Phi m^2/p$ and of $O(\Phi^2)$, we obtain from Eq. (3.4) the subsequent expression:

$$E_i \simeq p(1 + 2\gamma_i\Phi) + \frac{m_i^2}{2p} \tag{3.5}$$

The latter conducts us to the next expression:

$$\Delta E_{ij} = \frac{\Delta m_{ij}^2}{2E} + 2E\Delta\gamma_{ij} \tag{3.6}$$

where $\Delta\gamma_{ij} = \Phi(\gamma_i - \gamma_j)$.

In Eq. (3.6), we observe the two contributions to the energy shift; the first is due to the differences between neutrino mass eigenstates, and the second is because of the differences between neutrino gravitational eigenstates.

Since, the mass and gravitational eigenstates can be different, and accordingly, the mixing matrices that diagonalize their Hamiltonians on the flavor basis are not necessarily the same. The general procedure for the latter can be encountered in [162–166] and is assumed in our Hamiltonian approach.

We add to Eq. (1.8) a generic Hamiltonian on the flavor basis for the neutrino-gravitational eigenstates.

$$\mathbf{H}^{\mathbf{tot}}_{\mathrm{osc}} = \mathbf{H}^{\mathrm{f}}_{\mathrm{osc}} + \mathbf{H}^{\mathrm{f}}_{\mathrm{g}} \tag{3.7}$$

with

$$\mathbf{H}^{\mathrm{f}}_{\mathrm{g}} = 2EU_{\mathrm{g}}\mathbf{H}_{\mathrm{g}}U^{\dagger}_{\mathrm{g}} \tag{3.8}$$

$$\mathbf{H}_{\mathrm{g}} = \mathrm{diag}(0, \Delta\gamma_{21}, \Delta\gamma_{31}) \tag{3.9}$$

where U_{g} is the equivalent matrix to the PMNS matrix that combines the neutrino-gravitational eigenstates with the flavor eigenstates.

With the purpose of getting the formulas for oscillation probabilities that contain the matter and gravitational effects, we take the recipes given in [167], conceived in the context of nonstandard interactions, and make an exact replacement of the equivalent terms. Consequently, we make the following definitions.

$$\mathbf{V}_{\mathrm{g}} = 2E\mathbf{H}^{\mathrm{f}}_{\mathrm{g}} = 4E^2U_{\mathrm{g}}\mathbf{H}_{\mathrm{g}}U^{\dagger}_{\mathrm{g}} \tag{3.10}$$

where:

$$\mathbf{V}_{\rm g} = k_E \begin{pmatrix} v_{ee} & v_{e\mu}e^{i\phi_{e\mu}} & v_{e\tau}e^{i\phi_{e\tau}} \\ v_{e\mu}e^{-i\phi_{e\mu}} & v_{\mu\mu} & v_{\mu\tau}e^{i\phi_{\mu\tau}} \\ v_{e\tau}e^{-i\phi_{e\tau}} & v_{\mu\tau}e^{-i\phi_{\mu\tau}} & v_{\tau\tau} \end{pmatrix} \tag{3.11}$$

with $k_E = 4E^2$.

We express $U_{\rm g}\mathbf{H}_{\rm g}U_{\rm g}^{\dagger}$ in terms of the generic matrix elements v and their complex phases to easily match these elements with their corresponding ϵ (and their phases) present in the given prescription in [167]. Then, we can rewrite Eq.(3.7).

$$\mathbf{H}_{\rm osc}^{\mathbf{tot}} = \frac{1}{2E}\left[U\mathbf{H}_{\rm osc}U^{\dagger} + \mathbf{A}_{\rm matt} + \mathbf{V}_{\rm g}\right] \tag{3.12}$$

where:

$$\mathbf{A}_{\rm matt} + \mathbf{V}_{\rm g} = k_E \begin{pmatrix} \frac{A_{CC}}{k_E} + v_{ee} & v_{e\mu}e^{i\phi_{e\mu}} & v_{e\tau}e^{i\phi_{e\tau}} \\ v_{e\mu}e^{-i\phi_{e\mu}} & v_{\mu\mu} & v_{\mu\tau}e^{i\phi_{\mu\tau}} \\ v_{e\tau}e^{-i\phi_{e\tau}} & v_{\mu\tau}e^{-i\phi_{\mu\tau}} & v_{\tau\tau} \end{pmatrix} \tag{3.13}$$

Accordingly, for obtaining the matter oscillation probability formulae it is required to replace in Eq. (4) (Eq. (15)) presented in [167] ([168]) for the channels $\nu_\mu \to \nu_e$ ($\nu_\mu \to \nu_\mu$) the following:

$$\begin{gathered} \frac{A_{CC}}{k_E} + v_{ee} \to 1 + \epsilon_{ee} \\ k_E \to A \\ v \to \epsilon \\ \phi \to \phi \end{gathered} \tag{3.14}$$

In addition to these replacements, we present the next notation:

$$\begin{aligned} \tilde{A} = \frac{k_E}{EL} &= \frac{4E}{L} \\ \tilde{v}_{\alpha\beta} &= ELv_{\alpha\beta} \\ \tilde{A}\tilde{v}_{\alpha\beta} &= k_E v_{\alpha\beta} \end{aligned} \tag{3.15}$$

where L is the neutrino source-detector distance. After the details mentioned above are applied, we express the $\nu_\mu \to \nu_e$ oscillation probability as follows

$$
\begin{aligned}
&P^{\text{VEP}\bigoplus\text{SO}}_{\nu_\mu\to\nu_e} \simeq P^{\text{SO}}_{\nu_\mu\to\nu_e} \\
&+ 4\hat{A}\tilde{v}_{e\mu}\left\{xf\left[s^2_{23}f\cos\left(\phi_{e\mu}+\delta_{CP}\right)+c^2_{23}g\cos\left(\Delta+\delta_{CP}+\phi_{e\mu}\right)\right]\right. \\
&\left.+yg\left[c^2_{23}g\cos\phi_{e\mu}+s^2_{23}f\cos\left(\Delta-\phi_{e\mu}\right)\right]\right\} \\
&+ 4\hat{A}\tilde{v}_{e\tau}s_{23}c_{23}\left\{xf\left[f\cos\left(\phi_{e\tau}+\delta_{CP}\right)-g\cos\left(\Delta+\delta_{CP}+\phi_{e\tau}\right)\right]\right. \\
&\left.-yg\left[g\cos\phi_{e\tau}-f\cos\left(\Delta-\phi_{e\tau}\right)\right]\right\}+4\hat{A}^2g^2c^2_{23}|c_{23}\tilde{v}_{e\mu}e^{i\phi_{e\mu}}-s_{23}\tilde{v}_{e\tau}e^{i\phi_{e\tau}}|^2 \\
&+ 4\hat{A}^2f^2s^2_{23}|s_{23}\tilde{v}_{e\mu}e^{i\phi_{e\mu}}+c_{23}\tilde{v}_{e\tau}e^{i\phi_{e\tau}}|^2+8\hat{A}^2fgs_{23}c_{23}\left\{c_{23}\cos\Delta\left[s_{23}\left(\tilde{v}^2_{e\mu}-\tilde{v}^2_{e\tau}\right)\right.\right. \\
&\left.\left.+2c_{23}\tilde{v}_{e\mu}\tilde{v}_{e\tau}\cos\left(\phi_{e\mu}-\phi_{e\tau}\right)\right]-\tilde{v}_{e\mu}\tilde{v}_{e\tau}\cos\left(\Delta-\phi_{e\mu}+\phi_{e\tau}\right)\right\} \\
&+\mathcal{O}\left(s^2_{13}\tilde{v}_{\alpha\beta},s_{13}\tilde{v}^2_{\alpha\beta},\tilde{v}^3_{\alpha\beta}\right)
\end{aligned}
\tag{3.16}
$$

where

$$
\begin{aligned}
&x=2s_{13}s_{23},\quad y=2rs_{12}c_{12}c_{23},\quad r=|\Delta m^2_{21}/\Delta m^2_{31}|,\quad f,\bar{f}=\frac{\sin\left[\Delta\left(1\mp\hat{A}\tilde{v}'_{ee}\right)\right]}{1\mp\hat{A}\tilde{v}'_{ee}} \\
&g=\frac{\sin\left(\hat{A}\tilde{v}'_{ee}\Delta\right)}{\hat{A}\tilde{v}'_{ee}},\quad \tilde{v}'_{ee}=\frac{A_{CC}}{\tilde{A}}+\tilde{v}_{ee},\quad \Delta=\left|\frac{\Delta m^2_{31}L}{4E}\right|,\quad \hat{A}=\left|\frac{\tilde{A}}{\Delta m^2_{31}}\right|
\end{aligned}
\tag{3.17}
$$

and $s_{ij}=\sin\theta_{ij}$, $c_{ij}=\cos\theta_{ij}$. The antineutrino equation $\bar{\nu}_\mu \to \bar{\nu}_e$ is given by the Eq. (3.16), changing $\hat{A}\to-\hat{A}$ (then $\bar{f}$ instead of f), $\delta_{CP}\to-\delta_{CP}$ and $\phi_{\alpha\beta}\to-\phi_{\alpha\beta}$. For the inverted hierarchy $\Delta\to-\Delta$, $y\to-y$ and $\hat{A}\to-\hat{A}$. The $\tilde{v}_{\alpha\beta}$, one of the key parameters of expansion, is $\sim\Delta\tilde{\gamma}_{ij}=EL\Delta\gamma_{ij}$. For $\Delta\tilde{\gamma}_{ij}$ no greater than $\mathcal{O}(0.1)$, we obtain an error of less than 5% between our analytical formula and the numerical results for the energy range up to 7 GeV or up to 14 GeV, depending on the texture of the gravitational matrix. Other important parameters of expansion are the typical ones: $s_{13}\sim0.1$ and $r\equiv|\Delta m^2_{21}/\Delta m^2_{31}|\sim0.01$.

On the other hand, the oscillation probability for $\nu_\mu\to\nu_\mu$ disappear-

ance channel is expressed by:

$$
\begin{aligned}
&P^{\text{VEP}\bigoplus\text{SO}}_{\nu_\mu\to\nu_\mu} \simeq P^{\text{SO}}_{\nu_\mu\to\nu_\mu} \\
&- \tilde{v}_{\mu\tau}\hat{A}\cos\phi_{\mu\tau}\sin(2\theta_{23})\left[2\Delta s^2_{23}\sin(2\Delta) + 4\cos^2(2\theta_{23})\sin^2\Delta\right] \\
&+ \hat{A}\left(\tilde{v}_{\mu\mu} - \tilde{v}_{\tau\tau}\sin^2(2\theta_{23})\cos(2\theta_{23})\right)\left[\Delta\sin(2\Delta) - 2\sin^2\Delta\right] + \mathcal{O}(r, s_{13}, \tilde{v}^2_{\alpha\beta})
\end{aligned}
\tag{3.18}
$$

It is necessary to mention that we have rewritten the probabilities in such a way that the pure standard oscillation (SO) term, $P^{\text{SO}}_{\nu_\alpha\to\nu_\beta}$, is separated from those terms that combine the new physics parameters with the standard ones. Besides, when we use these oscillation probabilities formulas, Eq. (3.16) and Eq. (3.18), the $P^{\text{SO}}_{\nu_\alpha\to\nu_\beta}$ term is numerically calculated. This is done in order to achieve a better agreement between these (semi) analytical probabilities and those fully numerically calculated.

3.2 Lorentz violation interpretation

It is essential to mention that the VEP prescription shown in this Thesis so far, and its subsequent results, can be reinterpreted for a general energy exponent case. The aforementioned is set up because the only parameter in our oscillation probability formulas that contains the VEP effects is:

$$\Delta\tilde{\gamma}_{ij} = EL\Delta\gamma_{ij} \tag{3.19}$$

Consequently, for translating VEP into Lorentz invariance violation (LIV), it is adequate to substitute in Eq. (3.19) [169]:

$$2E \to E^{d-3} \implies E \to E^{d-3}/2 \tag{3.20}$$

where d represents the dimension of the operator. So that our oscillation probability formulas can be able to test for a power-law energy dependency for a given exponent and consequently extrapolate the results to a general case, we perform the following replacement equivalent to Eq.(3.20) in Eq. (3.8).

$$\mathbf{H^f_g \propto 2E \to H^f_g \propto E^{d-3}} \tag{3.21}$$

The cases when $d = 3, 4, 5, ..$ correspond with the isotropic Lorentz violating terms represented in the effective Hamiltonian of the SME [170], the minus sign in some coefficients can be reabsorbed in $\Delta\gamma_{ij}$.

3.3 VEP scenarios

Part of this chapter is to analyze different VEP cases related to the diverse textures of the $U_{\rm g}$ matrix and the $\Delta\tilde{\gamma}_{ij}$ parameter, deducing the oscillation probabilities from the general formulas shown in Eq.(3.16) and Eq.(3.18) for each arrangement. Our simplification criterion used in the probability formulas for each VEP scenario is to maintain only the most relevant terms, i.e., the primary ones responsible for the behavior patterns per VEP case.

We define a $U_{\rm g}$ with a similar parametrization to U. To this, we represent the parameters of the $U_{\rm g}$ matrix as θ^g_{ij} and δ^g. Therefore, taking into account that $\sin\theta^g_{ij} = s^g_{ij}$ and $\cos\theta^g_{ij} = c^g_{ij}$, for the neutrino appearance channel $\nu_\mu \to \nu_e$,

$$\tilde{v}_{ee} = (c^g_{13}s^g_{12})^2\Delta\tilde{\gamma}_{21} + (s^g_{13})^2\Delta\tilde{\gamma}_{31} \tag{3.22}$$

$$\phi_{e\mu} = \arctan\left[\frac{\sin\delta^g(k_2\Delta\tilde{\gamma}_{21} - k_3\Delta\tilde{\gamma}_{31})}{(k_1 - k_2\cos\delta^g)\Delta\tilde{\gamma}_{21} + k_3\cos\delta^g\Delta\tilde{\gamma}_{31}}\right] \tag{3.23}$$

$$\tilde{v}_{e\mu} = \frac{(k_1 - k_2\cos\delta^g)\Delta\tilde{\gamma}_{21} + k_3\cos\delta^g\Delta\tilde{\gamma}_{31}}{\cos\phi_{e\mu}} \tag{3.24}$$

$$\phi_{e\tau} = \arctan\left[\frac{-\sin\delta^g(k'_1\Delta\tilde{\gamma}_{21} + k'_3\Delta\tilde{\gamma}_{31})}{(k'_2 + k'_1\cos\delta^g)\Delta\tilde{\gamma}_{21} + k'_3\cos\delta^g\Delta\tilde{\gamma}_{31}}\right] \tag{3.25}$$

$$\tilde{v}_{e\tau} = \frac{(k'_2 + k'_1\cos\delta^g)\Delta\tilde{\gamma}_{21} + k'_3\cos\delta^g\Delta\tilde{\gamma}_{31}}{-\cos\phi_{e\tau}} \tag{3.26}$$

where

$$\begin{aligned} k_1 &= c^g_{12}c^g_{23}c^g_{13}s^g_{12},\ k_2 = s^g_{13}s^g_{23}c^g_{13}(s^g_{12})^2,\ k_3 = c^g_{13}s^g_{23}s^g_{13} \\ k'_1 &= c^g_{23}s^g_{13}c^g_{13}(s^g_{12})^2,\ k'_2 = c^g_{12}c^g_{13}s^g_{12}s^g_{23},\ k'_3 = c^g_{13}c^g_{23}s^g_{13} \end{aligned} \tag{3.27}$$

On the other hand, for the neutrino disappearance channel $\nu_\mu \to \nu_\mu$, we obtain the following:

$$\tilde{v}_{\mu\mu} = (c^g_{13}s^g_{23})^2\Delta\tilde{\gamma}_{31} + [(c^g_{12}c^g_{23})^2 + (s^g_{12}s^g_{13}s^g_{23})^2 - 2c^g_{12}c^g_{23}s^g_{12}s^g_{13}s^g_{23}\cos\delta^g]\Delta\tilde{\gamma}_{21} \tag{3.28}$$

$$\tilde{v}_{\tau\tau} = (c^g_{13}c^g_{23})^2\Delta\tilde{\gamma}_{31} + \Delta\tilde{\gamma}_{21}[(c^g_{12}s^g_{23})^2 + (s^g_{12}s^g_{13}c^g_{23})^2 - 2c^g_{12}s^g_{23}s^g_{12}s^g_{13}c^g_{23}\cos\delta^g] \tag{3.29}$$

$$\phi_{\mu\tau} = \arctan\left[\frac{\sin\delta^g(f_3+f_4)\Delta\tilde{\gamma}_{21}}{\Delta\tilde{\gamma}_{31}f_1 + \Delta\tilde{\gamma}_{21}[f_2+\cos\delta^g(f_3-f_4)]}\right] \tag{3.30}$$

$$\tilde{v}_{\mu\tau} = \frac{\Delta\tilde{\gamma}_{31}f_1 + \Delta\tilde{\gamma}_{21}[f_2+\cos\delta^g(f_3-f_4)]}{\cos\phi_{\mu\tau}} \tag{3.31}$$

with

$$\begin{aligned} f_1 &= s^g_{23}c^g_{23}(c^g_{13})^2,\ f_2 = c^g_{23}s^g_{23}(s^g_{12}s^g_{13})^2 - s^g_{23}c^g_{23}(c^g_{12})^2 \\ f_3 &= c^g_{12}s^g_{12}s^g_{13}(s^g_{23})^2,\ f_4 = c^g_{12}s^g_{12}s^g_{13}(c^g_{23})^2 \end{aligned} \tag{3.32}$$

Scenario A: $U_{\mathbf{g}} = U$

The most straightforward case study is to assume that the gravitational mixing matrix U_{g} is similar to the PMNS matrix U; consequently, we obtain the following:

$$\theta^g_{ij} = \theta_{ij} \tag{3.33}$$

$$\delta^g = \delta_{CP} \tag{3.34}$$

As mentioned in the previous section, we keep the terms of orders no greater than $\mathcal{O}(0.001)$. For the latter, we must take into account the following:

$$s_{13} \sim \mathcal{O}(0.1) \tag{3.35}$$

$$r \sim \mathcal{O}(0.01) \tag{3.36}$$

$$\Delta\tilde{\gamma}_{ij} \sim \mathcal{O}(0.1) \tag{3.37}$$

Consequently, in our oscillation probability formulas, we will preserve the terms not greater than $s^2_{13}\Delta\tilde{\gamma}_{ij}$, $r\Delta\tilde{\gamma}_{ij}$ or $s_{13}\Delta\tilde{\gamma}^2_{ij}$.

It is important to mention that during the present chapter, we consider the values in Table 3.1 as the best-fit values for the oscillation parameters.

Parameter	Value	Error
θ_{12}	33.62°	0.77°
θ_{13}(NH)	8.54°	0.15°
θ_{23}(NH)	47.2°	1.9°
Δm^2_{21}	$7.4 \times 10^{-5}\text{eV}^2$	$0.2 \times 10^{-5}\text{eV}^2$
Δm^2_{31}(NH)	$2.494 \times 10^{-3}\text{eV}^2$	$0.032 \times 10^{-3}\text{eV}^2$
Baseline	1300Km	-

Table 3.1: DUNE baseline and values for standard oscillation parameters taken from [171] (January 2018).

In the subsequent analyses, within the scenario $U_{\rm g} = U$, we study two cases:

- **Case 1:** $\Delta\gamma_{21} = 0 \neq \Delta\gamma_{31}$
- **Case 2:** $\Delta\gamma_{21} \neq 0 = \Delta\gamma_{31}$

Case 1

In this case, $\Delta\gamma_{21} = 0$ and $\Delta\gamma_{31} \neq 0$, the oscillation probability for the $\nu_\mu \to \nu_e$ neutrino appearance channel, is as follows:

$$P^{\rm VEP \bigoplus SO}_{\nu_\mu \to \nu_e} \simeq P^{\rm SO}_{\nu_\mu \to \nu_e} + C_1 s^2_{13} \Delta\tilde{\gamma}_{31} \tag{3.38}$$

$$C_1 = 8 f^2 s^2_{23}/\Delta \tag{3.39}$$

in addition, the oscillation probability for the $\nu_\mu \to \nu_\mu$ disappearance channel is given by:

$$P^{\rm VEP \bigoplus SO}_{\nu_\mu \to \nu_\mu} \simeq P^{\rm SO}_{\nu_\mu \to \nu_\mu} - \sin 2\Delta \sin^2 2\theta_{23} \Delta\tilde{\gamma}_{31} \tag{3.40}$$

In Fig. 3.1(a) and Fig. 3.1(b) we show the $\nu_\mu \to \nu_e$ appearance channel and observe that there are tiny differences, in the final part of the

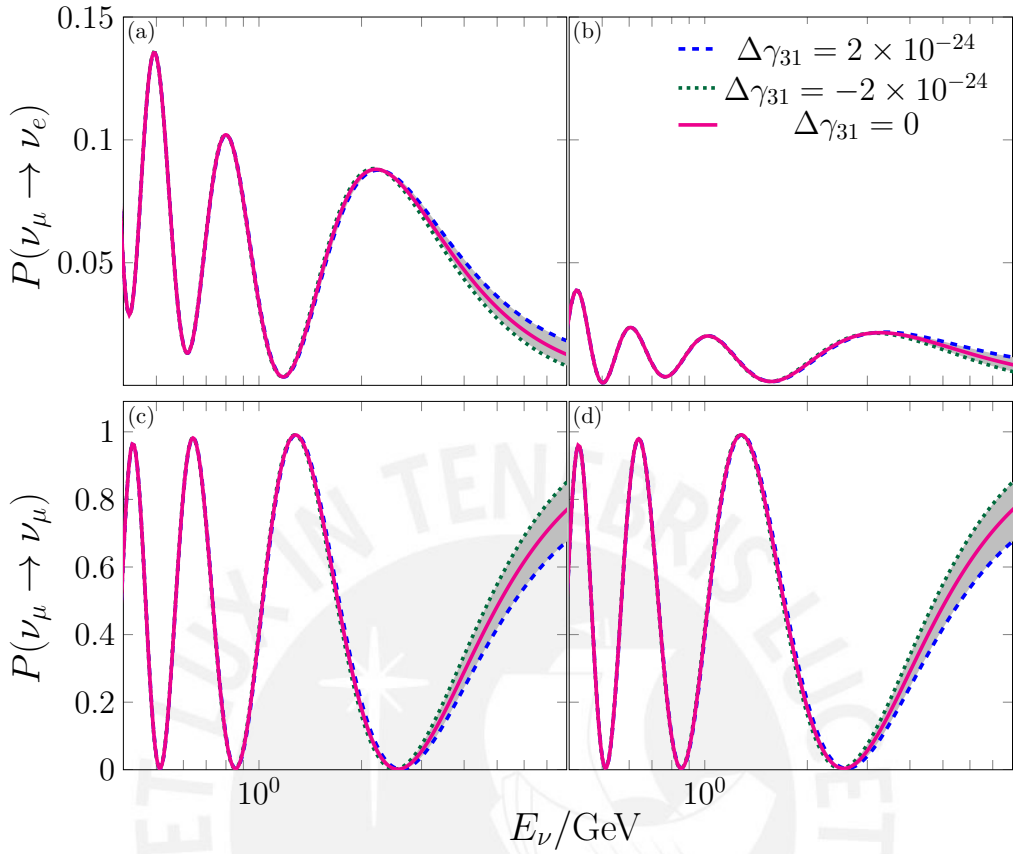

Figure 3.1: Oscillation probability depending on the neutrino energy and considering scenario A/case 1. Figures (b) and (d) represent the $\bar{\nu}_e$ appearance and $\bar{\nu}_\mu$ disappearance oscillation probability, respectively. We consider $\delta_{CP} = -\pi/2$ and $L = 1300$ km.

energy spectrum, between the pure SO and VEP$\bigoplus$SO. These minor differences in the $\nu_\mu \to \nu_e$ appearance channel are because only terms of order $s^2_{13}\Delta\tilde{\gamma}_{31} \sim \mathcal{O}(0.001)$ appear in the oscillation probability formula, as seen in Eq. (3.38).

On the other hand, the impact is slightly more meaningful in the $\nu_\mu \to \nu_\mu$ disappearance channel. The latter can be justified by the presence of terms of orders $\Delta\tilde{\gamma}_{31} \sim \mathcal{O}(0.1)$ in the oscillation probability expression, as shown in Eq. (3.40).

For the $\nu_\mu \to \nu_e$ channel, the VEP contribution has the same sign of $\Delta\tilde{\gamma}_{31}$, regardless it is a neutrino or an antineutrino due to the lack of $\delta_{\rm CP}$ phase in that term. Additionally, for the $\nu_\mu \to \nu_\mu$ channel the VEP contribution is opposite to the sign of $\Delta\tilde{\gamma}_{31}$, and is independent of being neutrino or antineutrino, i.e., there is no $\delta_{\rm CP}$ in the VEP term.

Case 2

In this case, $\Delta\gamma_{21} \neq 0$ and $\Delta\gamma_{31} = 0$, the oscillation probability for the $\nu_\mu \to \nu_e$ neutrino appearance channel is given by:

$$P^{\rm VEP \bigoplus SO}_{\nu_\mu \to \nu_e} \simeq P^{\rm SO}_{\nu_\mu \to \nu_e} + C_1 \cos\delta_{CP} s_{13} \Delta\tilde{\gamma}_{21} - C_2 \sin\delta_{CP} s_{13} \Delta\tilde{\gamma}_{21} + C_3 r \Delta\tilde{\gamma}_{21} - C_4 s^2_{13} \Delta\tilde{\gamma}_{21} + C_5 (\Delta\tilde{\gamma}_{21})^2 \tag{3.41}$$

with:

$$\begin{aligned} C_1 =& 8fg \cos\Delta s_{12} c_{12} s_{23} c_{23}/\Delta \\ C_2 =& 8fg \sin\Delta s_{12} c_{12} s_{23} c_{23}/\Delta \\ C_3 =& 8g^2 s^2_{12} c^2_{12} c^2_{23}/\Delta \\ C_4 =& 8f^2 s^2_{12} s^2_{23}/\Delta \\ C_5 =& 4g^2 s^2_{12} c^2_{12} c^2_{23}/\Delta^2 \end{aligned} \tag{3.42}$$

where the survival probability of $\nu_\mu \to \nu_\mu$ is:

$$P^{\rm VEP \bigoplus SO}_{\nu_\mu \to \nu_\mu} \simeq P^{\rm SO}_{\nu_\mu \to \nu_\mu} + \sin 2\Delta c^2_{12} \sin^2 2\theta_{23} \Delta\tilde{\gamma}_{21} \tag{3.43}$$

Unlike case 1, in the neutrino appearance channel $\nu_\mu \to \nu_e$, we observe a more significant difference between VEP $\bigoplus$ SO and the pure SO than the one shown in the $\nu_\mu \to \nu_\mu$ channel, see Fig. 3.2. The reason for the increment of the discrepancy in the $\nu_\mu \to \nu_e$ channel, with respect to the former case, relies on the fact that in the oscillation probability there are terms of order of $s_{13}\Delta\tilde{\gamma}_{21} \sim \mathcal{O}(0.01)$, as seen in Eq. (3.2). The sign of the overall contribution is positive (negative) for neutrinos and $\Delta\gamma_{21} > 0$ (and $\Delta\gamma_{21} < 0$), while it

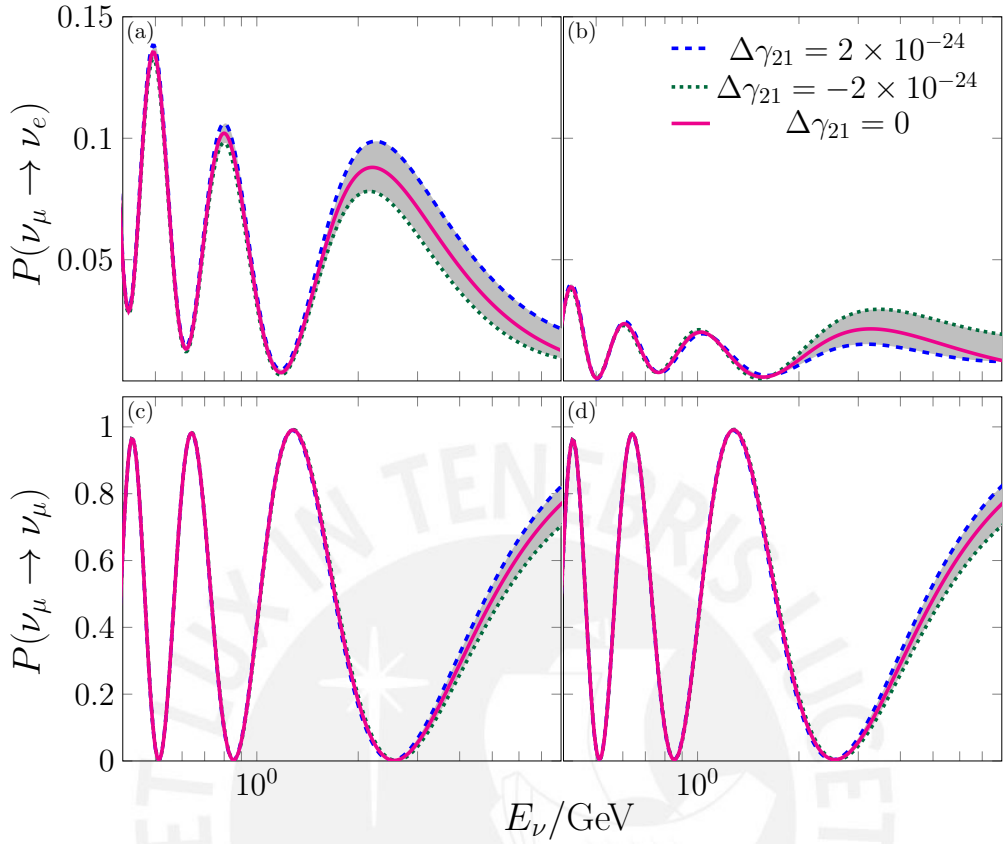

Figure 3.2: Oscillation probability depending on the neutrino energy and considering scenario A/case 2. Figures (b) and (d) represent the $\bar{\nu}_e$ appearance and $\bar{\nu}_\mu$ disappearance oscillation probability, respectively. We consider $\delta_{CP} = -\pi/2$ and $L = 1300$ km.

is negative (positive) for antineutrinos and $\Delta\gamma_{21} > 0$ (and $\Delta\gamma_{21} < 0$). The neutrino/antineutrino sign dependency appears due to the emergence of $\delta_{\rm CP}$ in the leading terms of the contribution. It is important to note that, given that $\delta_{\rm CP} = -\pi/2$, the term associated with C_1 vanishes.

I addition, for the $\nu_\mu \to \nu_\mu$ disappearance channel, even with a term of order $\Delta\tilde{\gamma}_{21} \sim \mathcal{O}(0.1)$, the discrepancy is less pronounced in comparison to the appearance channel. The latter occurs because the contribution of the VEP term is just smaller, by contrast with the magnitude of $P^{\rm SO}_{\nu_\mu \to \nu_\mu}$, than the corresponding ones for the transition channel.

On the other hand, it is interesting to mention that the oscillation probabilities for the degenerate case, $\Delta\gamma_{21} = \Delta\gamma = \Delta\gamma_{31}$, can be acquired just by replacing $s^2_{12} \to c^2_{12}$ in the term C_4 in Eq. (3.42). The observed effects on the neutrino oscillation probability are similar to those in the present case.

Scenario B: $U_{\mathbf{g}} \neq U$

In this chapter, we also analyze the general Ansatz for VEP where $U_{\rm g} \neq U$. For the latter, we develop three cases selected according to three different texture choices for the mixing matrix of the gravity eigenstates, $U_{\rm g}$. We denote each texture by $U^{ij}_{\rm g}$, which means that θ^g_{ij} is the only angle set as different from zero in the gravitational matrix.

Texture θ_{13}

For this case, the $U_{\rm g}$ matrix is given by the following expression:

$$U^{13}_{\rm g} = \begin{pmatrix} c^g_{13} & 0 & s^g_{13} \\ 0 & 1 & 0 \\ -s^g_{13} & 0 & c^g_{13} \end{pmatrix} \tag{3.44}$$

where $c^g_{ij} \equiv \cos\theta^g_{ij}$ and $s^g_{ij} \equiv \sin\theta^g_{ij}$. Selecting $\theta^g_{13} \neq 0$ implies a two-generation reduction of the probability formula preserving only $\Delta\gamma_{31}$ from the gravitational sector. After the replacements and simplifications the $\nu_\mu \to \nu_e$ oscillation probability channel takes the following form:

$$\begin{aligned} P^{\rm VEP \bigoplus SO}_{\nu_\mu\to\nu_e} \simeq\, & P^{\rm SO}_{\nu_\mu\to\nu_e} \\ & + C_1 \cos\delta_{CP} s_{13}\Delta\tilde{\gamma}_{31} + C_2 \sin\delta_{CP} s_{13}\Delta\tilde{\gamma}_{31} - C_3 r\Delta\tilde{\gamma}_{31} + C_4(\Delta\tilde{\gamma}_{31})^2 \end{aligned} \tag{3.45}$$

where:

$$\begin{aligned} C_1 =& 8f(f - g\cos\Delta)s^2_{23}c_{23}s^g_{13}c^g_{13}\ \Delta \\ C_2 =& 8fg\sin\Delta s^2_{23}c_{23}s^g_{13}c^g_{13}/\Delta \\ C_3 =& 8g(g - f\cos\Delta)s_{12}c_{12}s_{23}c^2_{23}s^g_{13}c^g_{13}/\Delta \\ C_4 =& 4(f^2 + g^2 - 2fg\cos\Delta)s^2_{23}c^2_{23}{s^g_{13}}^2{c^g_{13}}^2/\Delta^2 \end{aligned} \tag{3.46}$$

Similarly, the oscillation probability for the $\nu_\mu \to \nu_\mu$ disappearance channel is given by:

$$P^{\text{VEP}\bigoplus\text{SO}}_{\nu_\mu\to\nu_\mu} \simeq P^{\text{SO}}_{\nu_\mu\to\nu_\mu} - \frac{2}{\Delta}\sin\Delta(\Delta\cos\Delta - \sin\Delta) \times s_{23}c_{23}\sin 4\theta_{23}{c^g_{13}}^2\Delta\tilde{\gamma}_{31} \tag{3.47}$$

In Fig. 3.3, we observe that the differences in the oscillation probability for the $\nu_\mu \to \nu_e$ appearance channel are of the same order than in the previous case. The latter is due to the emergence of $s_{13}\Delta\tilde{\gamma}_{31} \sim \mathcal{O}(0.01)$ terms in the oscillation probability formula, similar to those in Eq. (3.41). Since $\Delta\gamma_{31}$ is taken as positive, the sign of the total contribution relies merely on whether they are neutrinos (negative) or antineutrinos (positive). Furthermore, from the oscillation probability, we observe that the maximum disparity with respect to the SO emerges when $\theta^g_{13} = \pm\pi/4$ because it maximizes/minimizes $\sin 2\theta^g_{13}$. The disparities between the $\nu_\mu \to \nu_\mu$ oscillation probabilities are insignificant because the term containing VEP is proportional to $\sin 4\theta_{23} \sim 0$, considering that θ_{23} is close to $\pi/4$.

Texture θ_{12}

For this texture, the U_{g} matrix is given by:

$$U^{12}_{\text{g}} = \begin{pmatrix} c^g_{12} & s^g_{12} & 0 \\ -s^g_{12} & c^g_{12} & 0 \\ 0 & 0 & 1 \end{pmatrix} \tag{3.48}$$

In this context, the oscillation probability formula for the $\nu_\mu \to \nu_e$ appearance channel finish as:

$$\begin{aligned} P^{\text{VEP}\bigoplus\text{SO}}_{\nu_\mu\to\nu_e} &\simeq P^{\text{SO}}_{\nu_\mu\to\nu_e} \\ &+ C_1\cos\delta_{CP}s_{13}\Delta\tilde{\gamma}_{21} - C_2\sin\delta_{CP}s_{13}\Delta\tilde{\gamma}_{21} + C_3 r\Delta\tilde{\gamma}_{21} + C_4(\Delta\tilde{\gamma}_{21})^2 \end{aligned} \tag{3.49}$$

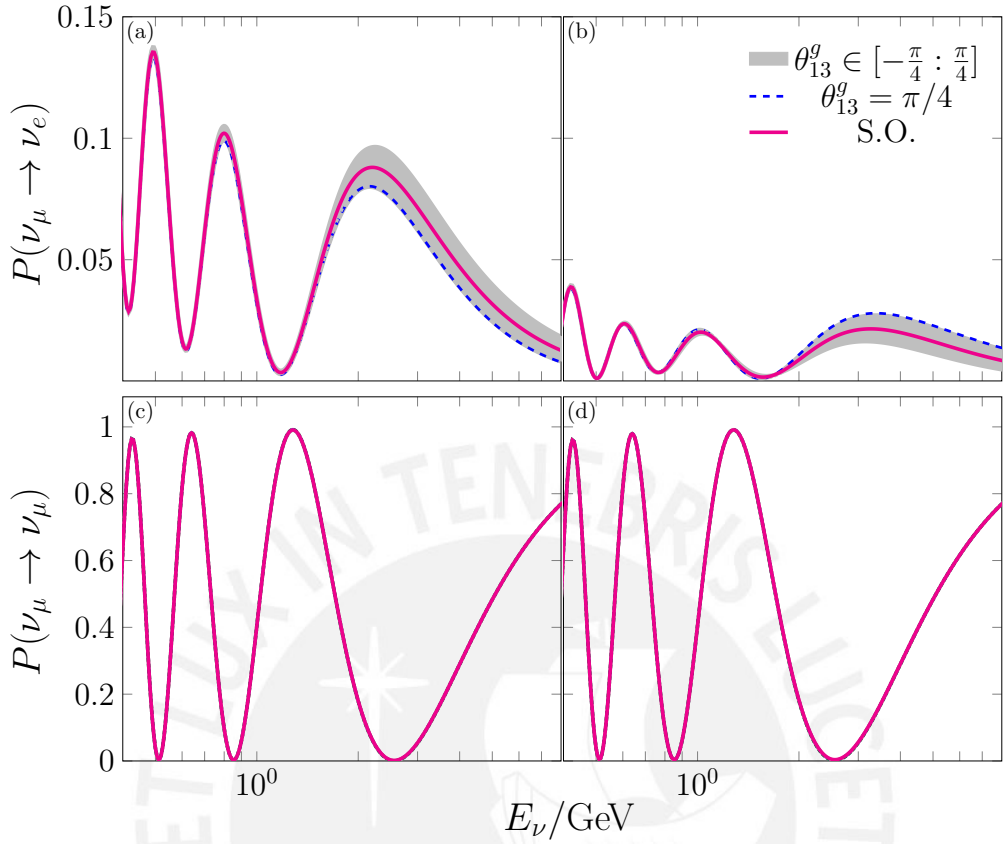

Figure 3.3: Oscillation probability depending on the neutrino energy and considering scenario B/texture θ_{13}. Figures (b) and (d) represent the $\bar{\nu}_e$ appearance and $\bar{\nu}_\mu$ disappearance oscillation probability, respectively. We consider $\Delta\gamma_{31} = 2 \times 10^{-24}$, $\delta_{CP} = -\pi/2$ and $L = 1300$ km.

where:

$$\begin{aligned} C_1 =& 8f(fs^2_{23} + gc^2_{23}\cos\Delta)s_{23}s^g_{12}c^g_{12}/\Delta \\ C_2 =& 8fg\sin\Delta s_{23}c^2_{23}s^g_{12}c^g_{12}/\Delta \\ C_3 =& 8g(fs^2_{23}\cos\Delta + gc^2_{23})s_{12}c_{12}c_{23}s^g_{12}c^g_{12}/\Delta \\ C_4 =& 4(f^2s^4_{23} + g^2c^4_{23} + 2fgs^2_{23}c^2_{23}\cos\Delta){s^g_{12}}^2{c^g_{12}}^2/\Delta^2 \end{aligned} \tag{3.50}$$

Additionally, the oscillation probability expression for the $\nu_\mu \to \nu_\mu$ disappearance channel is:

$$P^{\text{VEP}\bigoplus\text{SO}}_{\nu_\mu\to\nu_\mu} \simeq P^{\text{SO}}_{\nu_\mu\to\nu_\mu} + \frac{2}{\Delta}\sin\Delta(\Delta\cos\Delta - \sin\Delta) \times s_{23}c_{23}\sin 4\theta_{23}{c^g_{12}}^2\Delta\tilde{\gamma}_{21} \tag{3.51}$$

In Fig. 3.4, we note that the pattern of the oscillation probabilities is comparable to those shown in the previous case. Hence, the latter is plausible to anticipate in light of the similitudes in the formulae for both cases. Consequently, we can use the arguments to explain the previous texture in this case. The only difference for this case is that the sign of the general contribution that distinguishes VEP $\bigoplus$ SO from SO is positive for neutrinos and negative for antineutrinos in the $\nu_\mu \to \nu_e$ appearance channel. Consequently, for the oscillation probability in the $\nu_\mu \to \nu_\mu$ channel, as in the previous case, the discrepancies between VEP $\bigoplus$ SO and SO and are negligible.

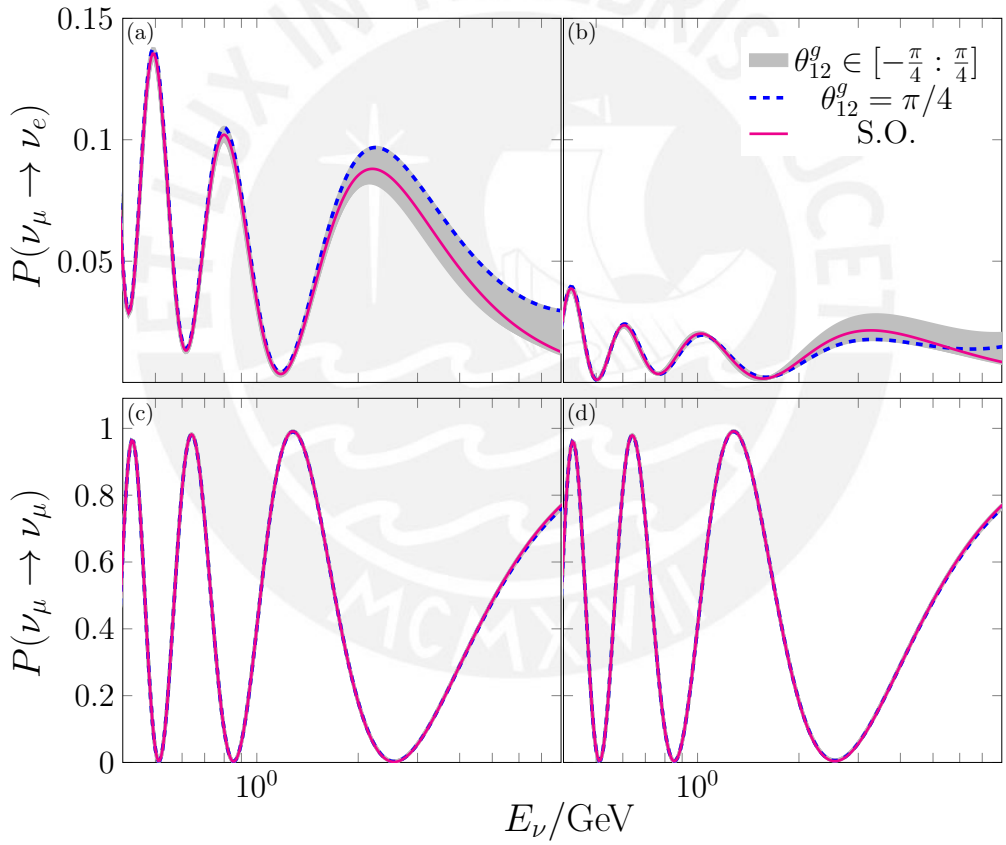

Figure 3.4: Oscillation probability depending on the neutrino energy and considering scenario B/texture θ_{12}. Figures (b) and (d) represent the $\bar{\nu}_e$ appearance and $\bar{\nu}_\mu$ disappearance oscillation probability, respectively. We consider $\Delta\gamma_{21} = 2 \times 10^{-24}$, $\delta_{CP} = -\pi/2$ and $L = 1300$ km.

Texture θ_{23}

In this section, we use the following texture for the gravitational matrix:

$$U_{\rm g}^{23} = \begin{pmatrix} 1 & 0 & 0 \\ 0 & c_{23}^{g} & s_{23}^{g} \\ 0 & -s_{23}^{g} & c_{23}^{g} \end{pmatrix} \tag{3.52}$$

Because the VEP parameter $\Delta\gamma_{23}$ can be expressed as a function of $\Delta\gamma_{31}$ and $\Delta\gamma_{21}$, we subdivide this particular texture into two different subcases.

$\Delta\gamma_{21} = 0$ **and** $\Delta\gamma_{31} \neq 0$

From Eq. (3.16), we can observe that all the VEP contributions in the oscillation probability for the $\nu_\mu \to \nu_e$ channel are up to $\mathcal{O}(10^{-3})$. Therefore, the oscillation probability for VEP $\bigoplus$ SO is very similar to the one for SO.

On the other hand, the oscillation probability for the the $\nu_\mu \to \nu_\mu$ channel has non-null VEP contribution due to the term $\Delta\tilde{\gamma}_{31} \sim \mathcal{O}(0.1)$. Therefore, the oscillation probability formula turns out to be as follows:

$$\begin{aligned} P_{\nu_\mu\to\nu_\mu}^{\rm VEP\bigoplus SO} \simeq\ & P_{\nu_\mu\to\nu_\mu}^{\rm SO} - \frac{4}{\Delta}\Big(\Delta\cos\Delta\sin 2\theta_{23}\cos(2(\theta_{23}-\theta_{23}^{g})) \\ & - \sin\Delta\cos 2\theta_{23}\sin(2(\theta_{23}-\theta_{23}^{g}))\Big) \times \sin\Delta s_{23}c_{23}\Delta\tilde{\gamma}_{31} \end{aligned} \tag{3.53}$$

$\Delta\gamma_{21} \neq 0$ **and** $\Delta\gamma_{31} = 0$

Analogous to the previous case, the oscillation probability for the $\nu_\mu \to \nu_e$ appearance channel for VEP $\bigoplus$ SO is not much different from SO due to the VEP contributions being terms scaled by factors of $\mathcal{O}(10^{-3})$, i.e., the VEP contributions are insignificant. In addition, the oscillation probability for the $\nu_\mu \to \nu_\mu$ channel has a non-negligible perturbative contribution, as seen as follows:

$$P^{\text{VEP}\bigoplus\text{SO}}_{\nu_\mu\to\nu_\mu} \simeq P^{\text{SO}}_{\nu_\mu\to\nu_\mu} + \frac{2}{\Delta}\Big(\sin\Delta(\Delta\cos\Delta - \sin\Delta)\times\sin 4\theta_{23}\cos 2\theta^g_{23} + \left(2\sin^2\Delta\cos^2 2\theta_{23} + \Delta\sin 2\Delta\sin^2 2\theta_{23}\right)\sin 2\theta^g_{23}\Big)s_{23}c_{23}\Delta\tilde{\gamma}_{21} \tag{3.54}$$

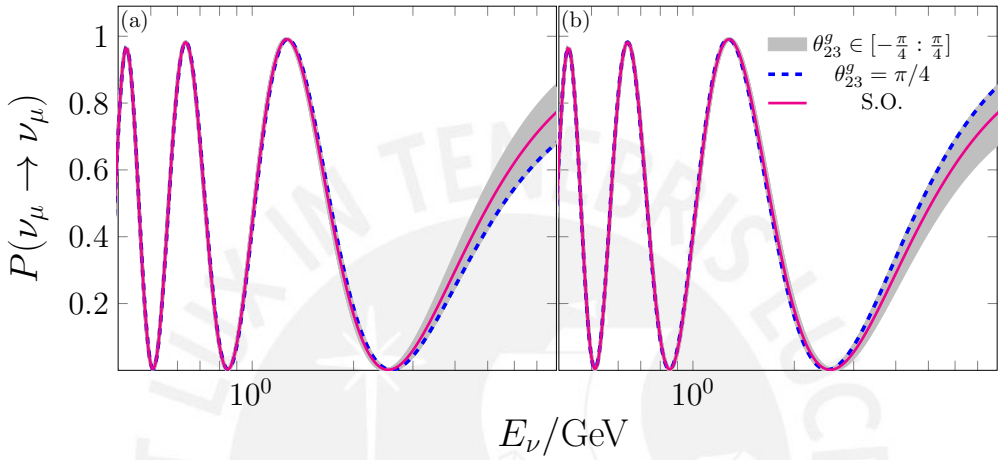

Figure 3.5: Oscillation probability depending on the neutrino energy and considering scenario B/texture θ_{23}. Figures (a) and (b) represent the subcases a and b, respectively. We consider $\Delta\gamma_{21} = 2\times10^{-24}$ for subcase a, $\Delta\gamma_{31} = 2\times10^{-24}$ for subcase b, $\delta_{CP} = -\pi/2$ and $L = 1300$ Km.

In Fig. 3.5, we observe the oscillation probabilities for the $\nu_\mu \to \nu_\mu$ channel, taking into account the scenario B and texture θ_{23}. From the latter, it is possible to observe noticeable discrepancies between VEP $\bigoplus$ SO and SO for the subcases a and b. The discrepancies due to the VEP effect are equivalent in magnitude for both subcases; however, for the subcase a, the VEP contribution is negative, while for b, the contribution is positive. Moreover, analogous to the previously analyzed textures (θ^g_{13} and θ^g_{12}), we reach the maximum VEP effect when the gravitational mixing angle is $\theta^g = \pm\pi/4$. Also, it is important to mention that the antineutrino counterpart has identical effects to those shown in Fig. 3.5.

3.4 Simulation and Results

For the DUNE simulation, we use the information from [52] taking into account the optimized fluxes with an exposure of 3.5 years for Forward Horn current (FHC) and Reverse Horn Current (RHC), neutrino and antineutrino mode, respectively. Additionally, we use the configuration of signal and background given by default by the DUNE collaboration [52, 53], as seen in Table 3.2.

Appearance mode	ν_e FHC	$\bar{\nu}_e$ RHC
Signal CC	$\nu_\mu \to \nu_e$	$\bar{\nu}_\mu \to \bar{\nu}_e$
Signal CC	$\bar{\nu}_\mu \to \bar{\nu}_e$	$\nu_\mu \to \nu_e$
Background CC	$\nu_e \to \nu_e$	$\bar{\nu}_e \to \bar{\nu}_e$
Background CC	$\bar{\nu}_e \to \bar{\nu}_e$	$\nu_e \to \nu_e$
Background CC	$\nu_\mu \to \nu_\mu$	$\bar{\nu}_\mu \to \bar{\nu}_\mu$
Background CC	$\bar{\nu}_\mu \to \bar{\nu}_\mu$	$\nu_\mu \to \nu_\mu$
Background CC	$\nu_\tau \to \nu_\tau$	$\bar{\nu}_\tau \to \bar{\nu}_\tau$
Background CC	$\bar{\nu}_\tau \to \bar{\nu}_\tau$	$\nu_\tau \to \nu_\tau$
Background NC	$\nu_\mu \to \nu_\alpha$	$\bar{\nu}_\mu \to \bar{\nu}_\alpha$
Background NC	$\bar{\nu}_\mu \to \bar{\nu}_\alpha$	$\nu_\mu \to \nu_\alpha$
Disappearance mode	**ν_μ FHC**	**$\bar{\nu}_\mu$ RHC**
Signal CC	$\nu_\mu \to \nu_\mu$	$\bar{\nu}_\mu \to \bar{\nu}_\mu$
Signal CC	$\bar{\nu}_\mu \to \bar{\nu}_\mu$	$\nu_\mu \to \nu_\mu$
Background CC	$\nu_\mu \to \nu_\tau$	$\bar{\nu}_\mu \to \bar{\nu}_\tau$
Background CC	$\bar{\nu}_\mu \to \bar{\nu}_\tau$	$\nu_\mu \to \nu_\mu$
Background NC	$\nu_\mu \to \nu_\alpha$	$\bar{\nu}_\mu \to \bar{\nu}_\alpha$
Background NC	$\bar{\nu}_\mu \to \bar{\nu}_\alpha$	$\nu_\mu \to \nu_\alpha$

Table 3.2: AEDL rules for DUNE experiment [52]

As mentioned above, in this chapter, we consider the values in Table 3.1 as the current best-fit values (CBFV). Because the probability distribution is not Gaussian, we estimate the uncertainty for the oscillation parameters by dividing their respective 3σ allowed region by six. We also assume $\delta_{CP} = -\pi/2$ because it is the closest value to the best fit. However, we do not consider priors due to the value of δ_{CP} is not well constrained. [171].

Additionally, we use the General Long Baseline Experiment Simula-

tor (GLoBES) package to simulate the DUNE experiment [155, 156]. On this basis, we consider the following definition for χ^2 [172]:

$$\chi^2(\zeta^{test}, \zeta^{true}) = \sum_i \frac{(N_i(\zeta^{test}) - N_i(\zeta^{true}))^2}{N_i(\zeta^{true})} \tag{3.55}$$

In case the priors are taken into account, the following expression is considered:

$$\chi^2 \to \chi^2 + \sum_j \frac{(\zeta_j^{test} - \zeta_j^{true})^2}{\sigma_j^2} \tag{3.56}$$

From the equations above, ζ^{true} defines the oscillation parameters that acquire their values according to Table 4.3. Also, ζ^{test} describes the parameters tested against the CBFV and assigned true VEP parameters. Finally, N_i represents the number of events in the ith bin, σ_j^2 is the error in the determination of ζ, and j is the number of oscillation parameters with nonzero errors.

Misinterpretation in the correlation of the SO parameters at DUNE.

In this section, we study the VEP effects on the correlation distortion of SO parameters. The distortion above is obtained considering the VEP effect in nature and fitting against the SO formula. Therefore, we simulate the data from DUNE per the ensuing parameters: $\Delta\gamma^{true} = 0$, 10^{-24}, or 2×10^{-24}, $\delta_{CP}^{true} = -\pi/2$ while the remaining true values for the SO parameters take the CBFV shown in Table 4.3. Then, taking $\Delta\gamma^{test} = 0$, we have marginalized over all SO parameters to locate the minimum χ^2, as shown below.

$$\chi^2(\theta_{13}^{test}, \delta_{CP}^{test}, \Delta\gamma_{ij}^{test} = 0, \theta_{13}^{true}, \delta_{CP}^{true}, \Delta\gamma_{ij}^{true}) \tag{3.57}$$

In order to analyze the $\Delta\chi^2$ contours in the $\sin^2\theta_{13}$ vs δ_{CP} plane, we use the following expression:

$$\begin{aligned}\Delta\chi^2 =& \chi^2(\theta_{13}^{test}, \delta_{CP}^{test}, \Delta\gamma_{ij}^{test} = 0, \theta_{13}^{true}, \delta_{CP}^{true}, \Delta\gamma_{ij}^{true}) \\ &- \chi^2_{min}(\theta_{13}^{fit}, \delta_{CP}^{fit}, \Delta\gamma_{ij}^{test} = 0, \theta_{13}^{true}, \delta_{CP}^{true}, \Delta\gamma_{ij}^{true})\end{aligned} \tag{3.58}$$

where the parameters that minimize the χ^2 are labeled θ_{13}^{fit} and δ_{CP}^{fit}. Same procedure as described in Eqs. (3.57) is used to obtain the contours in the plane Δm_{31}^2 vs δ_{CP}.

We can explain the discrepancies between the allowed regions obtained from data with non-null values for the VEP parameters and those with pure SO via the differences between the oscillation probabilities of VEP $\bigoplus$ SO and SO. The data fitting describes an exercise of shortening the discrepancies between the SO and the VEP $\bigoplus$ SO probabilities by increasing or reducing the value for the SO parameters.

Therefore, it is helpful to identify the approximated SO probabilities formulae employed in our work. First, the transition oscillation channel $\nu_\mu \to \nu_e$ given by:

$$P^{\rm SO}_{\nu_\mu \to \nu_e} \simeq C_1 s_{13}^2 + C_2 \cos\delta_{CP} r s_{13} - C_3 \sin\delta_{CP} r s_{13} + C_4 r^2 \tag{3.59}$$

where:

$$\begin{aligned} C_1 &= 4 f^2 s_{23}^2 \\ C_2 &= 8 f g \cos\Delta s_{12} c_{12} s_{23} c_{23} \\ C_3 &= 8 f g \sin\Delta s_{12} c_{12} s_{23} c_{23} \\ C_4 &= 4 g^2 s_{12}^2 c_{12}^2 c_{23}^2 \end{aligned} \tag{3.60}$$

All coefficients are positive for the most relevant part of the energy spectrum. Also, the coefficients f and g are taken from Eq. (3.17) without taking into account the VEP effects.

Secondly, another pertinent oscillation probability to consider is the survival channel, $\nu_\mu \to \nu_\mu$, which has the next expression:

$$P^{\rm SO}_{\nu_\mu \to \nu_\mu} \simeq 1 - 4\sin^2\Delta s_{23}^2 c_{23}^2 + 4\Delta \sin 2\Delta c_{12}^2 s_{23}^2 c_{23}^2 r \tag{3.61}$$

From the approximation presented in (3.61), we can notice that the term δ_{CP} does not appear. However, we can obtain terms proportional to $\cos\delta_{CP}$ if we consider higher orders. It is important to mention that we are not presenting the formula up to those higher-order terms since the size of the impact caused by the related terms is minimal.

Scenario A, Case 1

In Fig. 3.6 (a), we show the allowed regions for the Δm^2_{31} vs δ_{CP} correlation. For $\Delta\tilde{\gamma}_{31} > 0$, we observe a shift of the fitted value of Δm^2_{31} towards higher values compared with its corresponding CBFV. The shifting can be understood taking into account the distinct discrepancy between the VEP $\bigoplus$ SO and SO probabilities in the $\nu_\mu \to \nu_\mu$ channel, shown in Fig. 3.1. As we can observe there, to achieve a better pairing between these probabilities it is required to decrease the value of the SO probability for $\nu_\mu \to \nu_\mu$ channel, which can be obtained by increasing Δm^2_{31} (see Eq. (3.61)). Given the above explanation, when $\Delta\tilde{\gamma}_{31} < 0$, the behavior is exactly the opposite, which is observed in Fig. 3.6 (b). The plane $\sin^2\theta_{13}$ vs δ_{CP} is not shown since the variations between allowed regions are negligible. The behavior of the variations on the latter plane are correlated with the size of discrepancies between the VEP $\bigoplus$ SO and SO $\nu_\mu \to \nu_e$ probabilities, which are as a matter of fact small as shown in Fig. 3.1.

We have verified that if we choose, instead of VEP, any of the LV terms in the SME Hamiltonian (see Sec. 3.2), other than the one with d = 4 energy dependency, the behavior of the allowed regions follows a similar pattern. These similarities are present in scenarios A ($\mathbf{U} = \mathbf{U_g}$) and B ($\mathbf{U} \neq \mathbf{U_g}$), throughout all the cases.

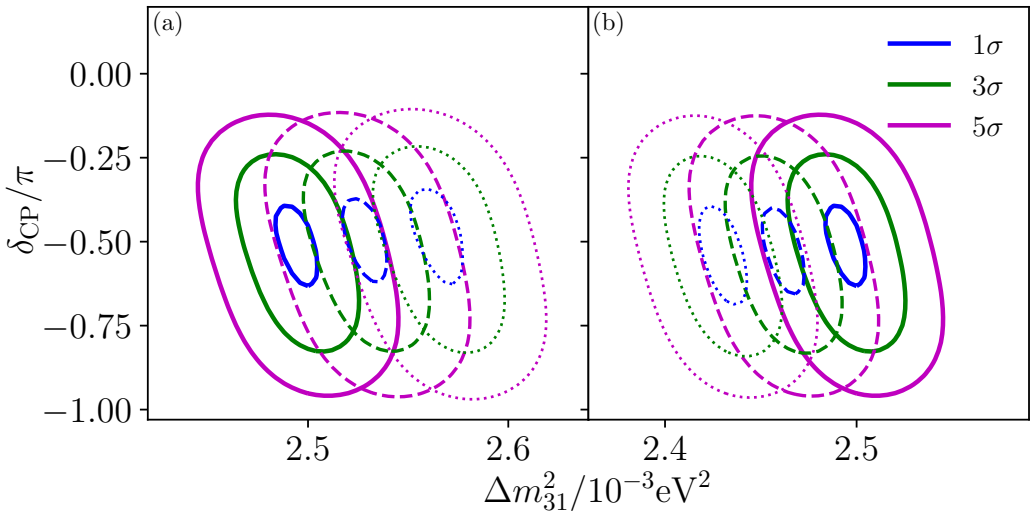

Figure 3.6: Scenario A/case 1. The solid lines are $\Delta\gamma_{31}^{true} = 0$ (SO) . Figure (a) represents VEP with $\Delta\gamma_{31}^{true} = 10^{-24}$ (dashed lines) and VEP with $\Delta\gamma_{31}^{true} = 2\times10^{-24}$ (dotted lines). While in Fig. (b) is shown VEP with $\Delta\gamma_{31}^{true} = -10^{-24}$ (dashed lines) and $\Delta\gamma_{31}^{true} = -2\times10^{-24}$ (dotted lines). We consider $\delta_{CP}^{true} = -\pi/2$.

Scenario A, Case 2

Contrary to the former case, in this one there are significant deviations between the allowed regions presented in the plane $\sin^2\theta_{13}$ vs δ_{CP}, as can be seen in Fig. 3.7. These changes, when $\Delta\gamma_{21} > 0$, are characterized by the shifting to higher values of $\sin^2\theta_{13}$ than the one of the SO best fit, as can be seen in Fig. 3.7 (a). This shifting is explained by the need to increase $\sin^2\theta_{13}$ in order to match the SO with the VEP $\bigoplus$ SO $\nu_\mu \to \nu_e$ probabilities, as it is shown in Fig. 3.2. This match can be attained by increasing the first term $C_1 s_{13}^2$, see Eq. (3.59). From Eq. (3.59), it is also clear that the need to decrease the SO antineutrino transition probability is satisfied through the flipped sign in term $C_3 \sin\delta_{CP} r s_{13}$. The shrinking of the allowed regions around the $\delta_{CP} \sim -\pi/2$, where its effect is maximal, happens because of the higher separation among the neutrino and antineutrino VEP $\bigoplus$ SO $\nu_\mu \to \nu_e$ probabilities than the corresponding for the SO neutrino antineutrino probability difference, evaluated

at the CBFV. Therefore, in order to mimic this separation for VEP $\bigoplus$ SO neutrino-antineutrino probabilities, the fitted SO probability needs to amplify the CP effects, which is accomplished by choosing a narrower set of values for the δ_{CP} interval around the maximal $\delta_{CP} \sim -\pi/2$. When $\Delta\gamma_{21} < 0$, there is a lower separation between the neutrino and antineutrino VEP $\bigoplus$ SO $\nu_\mu \to \nu_e$ probabilities and the corresponding for the SO neutrino antineutrino probability difference, at the CBFV. Then, and following the same reasoning for $\Delta\gamma_{21} > 0$, but seen in opposite way, we need to adjust the fitted SO probability in order to reduce the CP effects, diminishing (increasing) the neutrino (antineutrino) SO transition channel. This can be reached through the selection of δ_{CP} distant from where the maximal CP effect takes place, $\sim -\pi/2$, of the fitted SO probabilities, and, by opting for slightly smaller values of s_{13} that can help modulating the reduction (rise) of the neutrino (antineutrino) transition probability magnitude (see Eq. (3.59)). The aforementioned behavior is reflected in Fig. 3.7 (b). In the latter figure, we can observe a misconstrued δ_{CP}, which is a result of how the fitted SO probabilities try to emulate the VEP effect. Finally, there is no need to display the plane Δm^2_{31} vs δ_{CP} since the discrepancies in the survival probabilities, correlated with the results in this plane, are not relevant, as seen in Fig. 3.2.

Scenario B, Texture θ_{13}

From the probabilities point of view, see Fig. 3.3, this case can be seen as opposed to the preceding one. This means that for this case, $\Delta\gamma_{31} > 0$ ($\Delta\gamma_{31} < 0$) corresponds to $\Delta\gamma_{21} < 0$ ($\Delta\gamma_{21} > 0$) for scenario A/case 2. Therefore, the explanations for the former case could be applied to this one. On the other hand, as it can be noted in Fig. 3.3, the differences between the VEP $\bigoplus$ SO and SO $\nu_\mu \to \nu_\mu$ probabilities are almost null.

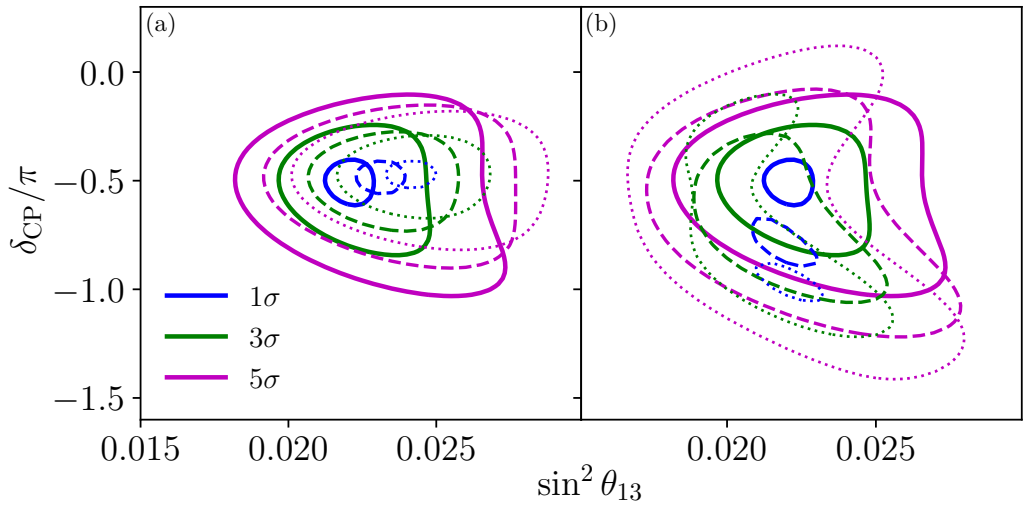

Figure 3.7: Scenario A/case 2. The solid lines are $\Delta\gamma_{21}^{true} = 0$ (SO) . Figure (a) represents VEP with $\Delta\gamma_{21}^{true} = 10^{-24}$ (dashed lines) and VEP with $\Delta\gamma_{21}^{true} = 2 \times 10^{-24}$ (dotted lines). While VEP with $\Delta\gamma_{21}^{true} = -10^{-24}$ (dashed lines) and $\Delta\gamma_{21}^{true} = -2 \times 10^{-24}$ (dotted lines) is shown in Fig. (b). We consider $\delta_{CP}^{true} = -\pi/2$.

Scenario B, Texture θ_{12}

This case is equivalent to scenario A/case 2. This equivalency is rooted in the similar conduct observed in the transition probabilities, shown in Fig. 3.4 and Fig. 3.2. Hence, the arguments used for explaining the allowed regions behavior for scenario A/case 2 are totally suitable to be applied to this case.

Scenario B, Texture θ_{23}

As pointed out in Secs. 3.3 and 3.3 only in the $\nu_\mu \to \nu_\mu$ channel the discrepancies between the VEP $\bigoplus$ SO and the SO are observable (evaluated at the CBFV). Therefore, the plane Δm^2_{31} vs δ_{CP} is the appropriate parameter space region, where the impact of these differences can be revealed. Scenario B/texture θ_{23}-a, $\Delta\gamma_{21} = 0$ and $\Delta\gamma_{31} \neq 0$, exhibits a quite similar behavior to that shown in Fig. 3.6 for scenario A/case 1. Scenario B/texture θ_{23}-b, $\Delta\gamma_{31} = 0, \Delta\gamma_{21} > 0$ ($\Delta\gamma_{21} < 0$) corresponds to $\Delta\gamma_{31} < 0$ ($\Delta\gamma_{31} > 0$) for

scenario A/case 1. Both tendencies in Fig. 3.6 (a) and (b) are in agreement to what is expected from the probabilities displayed in Fig. 3.5. For texture θ_{23}-a (θ_{23}-b), the fitted SO probability has to lessen (augment) its value to match with the VEP $\bigoplus$ SO, which means to increase (decrease) Δm^2_{31}, as can be checked in Eq. (3.61).

VEP sensitivity limits

We analyze the sensitivity of DUNE to VEP parameters generating a pure standard oscillation simulated data, fixing the following true values: $\Delta\gamma^{true} = 0$, and a given value of δ^{true}_{CP}, marginalizing over the remaining standard oscillation parameters.

$$\chi^2 = \chi^2\left(\Delta\gamma^{test}, \delta^{true}_{CP}, \Delta\gamma^{true} = 0\right) \tag{3.62}$$

The $\Delta\gamma^{test}$ is the test parameter paying attention that $\Delta\gamma^{true}(\Delta\gamma^{test})$ either would take the value of $\Delta\gamma^{true}_{31}(\Delta\gamma^{test}_{31})$ or $\Delta\gamma^{true}_{21}(\Delta\gamma^{test}_{21})$ depending on the case to be studied.

Scenario A

In Fig. 3.8 it is displayed the sensitivity to the VEP parameter for the different cases of scenario A. For case 1, the sensitivity to $\Delta\gamma_{31}$ is given by $[0.4, 1.1, 1.8] \times 10^{-24}$ and $-[0.4, 1.4, 2.4] \times 10^{-24}$ at the 1σ, 3σ, and 5σ levels, respectively. In this plot we can see that the sensitivity to $\Delta\gamma_{31}$ is almost constant irregardless the value of δ_{CP}. The latter can be inferred from the probabilities given in Eqs.(3.38) and (3.40), where δ_{CP} is not appearing, unless up to the perturbation order that we present in these formulas. When we consider negative values of $\Delta\gamma_{31}$, the formula predicts the same correction, which implies a same constant behavior, and rather similar values for the sensitivity, as the positive case. This can be seen in Fig. 3.8.

In this figure a plot for case 2 is shown, as well. For this case, the sensitivity to $\Delta\gamma_{21}$ for its positive values is $[0.3 \text{ - } 0.4, 1.1 \text{ - } 1.4, 1.8 \text{ - } 2.4] \times 10^{-24}$

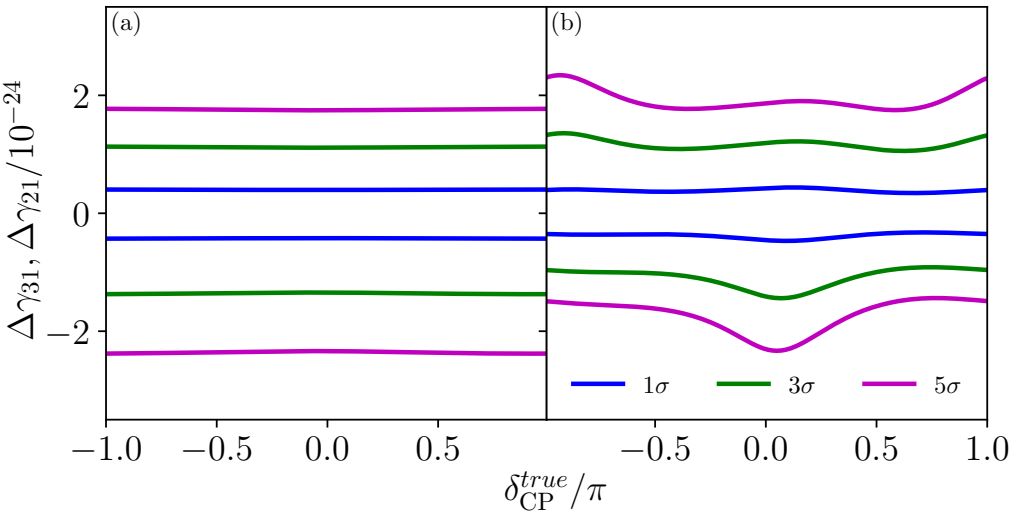

Figure 3.8: Sensitivity to VEP considering scenario A/case 1 (a) and case 2 (b), depending on δ_{CP}^{true}.

and for its negative values is $-\,[0.3$ - $0.5, 0.9$ - $1.4, 1.4$ - $2.3] \times 10^{-24}$ at the 1σ, 3σ, and 5σ levels. As it can be seen from Fig. 3.2, the highest discrepancies between VEP $\bigoplus$ SO and pure SO are present in the $\nu_\mu \to \nu_e$ transition channel. Consequently, it should be expected that the shape of the curve of the sensitivity is affected, at some degree, by the transition channel. Therefore, for getting a qualitative understanding of this shape we use the analytical expression of the $\nu_\mu \to \nu_e$ transition channel. In particular, the two lowest order perturbative (most relevant) terms in Eq. (3.41) can be grouped into a single term proportional to $\cos(\Delta + \delta_{CP})$. Fixing the neutrino energy at 2.5 GeV (the mean energy at DUNE), for which Δ is close to 0.5π, it is possible to have a rough idea about the location of the maximum and minimum sensitivities. Then, if Δ is close to 0.5π, it is expected that the maximum sensitivity points are located in values of δ_{CP} in the vicinity of -0.5π and 0.5π. This is what we observe for positive values of $\Delta\gamma_{21}$. Before we continue, it is convenient to point out that maximum sensitivity points correspond to the highest deflections of the VEP $\bigoplus$ SO -probability respect the SO one.

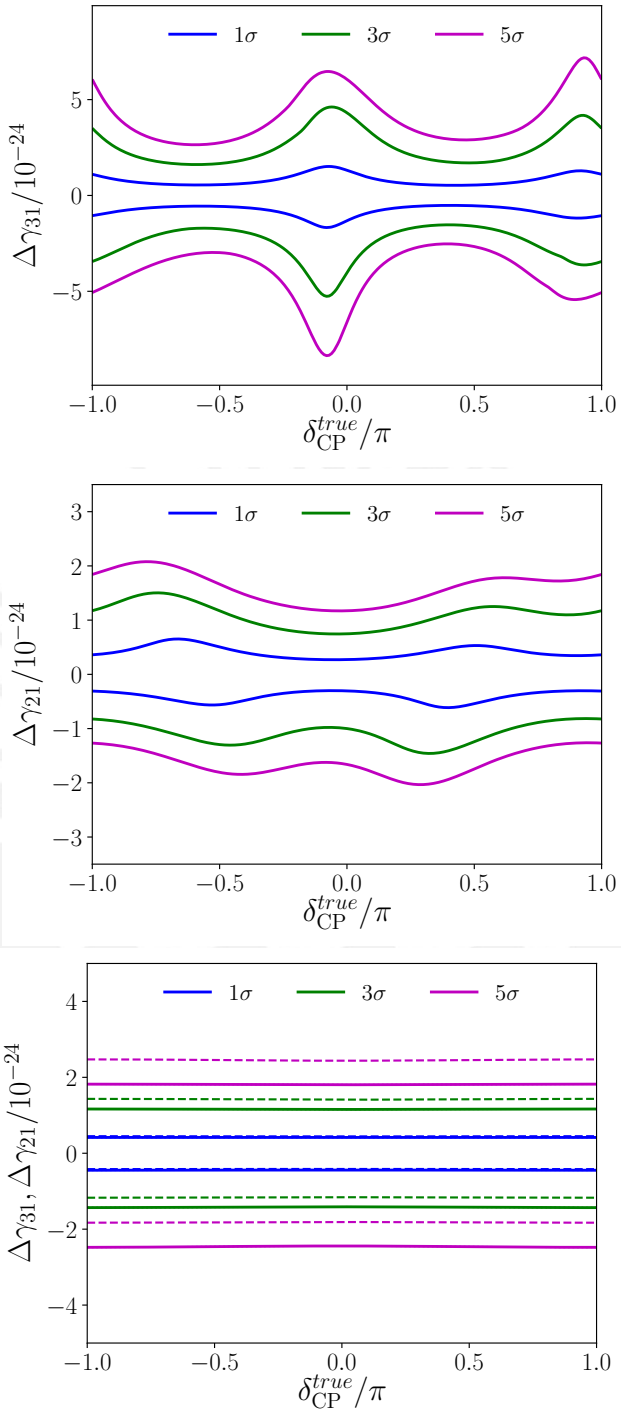

Figure 3.9: Sensitivity to VEP considering scenario B/textures θ_{13} (left), θ_{12} (center) and θ_{23} (right) depending on δ_{CP}^{true}. In the plot on the right, the solid and dashed lines represent the subcases a and b respectively. We consider θ_{12}^g, θ_{23}^g and θ_{13}^g equal to $\pi/4$.

On the other hand, minimum sensitivity is obtained for values of δ_{CP} at the vicinity of 0, π and $-\pi$. For negative values of $\Delta\gamma_{21}$, the minimum sensitivity for $\delta_{CP} \sim 0$ remains. However, the other minima and maxima vanish because of the influence of higher-order terms.

It should be stressed that the VEP phenomenom, in the framework of scenario A, was tested with IceCube-high energy atmospheric neutrinos obtaining the following upper limits: $|\Delta\gamma_{21}| \sim 9.1 \times 10^{-27}$ and $|\Delta\gamma_{31}| \sim 6 \times 10^{-27}$ at 90% C.L. [37]. Our limits within the DUNE framework and in the same confidence level are $|\Delta\gamma_{21}| \sim 5.2 \times 10^{-25}$ and $|\Delta\gamma_{31}| \sim 6.4 \times 10^{-25}$, which should be the best limits that could be attained by a man-made neutrino source.

Scenario B: $U_g \neq U$

In the same way, Fig. 3.9 shows the sensitivity to the new parameters for textures θ_{13}, θ_{12} and θ_{23} of scenario B. First we focus on texture θ_{13} and texture θ_{12}. For texture θ_{13}, the sensitivity to $\Delta\gamma_{31}$ is given by $[0.5 \text{ - } 1.5, 1.6 \text{ - } 4.6, 2.6 \text{ - } 7.2] \times 10^{-24}$ for the positive values and $-[0.5 \text{ - } 1.7, 1.5 \text{ - } 5.3, 2.5 \text{ - } 8.4] \times 10^{-24}$ for the negative ones at the 1σ, 3σ, and 5σ levels respectively. For texture θ_{12} of the same scenario, the sensitivity to $\Delta\gamma_{21}$ is given by $[0.3 \text{ - } 0.7, 0.7 \text{ - } 1.5, 1.2 \text{ - } 2.1] \times 10^{-24}$ and $-[0.3 \text{ - } 0.6, 0.8 \text{ - } 1.5, 1.3 \text{ - } 2] \times 10^{-24}$ at the 1σ, 3σ, and 5σ levels respectively.

The sensitivity behavior for theses textures, θ_{13} and θ_{12}, is almost absolutely dominated by the $\nu_\mu \to \nu_e$ transition channel, given that only in this channel there are (observable) discrepancies between VEP $\bigoplus$ SO and pure SO (see Figs. 3.3 and 3.4). In particular, it is possible to get an idea of the approximated position of the maximum and minimum sensitivity points analyzing the first two terms in the transition probabilities for both textures. These two terms are proportional to $C_1 \cos\delta_{CP} \pm C_2 \sin\delta_{CP}$. Then, when $C_1 < C_2 (C_1 > C_2)$ the maximum (minimum) sensitivity in δ_{CP} is located in the

neighborhood of 0.5π and -0.5π (0, π, and $-\pi$) for texture θ_{13} (textures θ_{12}). In the minimum (maximum) sensitivity point is where the lowest (highest) discrepancies between VEP $\bigoplus$ SO and pure SO are found. For both signs of $\Delta\gamma$ the behavior is similar, unless, of course, some shifts due to the influence of the other terms.

Fig. 3.9 presents the sensitivity to $\Delta\gamma_{31}$ and $\Delta\gamma_{21}$ in the context of scenario B, texture θ_{23} and subcases *a* and *b* respectively. Thus, the sensitivity to $\Delta\gamma_{31}$ ($\Delta\gamma_{21}$) is given by $[0.4, 1.2, 1.8] \times 10^{-24}$ and $-[0.4, 1.4, 2.5] \times 10^{-24}$ ($[0.4, 1.4, 2.5] \times 10^{-24}$ and $-[0.4, 1.2, 1.8] \times 10^{-24}$) at the 1σ, 3σ, and 5σ levels respectively. It is important to note that in both subcases the dependence on δ_{CP} is negligible, since, there are only deviations from SO in the $\nu_\mu \to \nu_\mu$ survival channel. For subcases *a* and *b*, there are no VEP-related terms in the transition probability $\nu_\mu \to \nu_e$ up to the level of the developed perturbation order. On the other hand, it is good to mention that there is a symmetric behavior for both signs of $\Delta\gamma_{ij}$.

Lorentz violation estimated sensitivities

As we have pointed out, we reapplied our VEP prescription to test the different isotropic Lorentz violating terms of the SME Hamiltonian with their respective energy dependencies, as discussed in Sec. 3.2. Here we have set up different sensitivities imposed on each of the terms mentioned above in the context of DUNE, working with them in an individual manner. Since this is an indirect result of this manuscript, we only present them in Table 3.3. Other similar works can be found in [173, 174].

Scenario $-\ \Delta\gamma$	$\times 10^{-23}$GeV $(d=3)$		$\times 10^{-24}$ $(d=4)$		$\times 10^{-25}$GeV^{-1} $(d=5)$		$\times 10^{-26}$GeV^{-2} $(d=6)$	
A/1 $-\ \Delta\gamma_{31}$	1.4	-1.3	2.2	-2.7	1.6	-3.3	0.9	-2.3
A/2 $-\ \Delta\gamma_{21}$	$[0.7-1.3]$	-$[0.7-1.3]$	$[2.1-2.7]$	-$[1.8-2.9]$	$[2.1-3.0]$	-$[1.4-2.3]$	$[1.3-1.8]$	-$[0.8-1.3]$
B/θ_{13} $-\ \Delta\gamma_{31}$	$[1.0-2.8]$	-$[0.9-3.0]$	$[3.2-9.2]$	-$[3.1-10.5]$	$[6.7-10.9]$	-$[6.5-9.9]$	$[5.1-7.3]$	-$[5.1-6.8]$
B/θ_{12} $-\ \Delta\gamma_{21}$	$[0.9-1.2]$	-$[0.8-1.2]$	$[1.5-3.0]$	-$[1.6-2.9]$	$[1.2-2.2]$	-$[1.3-2.2]$	$[0.7-1.2]$	-$[0.8-1.3]$
B/θ_{23}-a $-\ \Delta\gamma_{31}$	1.4	-1.4	2.3	-2.8	1.7	-3.3	1.0	-2.2
B/θ_{23}-b $-\ \Delta\gamma_{21}$	1.4	-1.4	2.8	-2.3	3.3	-1.7	2.3	-1.0

Table 3.3: Estimated sensitivities for Lorentz violation at 3σ level considering $\Delta\gamma > 0$ and $\Delta\gamma < 0$. For the scenario B, θ^g_{12}, θ^g_{23} and θ^g_{13} are considered equal to $\pi/4$.

Table 3.3 presents the sensitivity of DUNE experiment to LV. It can be seen that scenario B/texture θ_{12} shows the greatest constraint to the parameter $\Delta\gamma_{21}$ for almost all d. In the meantime, scenario B/texture θ_{13} presents precisely the opposite for constraining $\Delta\gamma_{31}$. This is exactly the same pattern found for VEP, whence the explanation is the same. Therefore, scenario B/texture θ_{13} is sensitive to higher $\Delta\gamma_{31}$ values, while scenario B/texture θ_{12} is sensitive to lower $\Delta\gamma_{21}$ values.

Table 3.4 shows the comparison between the previous estimations with those calculated in this work. These sensitivities can be also extracted from [175]. Scenario B has been considered because of the similarity with the textures used for Lorentz violation. We have translated our sensitivities in terms of $a_{e\mu}$, $a_{e\tau}$, and $a_{\mu\tau}$, where we have used the textures θ_{12}, θ_{13}, and θ_{23}, respectively. For $c_{\alpha\beta}$ we have proceed in the same way. The gravitational angle, θ^g , is considered equal to $\pi/4$ for all the textures. When $d = 3$, the estimations determined in this work are lower than the previous ones for $a_{e\mu}$ and $a_{e\tau}$ shown in [59, 174, 176, 177]. However, for $a_{\mu\tau}$, our bounds are lower than the preceding ones excluding the result in [170], which is lower than ours. For $d = 4$, lower values are obtained with the exception of those in [170] and [176], while for $d = 5$ and $d = 6$ we only have previous calculations established by [170]. which is much lower than the ones we have obtained. It is very important to note that in order to obtain our estimations we have treated separately each energy dependent term in the Hamiltonian, in contrast, for instance, with the procedure adopted in [170].

The sensitivity of DUNE to CP violation and mass hierarchy

CP violation sensitivity

This section discusses the effect of VEP on *CP* violation sensitivity at DUNE experiment. To refer to DUNE sensitivity to *CP* violation, the definition shown in [53, 172] are taken into account.

d		Previous Estimation	This work
3	$\lvert a_{e\mu}\rvert$	7.0×10^{-24}GeV [174]	2.8×10^{-24}GeV *
		2.5×10^{-23}GeV [176]	4.0×10^{-24}GeV †
		4.2×10^{-21}GeV [177]	
	$\lvert a_{e\tau}\rvert$	1.0×10^{-23}GeV [174]	3.0×10^{-24}GeV *
		5.0×10^{-23}GeV [176]	4.5×10^{-24}GeV †
		2.8×10^{-21}GeV [177]	
	$\lvert a_{\mu\tau}\rvert$	2.9×10^{-24}GeV [170]	4.5×10^{-24}GeV *
		1.7×10^{-23}GeV [174]	7.0×10^{-24}GeV †
		8.3×10^{-24}GeV [176]	
		5.9×10^{-23}GeV [59]	
		5.1×10^{-21}GeV [177]	
4	$\lvert c_{e\mu}\rvert$	1.1×10^{-26} [176]	3.8×10^{-25} *
		3.7×10^{-19} [177]	5.6×10^{-25} †
	$\lvert c_{e\tau}\rvert$	1.4×10^{-24} [176]	7.5×10^{-25} *
		2.5×10^{-19} [177]	1.2×10^{-24} †
	$\lvert c_{\mu\tau}\rvert$	3.9×10^{-28} [170]	6.0×10^{-25} *
		6.1×10^{-27} [176]	9.0×10^{-25} †
		5.0×10^{-24} [59]	
		4.5×10^{-19} [177]	
5	$\lvert a_{e\mu}\rvert$	–	4.5×10^{-26}GeV^{-1} *
		–	6.0×10^{-26}GeV^{-1} †
	$\lvert a_{e\tau}\rvert$	–	2.4×10^{-25}GeV^{-1} *
		–	3.3×10^{-25}GeV^{-1} †
	$\lvert a_{\mu\tau}\rvert$	2.3×10^{-32}GeV^{-1} [170]	6.0×10^{-26}GeV^{-1} *
			9.0×10^{-26}GeV^{-1} †
6	$\lvert c_{e\mu}\rvert$	–	2.0×10^{-27}GeV^{-2} *
		–	2.6×10^{-27}GeV^{-2} †
	$\lvert c_{e\tau}\rvert$	–	1.4×10^{-26}GeV^{-2} *
		–	2.0×10^{-26}GeV^{-2} †
	$\lvert c_{\mu\tau}\rvert$	1.5×10^{-36}GeV^{-2} [170]	2.6×10^{-27}GeV^{-2} *
			3.8×10^{-27}GeV^{-2} †

Table 3.4: Comparison between the existing bounds and the estimated sensitivities calculated in this work. Estimations marked * and † represent 95.5% and 99.7% C.L. respectively.

$$\begin{aligned}\Delta\chi^2_{CP} =& \text{Min}[\Delta\chi^2(\delta^{test}=0,\Delta\gamma^{test}=0,\delta^{true},\Delta\gamma^{true}),\\ &\Delta\chi^2(\delta^{test}=\pi,\Delta\gamma^{test}=0,\delta^{true},\Delta\gamma^{true})]\end{aligned} \tag{3.63}$$

To calculate $\Delta\chi^2_{CP}$, δ_{CP} and $\Delta\gamma$ are set as fixed while we marginalize over the rest of the parameters. The CP violation sensitivity is studied by fitting the data as SO and considering VEP as an unknown but existing effect. In most cases it is observed an increase in the significance level to reject the null hypothesis depending on δ^{true}_{CP}. However, some cases show a decrease of this significance level for certain values of δ^{true}_{CP}, all with respect to SO. This way of analysis is very important to study the consequences of omitting an existing VEP scenario in nature in our theoretical framework.

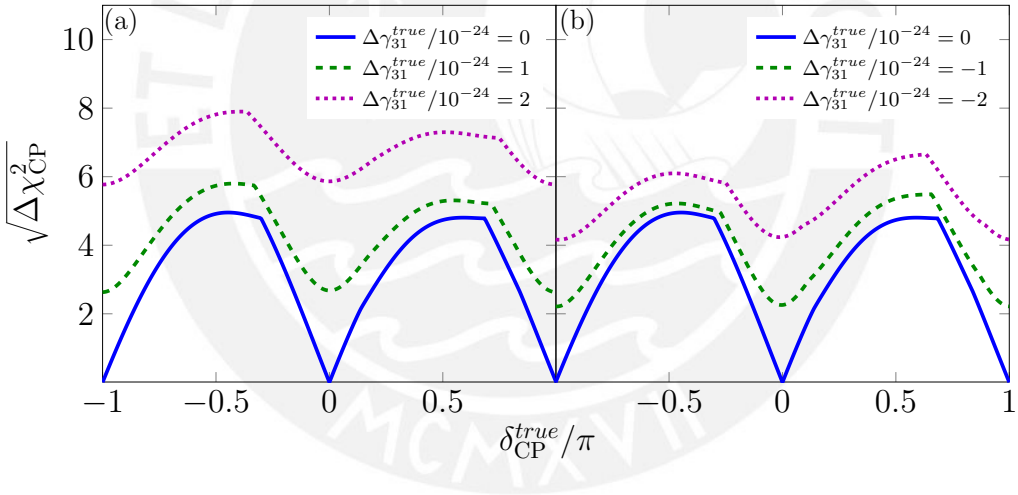

Figure 3.10: CP violation sensitivity for scenario A/case 1.

In Fig. 3.10, scenario A/case 1, an increase in the significance level to reject the null hypothesis can be observed even when $\delta^{true}_{CP}=0,\pm\pi$, generating a fake CPV. This is because there is a relatively constant increment on sensitivity and is a reflection of the δ_{CP}-independent discrepancy between the VEP $\bigoplus$ SO and SO in the ν_μ (and $\bar{\nu}_\mu$) disappearance probabilities for scenario A/case 1 (see Eq. (3.40). The increase of the number of events for the $\Delta\gamma<0$

reduces the $\sqrt{\Delta\chi^2}$ making it harder to achieve similar values of sensitivity to those obtained for the $\Delta\gamma > 0$ case. These results are qualitatively similar to those shown in scenario B/texture θ_{23}-a. Additionally, scenario B/texture θ_{23}-b $\Delta\gamma_{21} > 0$ ($\Delta\gamma_{21} < 0$) corresponds to $\Delta\gamma_{31} < 0$ ($\Delta\gamma_{31} > 0$) for scenario A/case 1.

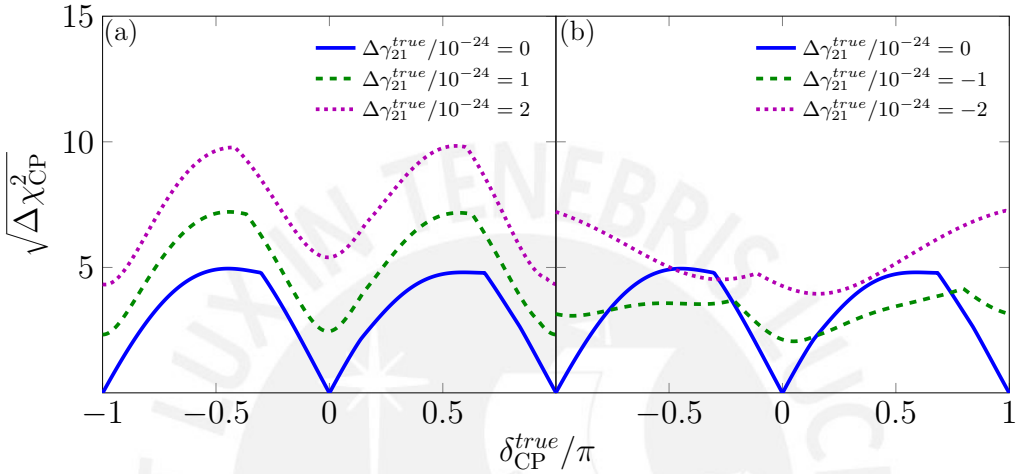

Figure 3.11: *CP* Violation sensitivity for scenario A/case 2.

In Fig. 3.11 (a), scenario A/case 2, the displayed results are due to the increased asymmetry between the $\nu_\mu \to \nu_e$ and $\bar{\nu}_\mu \to \bar{\nu}_e$ appearance channels amplifying the discrimination of the *CP* violation case, see Fig. 3.2. This also includes an extra fake CPV caused by the connection between the VEP term and the matter potential. Notwithstanding, as a consequence of the opposite behavior (decrease) of the asymmetry between the $\nu_\mu \to \nu_e$ and $\bar{\nu}_\mu \to \bar{\nu}_e$ appearance channels, when $\Delta\gamma_{21} < 0$, it is observed a decrease in the level of significance, that could be even lower to the SO case in the neighborhood of $\delta_{CP}^{true} = \pm\pi/2$, where this case reaches its peak of sensitivity. This means that the capacity to reject the null *CP*-hypothesis when δ_{CP}^{true} takes values close to its maximum would be reduced. As already stated, the results for scenario A/case 2 are qualitatively similar to those shown in scenario B/texture θ_{12}. Moreover, scenario B/texture θ_{13} $\Delta\gamma_{31} > 0$ ($\Delta\gamma_{31} < 0$) corresponds to

$\Delta\gamma_{21} < 0$ ($\Delta\gamma_{21} > 0$) for scenario A/case 2. Therefore, we could apply Fig. 3.11 and explanations for scenario A/case 2 to these ones.

Mass hierarchy sensitivity

One of the main goals of DUNE experiment is to figure out the mass hierarchy (MH). This is related to the fact that one of the main features of DUNE experiment is its baseline (1300 Km), resulting in a high sensitivity to the matter effect. This means that a considerable difference in the oscillation channels $\nu_\mu \to \nu_e$ and $\bar{\nu}_\mu \to \bar{\nu}_e$ is expected as a result, on which MH depends. Therefore, studying the sensitivity to MH is extremely important, since we have shown VEP scenarios where the asymmetry of these channels is clearly affected. The MH sensitivity is obtained as follows [53, 172].

$$\Delta\chi^2_{\rm MH} = \chi^2(\Delta m^{2\ test}_{31} < 0, \Delta\gamma^{test} = 0, \Delta m^{2\ true}_{31} > 0, \delta^{true}_{CP}, \Delta\gamma^{true}) \qquad (3.64)$$

Taking into account the analysis explained in the previous section we study the impact on the MH sensitivity considering VEP/NH in nature and assuming SO/IH as theoretical hypothesis. We do not display the scenarios with low discrepancies on $\nu_\mu \to \nu_e$, which are scenario A/case 1 and scenario B/texture θ_{23}-a and texture θ_{23}-b since those scenarios have MH sensitivities rather similar to SO MH.

In Fig. 3.12 the MH sensitivities for scenario A/case 2 are presented. In order to explain the behavior of these sensitivity curves we define two probability differences: $\Delta P^{\rm SO} = P^{\rm SO(NH)}_{\nu_\mu\to\nu_e} - P^{\rm SO(IH)}_{\nu_\mu\to\nu_e}$ and $\Delta P^{\rm VEP} = P^{\rm VEP\bigoplus SO(NH)}_{\nu_\mu\to\nu_e} - P^{\rm SO(IH)}_{\nu_\mu\to\nu_e}$ with $\Delta^{\text{VEP-SO(NH)}} = \Delta P^{\rm VEP} - \Delta P^{\rm SO}$. The $\Delta P^{\rm VEP}$ is associated with the VEP sensitivity while $\Delta P^{\rm SO}$ is related to the SO one. For this scenario the most important VEP-terms of $s_{13}\Delta\tilde{\gamma}_{21} \sim \mathcal{O}(0.01)$ of the transition probability (see Eq. (3.41)) can be written into a single term proportional to $fg\Delta\tilde{\gamma}_{21}$, considering $\Delta \sim \pi/2$. For $\Delta\gamma_{21} > 0$, $\Delta^{\text{VEP-SO(NH)}} \propto fg\Delta\tilde{\gamma}_{21}$ at

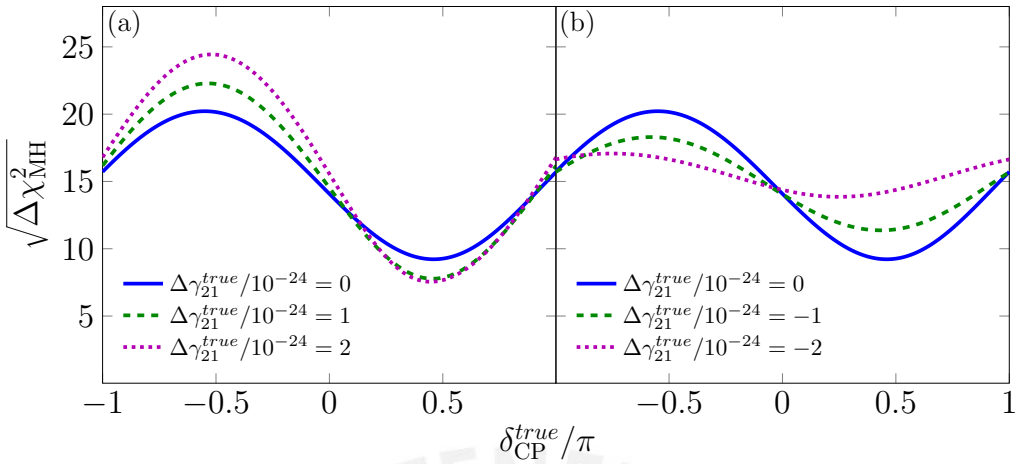

Figure 3.12: Mass hierarchy sensitivity for scenario A/case 2.

$\delta_{CP}^{true} = -\pi/2$, therefore the VEP sensitivity reaches a higher significance than the SO one. While, at $\delta_{CP}^{true} = \pi/2$, $\Delta^{\text{VEP-SO(NH)}} \propto -fg\Delta\tilde{\gamma}_{21}$, which means that the VEP sensitivity attains lower significance than the SO one. For $\Delta\gamma_{21} < 0$, what happens is exactly the opposite. These results are applicable for scenario B/texture θ_{13} and texture θ_{12}, as well.

3.5 Summary and Conclusions

We have tested the impact of fitting simulated data generated for different VEP scenarios, and considering pure standard oscillation as theoretical hypothesis. Among our findings, we have found the displacement of the Δm^2_{31}, the increase of $\sin^2\theta_{13}$ ($\Delta\gamma > 0$) or the change of $\delta_{\rm CP}$ ($\Delta\gamma > 0$) toward the decrease of the magnitude of CP violation, which are scenario-dependent effects. Furthermore, the DUNE CP sensitivity, treating VEP as before, increases for the majority of scenarios having all in common the introduction of a fake CP violation. The DUNE significance for identifying the MH for $\Delta\gamma > 0$ ($\Delta\gamma < 0$) increases (decreases) and decreases (increases) for $\delta_{\rm CP} \in [-\pi, 0]$ and $\delta_{\rm CP} \in [0, \pi]$. In addition, we have also found sensitivities for VEP, for the variety of scenarios under study, being the most stringent $\Delta\gamma \sim 0.7 \times 10^{-24}$ GeV which corresponds to the scenario B/texture θ_{12}. Finally, we have estimated

sensitivity limits for LV terms of the SME Hamiltonian, with different energy dependencies. The most restrictive one corresponds to the scenario B/texture θ_{12}, as well, and is $\Delta\gamma = \{8, 1.5, 0.12, 0.007\} \times 10^{-24}$ GeV^{4-d} that corresponds to $d = 3, 4, 5, 6$, respectively at 99.7% C.L. These limits are going to be the best that we can achieve using a manmade neutrino source.

CHAPTER 4

QUANTUM DECOHERENCE

4.1 Neutrino as an open quantum system

We aim to treat the neutrino as a subsystem that weakly interacts with a large and unknown environment. Therefore, we obtain the linear evolution of the neutrino subsystem mentioned above using the Lindblad Master equation [60, 61].

$$\frac{\partial \rho(t)}{\partial t} = -i[H, \rho(t)] + \mathcal{D}[\rho(t)], \tag{4.1}$$

where $\rho(t)$ is the reduced (neutrino) density matrix, obtained after trace over the degrees of freedom of the environment, H is the Hamiltonian of the neutrino subsystem and $\mathcal{D}[\rho(t)]$ is the dissipative term where the decoherence phenomena is encoded. This dissipative factor is written as follows:

$$\mathcal{D}[\rho(t)] = \frac{1}{2}\sum_j \left([A_j, \rho(t) A_j^\dagger] + [A_j \rho(t), A_j^\dagger] \right). \tag{4.2}$$

Considering a three-level system we can expand the operators in Eq. (4.1) in the basis of the Gell-Mann matrices from $SU(3)$ group plus the identity

matrix:

$$\rho = \sum \rho_\mu t_\mu \tag{4.3}$$

$$H = \sum h_\mu t_\mu \tag{4.4}$$

$$A_j = \sum a_\mu^j t_\mu \tag{4.5}$$

where μ is running from 0 to 8, being t_0 the identity matrix and t_k the Gell-Mann matrices ($k = 1, ..., 8$), which satisfy the follows:

$$[t_a, t_b] = i \sum_c f_{abc} t_c \tag{4.6}$$

where f_{abc} are the structure constants of $SU(3)$. Moreover, for the dissipative term to satisfy that the Von Neumann entropy increases with time, the $\hat{A}_j$ operators must be Hermitian. Therefore, the dissipative term can be expressed as the matrix [70]:

$$D_{kj} = \frac{1}{2} \sum_{l,m,n} (a_{nl}) f_{knm} f_{mlj}, \quad a_{nl} = \vec{a}_n . \vec{a}_l, \tag{4.7}$$

The dissipative matrix defined by Eq. (4.7) can be parameterized, in general, by 36 free parameters in the following form:

$$\mathbf{D} = \begin{pmatrix} -\gamma_1 & \beta_{12} & \beta_{13} & \beta_{14} & \beta_{15} & \beta_{16} & \beta_{17} & \beta_{18} \\ \beta_{12} & -\gamma_2 & \beta_{23} & \beta_{24} & \beta_{25} & \beta_{26} & \beta_{27} & \beta_{28} \\ \beta_{13} & \beta_{23} & -\gamma_3 & \beta_{34} & \beta_{35} & \beta_{36} & \beta_{37} & \beta_{38} \\ \beta_{14} & \beta_{24} & \beta_{34} & -\gamma_4 & \beta_{45} & \beta_{46} & \beta_{47} & \beta_{48} \\ \beta_{15} & \beta_{25} & \beta_{35} & \beta_{45} & -\gamma_5 & \beta_{56} & \beta_{57} & \beta_{58} \\ \beta_{16} & \beta_{26} & \beta_{36} & \beta_{46} & \beta_{56} & -\gamma_6 & \beta_{67} & \beta_{68} \\ \beta_{17} & \beta_{27} & \beta_{37} & \beta_{47} & \beta_{57} & \beta_{67} & -\gamma_7 & \beta_{78} \\ \beta_{18} & \beta_{28} & \beta_{38} & \beta_{48} & \beta_{58} & \beta_{68} & \beta_{78} & -\gamma_8 \end{pmatrix}. \tag{4.8}$$

being the matrix $\mathbf{D} \equiv D_{kj}$ symmetric, with components $D_{\mu 0} = D_{0\mu} = 0$, and $\vec{a}_r = \{a_r^1, a_r^2, ..., a_r^8\}$. The complete positivity condition requires that the eigenvalues of the mixing matrix $\rho(t)$ should be positive at any time, this is achieved demanding that the matrix $\mathbf{A} \equiv a_{nl}$ is positive [60, 61]. The scalar

product structure present in the elements D_{kj} makes them to respect the Cauchy-Schwartz inequalities. Including conservation of the probability to all that we have said, we have that the evolution equation of $\rho(t)$ is given by:

$$\dot{\rho}_0 = 0, \quad \dot{\rho}_k = (H_{kj} + D_{kj})\rho_j = M_{kj}\rho_j, \tag{4.9}$$

where $H_{kj} = \sum_i h_i f_{ijk}$. The solution of the Eq. (4.9) written in matricial form is:

$$\varrho(t) = e^{\mathbf{M}t}\varrho(0), \tag{4.10}$$

where ϱ is an eight column vector compose by the ρ_k and $\mathbf{M} \equiv M_{kj}$. Therefore, we can obtain a general expression for the neutrino oscillation probability $\nu_\alpha \to \nu_\beta$:

$$P_{\nu_\alpha \to \nu_\beta} = \frac{1}{3} + \frac{1}{2}(\varrho^\beta)^T \varrho^\alpha(t) \tag{4.11}$$

Written in terms of the coefficients $\rho_j^\alpha(0)$, we have:

$$P_{\nu_\alpha \to \nu_\beta} = \frac{1}{3} + \frac{1}{2}\sum_{i,j} \rho_i^\beta \rho_j^\alpha [e^{\mathbf{M}t}]_{ij}. \tag{4.12}$$

where $\beta, \alpha = e, \mu, \tau$ and $i, j = 1, ..., 8$. For the vacuum case, the ρ_i^α are given by:

$$\begin{aligned}
\rho_0^\alpha &= \sqrt{2/3}, \\
\rho_1^\alpha &= 2\,\mathrm{Re}\left(U_{\alpha 1}^* U_{\alpha 2}\right), \\
\rho_2^\alpha &= -2\,\mathrm{Im}\left(U_{\alpha 1}^* U_{\alpha 2}\right), \\
\rho_3^\alpha &= |U_{\alpha 1}|^2 - |U_{\alpha 2}|^2, \\
\rho_4^\alpha &= 2\,\mathrm{Re}\left(U_{\alpha 1}^* U_{\alpha 3}\right), \\
\rho_5^\alpha &= -2\,\mathrm{Im}\left(U_{\alpha 1}^* U_{\alpha 3}\right), \\
\rho_6^\alpha &= 2\,\mathrm{Re}\left(U_{\alpha 2}^* U_{\alpha 3}\right), \\
\rho_7^\alpha &= -2\,\mathrm{Im}\left(U_{\alpha 2}^* U_{\alpha 3}\right), \\
\rho_8^\alpha &= \frac{1}{\sqrt{3}}\left(|U_{\alpha 1}|^2 + |U_{\alpha 2}|^2 - 2|U_{\alpha 3}|^2\right),
\end{aligned} \tag{4.13}$$

where the $U_{\alpha j}$ refers to an element of the Pontecorvo-Maki-Nakagawa-Sakata (PMNS) without taking into account the Majorana phases. [178, 179]. If we want to solve the Eq. (4.12) for the antineutrino case is enough to make $U_{\alpha j} \to U^*_{\alpha j}$.

Perturbative approach for oscillation probability

Our selected texture of decoherence matrix $\mathbf{D}$ in the mass vacuum basis (MVB), can be seen as composed by two matrices: one is a diagonal one with all its element equal $\mathbf{D^d} = -\Gamma \times \mathbb{I}$. The other one, $\mathbf{D^{nd}}$, is composed by its off-diagonal part, having as non-null only a unique $[\mathbf{D^{nd}}]_{ij} = -\beta_{ij} (= -\beta_{ji})$ elements (the diagonal is zero). Since in our case, the neutrinos are going to be propagating in matter, and in order to solve Eq. (4.9), we need to rotate the decoherence matrix D to the mass matter basis (MMB). In the MMB the decoherence matrix $\mathbf{D_m}$ is defined as:

$$\mathbf{D_m} = \mathbf{D^d_m} + \mathbf{D^{nd}_m}, \tag{4.14}$$

where $\mathbf{D^d_m} = -\Gamma \times \mathbb{I}$ is purely diagonal, $\mathbf{D^d}$ is unaltered by the rotation, while $\mathbf{D^{nd}_m}$ is the rotated matrix of the non-diagonal matrix $\mathbf{D^{nd}}$ in the MVB.

Considering, that the transition probability when neutrinos travel through matter is:

$$P_{\nu_\alpha \to \nu_\beta} = \frac{1}{3} + \frac{1}{2}(\varrho^\beta_m(0))^T \varrho^\alpha_m(t), \tag{4.15}$$

where $\varrho^\alpha_m(t) = e^{\mathbf{M}t}\varrho^\alpha_m(0)$, with $\mathbf{M} = \mathbf{H_m} + \mathbf{D_m}$. $\mathbf{H_m}$ is the Hamiltonian is written in the MMB. Since $\mathbf{D^d_m}$ is proportional to the identity matrix, this commutes with $\mathbf{H_m}$, then we have:

$$\varrho^\alpha_m(t) = e^{-\Gamma t} e^{(\mathbf{H_m} + \mathbf{D^{nd}_m})t} \varrho^\alpha_m(0) = e^{-\Gamma t} \varrho'^\alpha_m(t) \tag{4.16}$$

Given that $\varrho^\alpha_m(0) = \varrho'^\alpha_m(0)$ we can rewrite the probability in the following way:

$$P_{\nu_\alpha \to \nu_\beta} = \frac{1}{3} + \frac{1}{2} e^{-\Gamma t} (\varrho'^\beta_m(0))^T \varrho'^\alpha_m(t). \tag{4.17}$$

The solution of $\varrho'^{\alpha}_{m}(t)$, which is based on a power series solution expanded in θ_{13}, $\alpha_{\Delta} = \Delta m^2_{12}/\Delta m^2_{13}$ and a single $\bar{\beta}_{ij} = \beta_{ij}t$ follows the procedure given in [29]. For solving $\varrho'^{\alpha}_{m}(t)$ we must start with the next differential equation:

$$\dot{\varrho'^{\alpha}_{m}} = (\mathbf{H_m} + \mathbf{D^{nd}_m})\varrho'^{\alpha}_{m}, \tag{4.18}$$

The Eq.(4.18) can be simplified using this change of variable:

$$\varrho'^{\alpha}_{m}(t) = e^{\mathbf{H_m}t}\tilde{\varrho}^{\alpha}(t), \tag{4.19}$$

then, the Eq. (4.18) :

$$e^{\mathbf{H_m}t}\dot{\tilde{\varrho}}^{\alpha} + \mathbf{H}_m e^{\mathbf{H_m}t}\tilde{\varrho}^{\alpha} = (\mathbf{H_m} + \mathbf{D^{nd}_m})e^{\mathbf{H_m}t}\tilde{\varrho}^{\alpha} \tag{4.20}$$

thus we get:

$$\dot{\tilde{\varrho}}^{\alpha} = e^{-\mathbf{H_m}t}\mathbf{D^{nd}_m}e^{-\mathbf{H_m}t}\tilde{\varrho}^{\alpha}, \tag{4.21}$$

the matrix $e^{-\mathbf{H_m}t}\mathbf{D^{nd}_m}e^{-\mathbf{H_m}t}$ can be expanded perturbatively in power series of the small parameters θ_{13}, and α_{Δ} which turns out to be:

$$e^{-\mathbf{H_m}t}\mathbf{D^{nd}_m}e^{-\mathbf{H_m}t} = \beta_{ij}(\tilde{D}^{(0)} + \theta_{13}\tilde{D}^{(\theta_{13})} + \alpha_{\Delta}\tilde{D}^{(\alpha_{\Delta})} + ...) \tag{4.22}$$

we can factor out the decoherence parameter β_{ij} since it is a common factor of all the elements in the decoherence matrix $\mathbf{D^{nd}_m}$ in the MMB (a consequence of its definition in the mass vacuum basis that is an off-diagonal matrix with only non-null terms in a given $-\beta_{ij}$ element). Replacing Eq.(4.22) into Eq.(4.21):

$$\dot{\tilde{\varrho}}^{\alpha} = \beta_{ij}(\tilde{D}^{(0)} + \theta_{13}\tilde{D}^{(\theta_{13})} + \alpha_{\Delta}\tilde{D}^{(\alpha_{\Delta})} + ...)\tilde{\varrho}^{\alpha} \tag{4.23}$$

the above equation can be solved perturbatively treating $\tilde{\varrho}^{\alpha}$ as a power series in θ_{13}, α_{Δ} and β_{ij}:

$$\begin{aligned}\tilde{\varrho}^{\alpha} = \tilde{\varrho}^{(0)} + \theta_{13}\tilde{\varrho}^{(\theta)} + \alpha_{\Delta}\tilde{\varrho}^{(\alpha_{\Delta})} + \alpha_{\Delta}\theta_{13}\tilde{\varrho}^{(\alpha_{\Delta}\theta_{13})} + ... \\ + \beta_{ij}\tilde{\varrho}^{(\beta_{ij})} + \beta_{ij}\theta_{13}\tilde{\varrho}^{(\beta_{ij}\theta_{13})} + \beta_{ij}\alpha_{\Delta}\tilde{\varrho}^{(\beta_{ij}\alpha_{\Delta})} + ...\end{aligned} \tag{4.24}$$

Then substituing Eq.(4.24) into Eq.(4.23) we produce a sequence of first order differential equations each of them collecting equal power terms. The β_{ij}-independent terms of the $\tilde{\varrho}^{\alpha}$ expansion: $\tilde{\varrho}^{(0)} + \theta_{13}\tilde{\varrho}^{(\theta)} + \alpha_{\Delta}\tilde{\varrho}^{(\alpha_{\Delta})} + \alpha_{\Delta}\theta_{13}\tilde{\varrho}^{(\alpha_{\Delta}\theta_{13})} +$

... corresponds to the initial condition $\tilde{\varrho}^{\alpha}(0)$, which is constant in time and coincides with the initial condition for the standard oscillation case, since at that instant the environment is decoupled (not interacting) with the neutrino system. Additionally, considering $\varrho'^{\alpha}_{m}(0) = \tilde{\varrho}^{\alpha}(0)$, we can rewrite Eq.(4.19) as follows:

$$\varrho'^{\alpha}_{m}(t) = e^{\mathbf{H_m}t}(\varrho'^{\alpha}_{m}(0) + \bar{\beta}_{ij}(...))., \tag{4.25}$$

with $\bar{\beta}_{ij} = \beta_{ij}t$. The second term at the right-hand side of the equation above contains the explicit solution of the power series of ϱ^{α}.

4.2 Quantum decoherence and CPT violation

We will test the CPT symmetry in the context of DUNE using the simulated total rates associated to the ν_μ and the $\bar{\nu}_\mu$ survival channels, where the matter effects are unimportant. The latter fact implies that the vacuum probabilities formulae for oscillation (plus decoherence) are going to be well enough for understanding the corresponding features of CPTV effects. Thus, all the formulae in this section will be developed under the vacuum framework. It is important to mention that we introduce the matter effects numerically. Before starting, it is of utmost importance to remark that the decoherence phenomena entails the transition from pure to mixed states, which implies that the time reversal operation is, as itself, meaningless for this situation [75]. The tool for revealing these, implicit, CPTV effects is the difference between the ν_μ and $\bar{\nu}_\mu$ survival probabilities channels, which written for a generic flavor ν_α is:

$$\Delta P_{\not{\text{CPT}}} = P_{\nu_\alpha \to \nu_\alpha} - P_{\bar{\nu}_\alpha \to \bar{\nu}_\alpha}. \tag{4.26}$$

With the aim of simplifying the analytical form of the latter expression we work under three assumptions:

- The diagonal elements (damping parameters) of the dissipative matrix **D** are all equal to a single parameter Γ.

- The dissipative matrix for neutrinos is equal to the corresponding for antineutrinos, $\mathbf{D} = \bar{\mathbf{D}}$.

- The $\mathbf{D}$ matrix is containing no more than one non-diagonal elements at a time we study the $\Delta P_{\not{CPT}}$.

As a general feature, we have that a non-zero $\Delta P_{\not{CPT}}$ is obtained when in the survival neutrino oscillation probability there is a term with β_{ij} (non-diagonal term) coupled to $\rho_i^\alpha \rho_j^\alpha$ that contains $\sin\delta_{CP}$, therefore, when its corresponding antineutrino term is subtracted for getting $\Delta P_{\not{CPT}}$ they do not cancel each other because of the flipping of the sign of $\sin\delta_{CP}$. We find that the aforementioned situation (i.e. non null $\Delta P_{\not{CPT}}$) is fulfilled by fifteen β_{ij} where one coefficient in the product $\rho_i^\alpha \rho_j^\alpha$ is: ρ_2^α, ρ_5^α or ρ_7^α and the other one : ρ_1^α, ρ_3^α, ρ_4^α, ρ_6^α or ρ_8^α summarizing in total fifteen cases. The remaining β_{ij} do not produce non-null $\Delta P_{\not{CPT}}$ given that they are not connected with $\rho_i^\alpha \rho_j^\alpha$ terms that contain $\sin\delta_{CP}$, similar to what happen for the survival probabilities, in the pure oscillation case, where there are no terms involving $\sin\delta_{CP}$ then these do not flip sign when we switch neutrinos to antineutrinos conserving CPT.

Based on the similarities of the structure of the form for $\Delta P_{\not{CPT}}$ we can divide these fifteen cases in two groups, each group related to different set of β_{ij}, that we present as follows.

Group 1

The $\Delta P_{\not{CPT}}$ expression for the first group is given by:

$$\Delta P_{\not{CPT}} = \beta_{ij} \frac{\left(e^{\Omega_{\beta_{ij}} t} - e^{-\Omega_{\beta_{ij}} t}\right)}{\Omega_{\beta_{ij}}} \rho_i^\alpha \rho_j^\alpha \; e^{-\Gamma t}, \tag{4.27}$$

where

$$\Omega_{\beta_{ij}} = \sqrt{\beta_{ij}^2 - {\Delta_{\beta_{ij}}}^2}, \tag{4.28}$$

with $\Delta_{\beta_{ij}} = \Delta m^2_{\beta_{ij}}/2E$, where E is energy and $\Delta m^2_{\beta_{ij}}$, corresponds to standard square mass differences of neutrino masses, according to its indices ij (see Table 4.1). This formula applies for nine β_{ij}, the details are given in Table 4.1.

(i,j)	$\Delta_{\beta_{ij}}$
$(1,2),(2,3),(2,8)$	Δ_{12}
$(4,5),(5,3),(5,8)$	Δ_{13}
$(6,7),(7,3),(7,8)$	Δ_{23}

Table 4.1: Here it is displayed each group of indices (i,j), which corresponds to a one of the nine β_{ij}. The (i,j) in the same row are associated to the $\Delta_{\beta_{ij}}$ in the same line

As an example, the exact probability from where we can extrapolate the $\Delta P_{\not{\text{CPT}}}$ for β_{12} is.

$$P_{\nu_\alpha\to\nu_\alpha} = \frac{1}{3} + \frac{1}{2}\Bigg(\left((\rho_1^\alpha)^2 + (\rho_2^\alpha)^2\right)\frac{\left(e^{\Omega_{12}t} + e^{-\Omega_{12}t}\right)}{2} + \left((\rho_4^\alpha)^2 + (\rho_5^\alpha)^2\right)\cos\Delta_{13}t$$
$$+ \left(\left(\rho_6^\alpha\right)^2 + (\rho_7^\alpha)^2\right)\cos\Delta_{23}t + (\rho_3^\alpha)^2 + (\rho_8^\alpha)^2 + \beta_{12}\frac{\left(e^{\Omega_{12}t} - e^{-\Omega_{12}t}\right)}{\Omega_{12}}\rho_1^\alpha\rho_2^\alpha\Bigg)e^{-\Gamma t}. \tag{4.29}$$

Group 2

The $\Delta P_{\not{\text{CPT}}}$ for the remaining six β_{ij}: $\beta_{15}, \beta_{24}, \beta_{17}, \beta_{26}, \beta_{47}$ and β_{56}, is also proportional to β_{ij}, but it is rather a cumbersome expression in comparison to the one in Eq. 4.27. In fact, it is the addition of two terms, one of them is proportional to $\rho_i^\alpha\rho_j^\alpha$ while the other one, is proportional to $\rho_k^\alpha\rho_l^\alpha$. For a given ij indices, there is a specific kl, with each one of these indices associated to an specific mass squared difference value, for the complete details see Table 4.2. The six expressions for the CPTV formula are obtained per each pair ij, kl plus exchanging $ij \leftrightarrow kl$, with all its correspondent terms associated with them. The explicit formula is given by:

$$\Delta P_{\not{\text{CPT}}} = \beta_{ij}\frac{1}{\sqrt{\Omega^4 - 4\Delta_{\beta_{ij}}^2\Delta_{\beta_{kl}}^2}} \times \Bigg[\left(\Omega_+\left(e^{\Omega_+ t} - e^{-\Omega_+ t}\right) - \Omega_-\left(e^{\Omega_- t} - e^{-\Omega_- t}\right)\right)\rho_i^\alpha\rho_j^\alpha$$
$$+ \Delta_{\beta_{ij}}\Delta_{\beta_{kl}}\left(\frac{e^{\Omega_+ t} - e^{-\Omega_+ t}}{\Omega_+} - \frac{e^{\Omega_- t} - e^{-\Omega_- t}}{\Omega_-}\right)\rho_k^\alpha\rho_l^\alpha\Bigg]e^{-\Gamma t}, \tag{4.30}$$

where

$$\Omega^2 = \beta_{ij}^2 - \Delta_{\beta_{ij}}^2 - \Delta_{\beta_{kl}}^2 \tag{4.31}$$

$$\Omega_\pm = \tfrac{1}{\sqrt{2}}\sqrt{\Omega^2 \pm \sqrt{\Omega^4 - 4\Delta_{\beta_{ij}}^2\Delta_{\beta_{kl}}^2}} \tag{4.32}$$

As in the case of group one, we can write the oscillation probability for β_{24}. From there, we can extract the corresponding $\Delta P_{\not{CPT}}$.

$$\begin{aligned} P_{\nu_\alpha\to\nu_\alpha} =& \frac{1}{3} + \frac{e^{-\Gamma t}}{2}\Bigg(\frac{\left(e^{\Omega_+ t} + e^{-\Omega_+ t}\right)}{2\sqrt{\Omega^4 - 4\Delta_{12}^2\Delta_{13}^2}} \times g_{+,2}^{-,1} + \frac{\left(e^{\Omega_- t} + e^{-\Omega_- t}\right)}{2\sqrt{\Omega^4 - 4\Delta_{12}^2\Delta_{13}^2}} g_{-,2}^{+,1} \\ &+ \frac{\left(e^{\Omega_+ t} + e^{-\Omega_+ t}\right)}{2\sqrt{\Omega^4 - 4\Delta_{12}^2\Delta_{13}^2}} g_{-,5}^{+,4} + \frac{\left(e^{\Omega_- t} + e^{-\Omega_- t}\right)}{2\sqrt{\Omega^4 - 4\Delta_{12}^2\Delta_{13}^2}} g_{+,5}^{-,4} + \left(\left(\rho_6^\alpha\right)^2 + (\rho_7^\alpha)^2\right)\cos\Delta_{23}t \\ &+ (\rho_3^\alpha)^2 + (\rho_8^\alpha)^2 + \beta_{24}\frac{1}{\sqrt{\Omega^4 - 4\Delta_{12}^2\Delta_{13}^2}}\rho_2^\alpha\rho_4^\alpha \\ &+ \Delta_{12}\Delta_{13}\left(\frac{e^{\Omega_+ t} - e^{-\Omega_+ t}}{\Omega_+} - \frac{e^{\Omega_- t} - e^{-\Omega_- t}}{\Omega_-}\right)\rho_1^\alpha\rho_5^\alpha\Bigg]\Bigg) \end{aligned} \tag{4.33}$$

where:

$$g_{(\pm)_{\text{down}},j}^{(\pm)_{\text{up}},i} = \left((\pm)_{\text{up}}(\Delta_{12}^2 + \Omega'^2_{(\pm)_{\text{up}}})(\rho_i^\alpha)^2(\pm)_{\text{down}}(\Delta_{13}^2 + \Omega'^2_{(\pm)_{\text{down}}})(\rho_j^\alpha)^2\right),$$

with

$$\Omega'^2_\pm = \frac{1}{2}\left(\Omega^2 \pm \sqrt{\Omega^4 - 4\Delta_{12}^2\Delta_{13}^2}\right) \tag{4.34}$$

$\{(i,j),\Delta_{\beta_{ij}}\} \leftrightarrow \{(k,l),\Delta_{\beta_{kl}}\}$
$\{(1,5),\Delta_{12}\} \leftrightarrow \{(2,4),\Delta_{13}\}$
$\{(1,7),\Delta_{12}\} \leftrightarrow \{(2,6),\Delta_{23}\}$
$\{(4,7),\Delta_{13}\} \leftrightarrow \{(5,6),\Delta_{23}\}$

Table 4.2: Here it is shown how is the relation between the six indices (i,j) and (k,l), each of them associated to its corresponding β and its neutrino mass square differences.

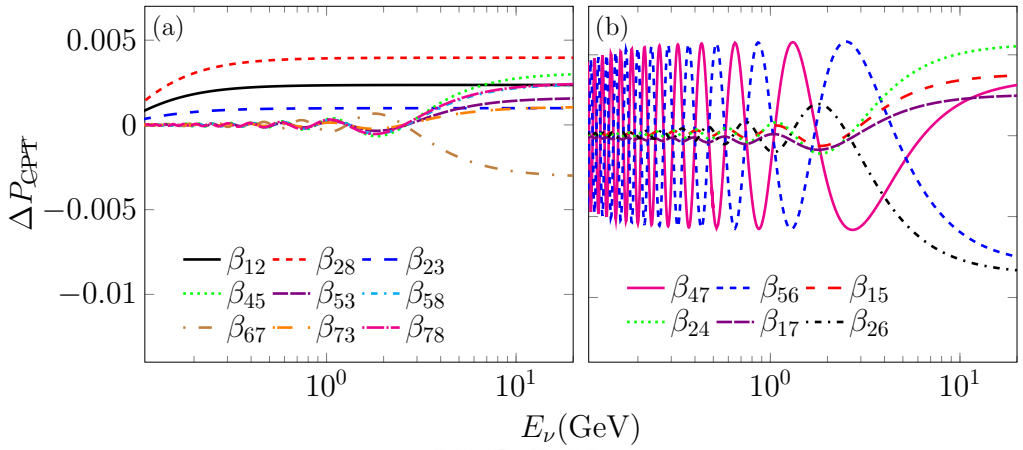

Figure 4.1: $\Delta P_{\not CPT}$ versus E_ν, evaluated for $\Gamma = 10^{-23}$ GeV and $\delta_{CP} = 3\pi/2$. At (a) it is displayed the group 1 with $\beta_{28}, \beta_{53}, \beta_{73} = \Gamma/\sqrt{3}$, $\beta_{58}, \beta_{78} = \Gamma/\sqrt{7}$, $\beta_{12}, \beta_{23}, \beta_{45}, \beta_{67} = \Gamma/3$, while at (b) it is displayed group 2 with all β's are equal to $\Gamma/\sqrt{3}$. The remaining parameters are given in Table 4.3.

Parameter	Value
θ_{12}	$33.63°$
θ_{13}(NH)	$8.52°$
θ_{23}(NH)	$48.7°$
Δm^2_{21}	$7.4 \times 10^{-5}\text{eV}^2$
Δm^2_{31}(NH)	$2.515 \times 10^{-3}\text{eV}^2$
Baseline	1300Km

Table 4.3: DUNE baseline and values for standard oscillation parameters taken from [171].

Analytical results for $\Delta P_{\not CPT}$

It is important to point out that, from now on, all the results that we will present the $\Delta P_{\not CPT}$ will be calculated for $\alpha = \mu$. In Fig. 4.1, we present $\Delta P_{\not CPT}$ in two separated plots all β's for group 1 and group 2, for neutrino energies from 0.1 to 20 GeV, which encloses the DUNE energy range. We have evaluated this effect in an isolated manner per each β, i.e., we consider all the rest of β's as zero. For the latter, we obtain its maximum value from the inequalities and positivity conditions given in Appendix A, having as result

the following:

$$\beta_{28}, \beta_{53}, \beta_{73} = \Gamma/\sqrt{3} \tag{4.35}$$

$$\beta_{58}, \beta_{78} = \Gamma/\sqrt{7} \tag{4.36}$$

$$\beta_{12}, \beta_{23}, \beta_{45}, \beta_{67} = \Gamma/3 \tag{4.37}$$

and the maximum values for the remaining β's are $\Gamma/\sqrt{3}$, it is essential to mention that we have taken their positive values. For all these plots it is also fixed $\delta_{CP} = 3\pi/2$ and $\Gamma = 10^{-23}$ GeV, with the remaining parameters displayed in Table 4.3. The parameters given in Table 4.3 will be used throughout this thesis. We note, for group one, that the β_{28} is producing the highest amplitude for $\Delta P_{\not{CPT}}$ in all the energy range, being followed by β_{12}. In the case of group two, β_{47} and β_{56} give the maximum values of amplitudes of $\Delta P_{\not{CPT}}$ up to neutrino energies a bit less than 5 GeV.

In Fig. 4.2, we have four plots which show iso-contour curves of $\Delta P_{\not{CPT}}$ at the plane Γ versus δ_{CP}, two of them corresponds to the vacuum oscillation case (top) and the other two to the matter oscillation case (bottom). For all plots the neutrino energy is fixed at 2.4 GeV keeping the remaining parameters at the same values than those used for Fig 4.1. Two plots are for β_{28} (group one) for vacuum and matter, and the corresponding other two are for β_{56} (group two). All β's are equal to $\Gamma/\sqrt{3}$. We have chosen these particular β's since they are those who generate the biggest amplitudes for $\Delta P_{\not{CPT}}$ per each group. Among the general features, we have that other than the maximum (and minimum) value of the $\Delta P_{\not{CPT}}$ the behaviour of all plots are rather similar. Other common detail is that the $\Delta P_{\not{CPT}}$ grows with Γ until reaching a region where the maximum amplitude is located, then starts to decrease. Outside the regions around the peaks, i.e. for lower and higher values than the Γ at the peak, the $\Delta P_{\not{CPT}}$ is zero. The vacuum and the matter case exhibit a very similar pattern, and there is no a qualitative difference between the plots for β_{28} (group one) and β_{56} (group two). Therefore, we can use for getting a full understanding of what happens the vacuum formula

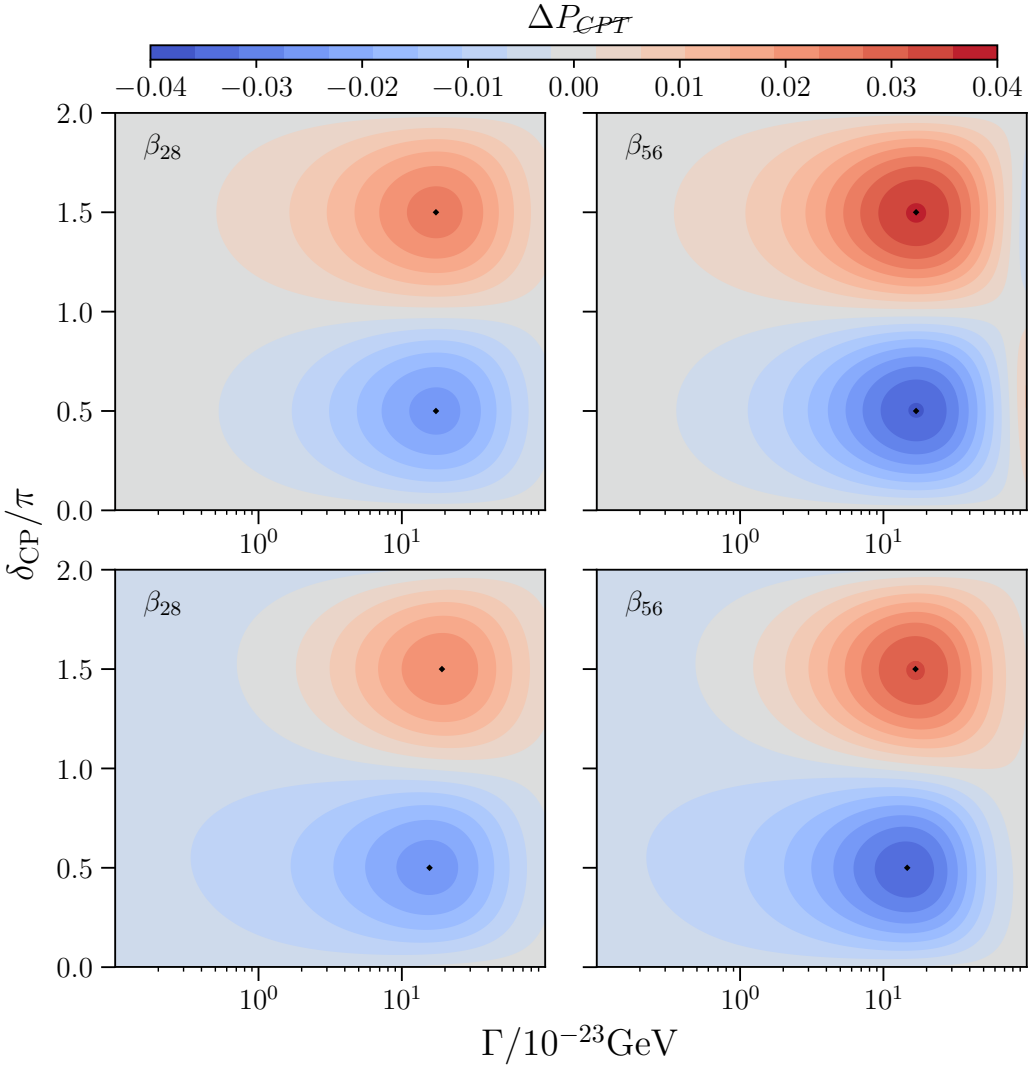

Figure 4.2: Iso-contour curves of $\Delta P_{\not{CPT}}$ at the plane Γ versus δ_{CP} evaluated for $\beta_{28} = \Gamma/\sqrt{3}$ and $\beta_{56} = \Gamma/\sqrt{3}$ and for a fixed $E_\nu = 2.4$ GeV. The two plots at the top correspond to the vacuum oscillation case, meanwhile, the two plots at the bottom correspond to the matter oscillation case.

given for group one, Eq. (4.27). Hence, from Eq. (4.27), we see that $\Delta P_{\not{CPT}}$ is suppressed for low values of Γ, which implies low values of $\beta_{28}(= \Gamma/\sqrt{3})$ that are directly proportional to the value of $\Delta P_{\not{CPT}}$. On the other hand, $\Delta P_{\not{CPT}}$ is reduced for higher values of Γ, given that the latter diminishes the factor $\exp^{-\Gamma t}$. From the maximization of the Eq. (4.27) the value of the Γ at the peak can be extracted, for β_{28} the peak is at $\Gamma \sim 1.7 \times 10^{-22}$ GeV, similarly, if

we maximize Eq. (4.30) we obtain the peak for β_{56} at $\Gamma \sim 1.6 \times 10^{-22}$ GeV. In general, a very reasonable estimation for the value of Γ at the peak is obtained from $\Gamma L \sim 1$ then $\Gamma \sim 1/L$, which for $L = 1300$ km is $\sim 1.5 \times 10^{-22}$ GeV. The corresponding values of $\delta_{CP} = \pi/2$ and $3\pi/2$, for β_{28}, can be directly inferred from the unique presence of $\sin\delta_{CP}$ in the factor $\rho_2^\mu \rho_8^\mu$, the values of δ_{CP} for β_{56} are very close to $\pi/2$ and $3\pi/2$ for similar reasons, but they are slightly distorted due to ρ_6^μ is composed by two terms, being one of them proportional to $\cos\delta_{CP}$. In spite of, the vacuum and matter case looks pretty alike, we must note that the matter effects produces a $\Delta P_{\not{CPT}} \neq 0$ even in the absence of decoherence. Actually, in the experimental (simulated) searches of CPTV that we will present in the following sections, the CPTV, due to matter effects, will play the role of normalization factor.

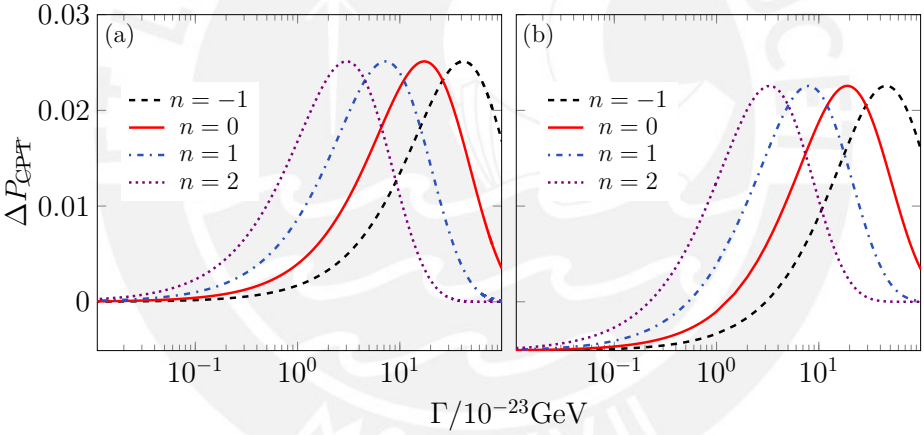

Figure 4.3: $\Delta P_{\not{CPT}}$ versus Γ, evaluated for different energy dependence $n = -1, 0, 1, 2$, $E_\nu = 2.4$ GeV, $\delta_{CP} = 3\pi/2$ and fixing $\beta_{28} = \Gamma/\sqrt{3}$. We have the vacuum oscillation case (a) and the matter oscillation case (b). In both plots we use the same scale.

Energy dependency of the decoherence parameters

From a more general view the entries of the decoherence matrix could be energy dependent, particularly, in this thesis we will adopt this dependence as follows:

$$\Gamma_{E_\nu} = \Gamma \left(\frac{E_\nu}{\text{GeV}} \right)^n , \tag{4.38}$$

where n can be $-1, 0, 1$ and 2. The $n = -1$ is taken because it imitates the oscillation energy dependence. The motivation for $n = 1$ and $n = 2$ can be found in [77] and [78], respectively.

In Fig. 4.3 we study the $\Delta P_{\not CPT}$ for the aforementioned energy dependence and setting $\beta_{28} = \Gamma/\sqrt{3}$, the neutrino energy in 2.4 GeV (the DUNE energy peak) and $\delta_{CP} = 3\pi/2$, for the vacuum and matter oscillation case. In these figures we note that the energy dependency on Γ only change their values at the peak but do not affect the amplitudes of $\Delta P_{\not CPT}$. As we have discussed in section 4.2, at the peak obtained approximately when the next relation is satisfied: $\Gamma_{E_\nu} L \sim 1$ then $\Gamma \sim 1/(LE^n)$ which turns out to be in $\Gamma \sim \{4.0,\ 1.5,\ 0.6,\ 0.3\}\times 10^{-22}$ GeV for $n = -1, 0, 1$ and 2 respectively. As expected we have a non negligible negative value of $\Delta P_{\not CPT}$ when Γ goes to zero for the matter oscillation case.

Decoherence matrix texture for optimal $\Delta P_{\not CPT}$

For maximizing the $\Delta P_{\not CPT}$ we simultaneously turn on β_{28}, β_{12}, β_{56} and β_{47} in the following values: $\beta_{28} = \Gamma/\sqrt{3}$, $\beta_{12} = (\sqrt{2/3})\Gamma/3$ and $\beta_{56} = -\beta_{47} = \Gamma/3$. These values has been set according to the following steps: First, we fix $\beta_{28} = \Gamma/\sqrt{3}$, given that this β produces the major effect on $\Delta P_{\not CPT}$. Second, once β_{28} have been defined we obtain the maximum allowed value for β_{12}, which is the second in importance regarding to its impact on $\Delta P_{\not CPT}$. By last, with β_{28} and β_{12} already set up, we get the maximum values of β_{56} and β_{47}, where we have taken $\beta_{56} = -\beta_{47}$ in order to obtain a constructive effect between them. The restrictions imposed by the Schwarz inequalities and positivity conditions, fully described in the Appendix A, have been considered for getting the aforementioned values of β's.

CPT violation in matter

As we have already mentioned, when the neutrinos are traveling through matter, we have a non-zero CPTV value for pure standard oscillation,

even for zero CP phase. From now on, when we refer to the term standard oscillation (SO), it means that the matter effects are included. If we add the decoherence to SO, the non-zero value of CPTV is still preserved, but, it has a different magnitude with respect to its corresponding in the pure SO, because, as expected, it is distorted by the presence of the quantum decoherence parameters. In particular, it is interesting to note that this happens even when a single parameter diagonal decoherence matrix (DDM) proportional to the identity is considered ($\mathbf{D^{nd}} = 0$), in contrast with the DDM case in vacuum, where a non-zero CPTV is not brought to light. The matter neutrino oscillation probabilities for a single parameter DDM can be derived only replacing the vacuum mixing angles and mass squared for their corresponding ones in matter, in, for instance, the three generation formula displayed in [70]. Of course, it also includes the replacement of a singular decoherence parameter. The application of the latter procedure is fully justified and it has been very well explained in [29]. Therefore, we have that the structure of the formula is given by:

$$P^{\mathrm{SO}\bigoplus\mathrm{DDM}}_{\nu_\alpha\to\nu_\rho} = \frac{1}{3}(1 - e^{-\Gamma t}) + e^{-\Gamma t} P^{\mathrm{SO}}_{\nu_\alpha\to\nu_\rho}, \tag{4.39}$$

where α, ρ, are neutrino flavours, and $\mathrm{SO}\bigoplus\mathrm{DDM}$ stands for standard oscillation plus diagonal decoherence. It is clear that: $\Delta P^{\mathrm{SO}\bigoplus\mathrm{DDM}}_{\not{C}\not{P}\not{T}} = e^{-\Gamma t}\Delta P^{\mathrm{SO}}_{\not{C}\not{P}\not{T}}$, which goes to zero for high values of Γ and t. Nonetheless, when we deal with a real situation, the latter does not occur, since, we have to convolute the neutrino (antineutrino) oscillation probabilities with the fluxes, cross sections, efficiencies and resolution, being that, for this context, the $1/3$ from the first term at the RHS in Eq.(4.39) is the only one that survives for high values of Γ, leading us to find a non-zero constant value. We will see this type of behaviour further ahead in our section of results.

In this study we are not going to derive an analytical formula for the neutrino matter oscillation probability, for the non-diagonal decoherence matrices (NDM) cases that we have presented before. This is because it is

a rather complicated task and, besides, as we have already argued, the vacuum oscillation probabilities formulas are going to be enough for having a qualitative understanding of our results.

4.3 Simulation and results: CPT Violation

For the simulation of DUNE experiment, we assume the configuration of 80 GeV energy with 1.07 MW power in the primary proton beam from the Main Injector running over 5 years for exposure for each mode, the forward horn current (FHC) and the reverse horn current (RHC). In our simulation of DUNE, the GLoBES package [155, 156] is used and feeding with the information of the cross section, neutrino fluxes, resolution function and efficiency extracted from [52]. While, the matter neutrino oscillation probabilities plus decoherence was calculated with nuSQuIDS [157].

For testing the CPTV effects the following experimental observable is defined:

$$\mathcal{R} = \frac{\Delta N^{\mathrm{SO}\bigoplus\mathrm{DEC}}}{\Delta N^{\mathrm{SO}}}, \tag{4.40}$$

where $\Delta N^{\mathrm{SO}\ (\mathrm{SO}\bigoplus\mathrm{DEC})}$ is the difference between the total events rates for neutrino (N_{ν_μ}) and antineutrino ($N_{\bar{\nu}_\mu}$), as seen in Eq. (4.41). Additionally, DEC stands for any case of decoherence.

$$\Delta N = N_{\nu_\mu} - N_{\bar{\nu}_\mu} \tag{4.41}$$

The total event rates have been calculated using the prescription given in [53], where the signal is composed by $\nu_\mu + \bar{\nu}_\mu$ charge current event rates while the background is composed by neutral current event rates and the $\nu_\tau + \bar{\nu}_\tau$ charge current event rates, as shown in Table 3.2. Our observable is normalized with the SO difference of events ΔN^{SO}, which is non-zero due to matter effects plus the intrinsic differences between the cross sections, fluxes, etc, for neutrinos and antineutrinos. Given our definition, when decoherence is absent $\mathcal{R} = 1$.

$\Gamma = 10^{-23}$ GeV	Std	$n = -1$	$n = 0$	$n = 1$	$n = 2$
Neutrino mode					
$\nu_\mu + \bar{\nu}_\mu$ CC Signal	11749	11841	11965	11573	11932
NC Background	109	109	109	109	109
$\nu_\tau + \bar{\nu}_\tau$ CC Background	43	43	46	74	87
Antineutrino mode					
$\bar{\nu}_\mu + \nu_\mu$ CC Signal	5903	5897	5846	5237	4816
NC Background	58	58	58	58	58
$\nu_\tau + \bar{\nu}_\tau$ CC Background	27	27	29	50	60

Table 4.4: Total rates for the signal of ν_μ and $\bar{\nu}_\mu$ disappearance channels and their corresponding background. We consider $\delta_{\rm CP} = 3\pi/2$.

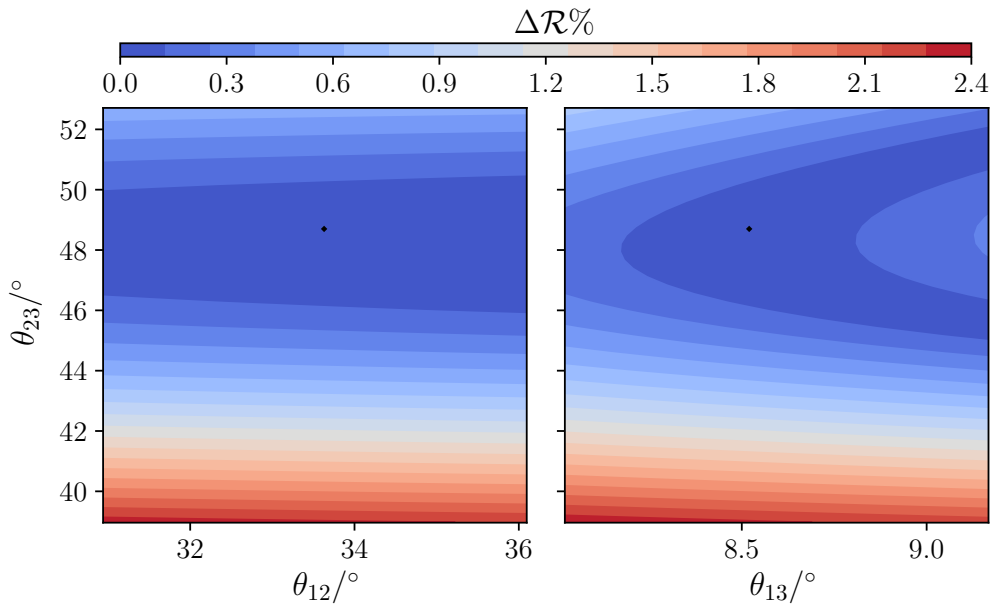

Figure 4.4: Contour plots for: θ_{23} vs θ_{12} and θ_{23} vs θ_{13}, varying the mixing angles within the 3σ range, showing the percentual variation of $\mathcal{R}$ with respect to the value obtained for the best fit oscillation parameters given in Table 4.3. The mixing angle that does not appear in the corresponding plot is fixed at its best fit value. In all the plots we fix $\Gamma = 10^{-23}$GeV and $\delta_{CP} = 3\pi/2$.

For giving an idea of the impact of decoherence into SO physics, we display in Table 4.4, the total rates for four energy dependent decoherence scenarios. We are not considering within this table the tau contamination [180] [181] since this contribution is negligible.

Using the values of this table we displayed at Fig. 4.5 the evaluation of $\mathcal{R}$ for the signal and backgrounds event rates, separately. We clearly see that the size of $\mathcal{R}$ for the backgrounds is very small in comparison with the corresponding one for the signal.

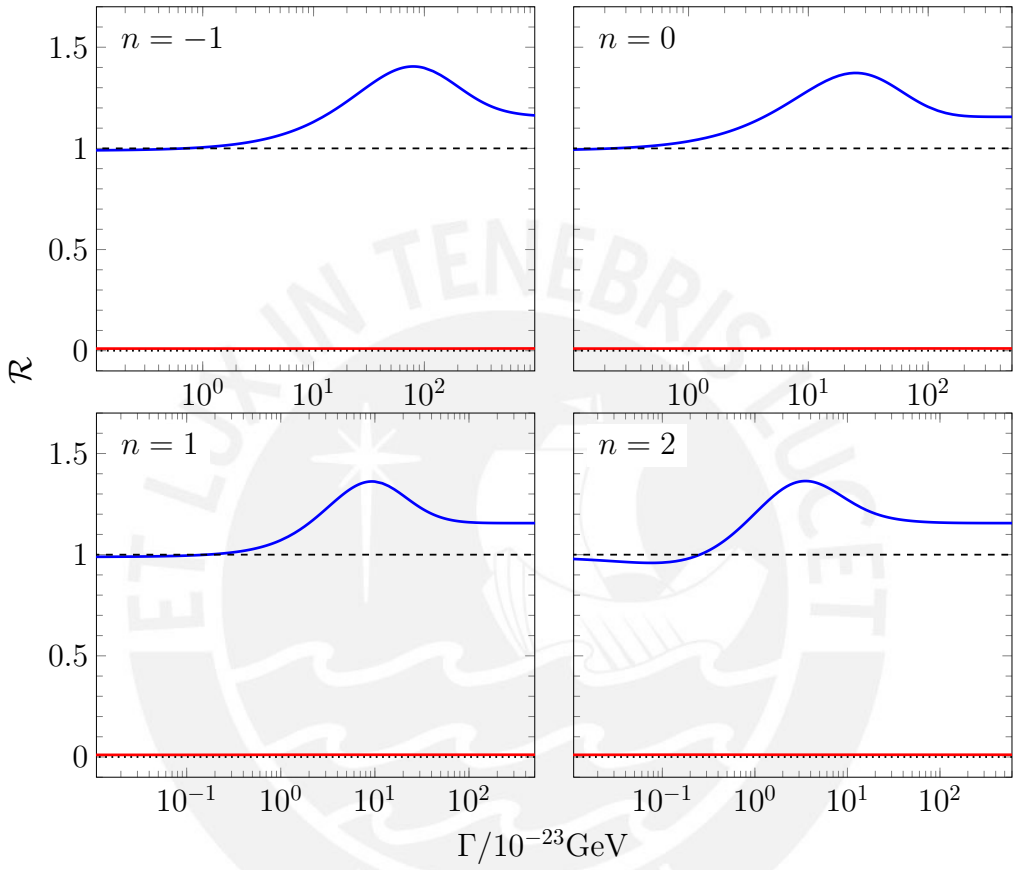

Figure 4.5: Here we display $\mathcal{R}$ versus Γ for the four energy dependence: $n = -1, 0, 1$ and 2. For the signal (blue) and backgrounds (red). We consider $\delta_{\rm CP} = 3\pi/2$.

We also displayed in Fig. 4.4 two plots: θ_{23} vs θ_{12} and θ_{23} vs θ_{13}, varying the mixing angles within the 3σ range, showing the percentual variation of $\mathcal{R}$ ($\Delta\mathcal{R}\%$) with respect to the value obtained for the best fit oscillation parameters given in Table 4.3 for $\Gamma = 10^{-23}$GeV and $\delta_{CP} = 3\pi/2$. We observe in the two plots that the $\Delta\mathcal{R}\%$ varies at maximum $\sim 2.3\%$. We do not display the case of θ_{13} vs θ_{12} since the variation is much lower.

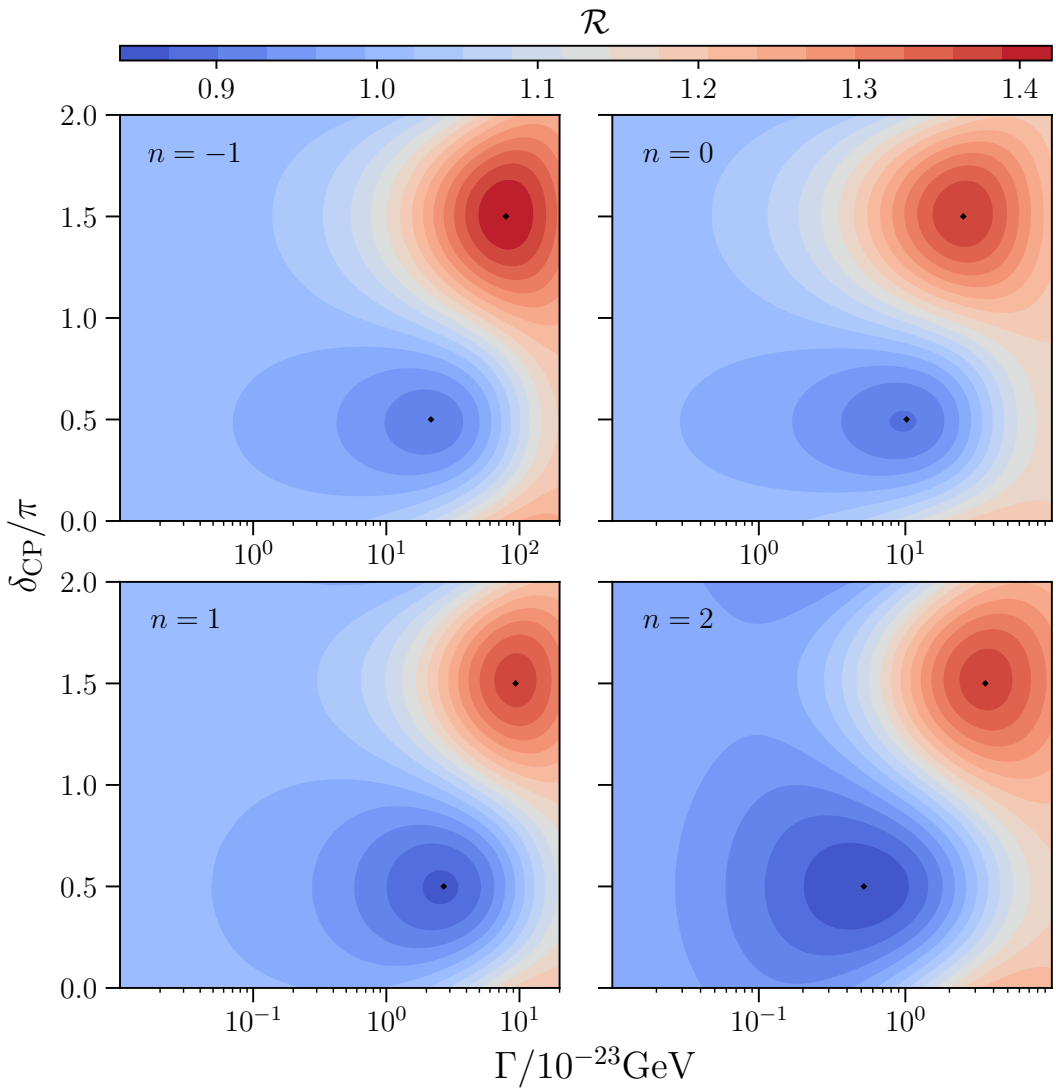

Figure 4.6: We analyze the confidence levels for the maximum values for $\mathcal{R}$. For $\delta_{\rm CP} \sim \pi/2$ we have 2.9σ, 3.4σ, 4.7σ and 5.5σ of confidence for $n = -1$, 0, 1 and 2 respectively. On the other hand, for $\delta_{\rm CP} \sim 3\pi/2$ we have 10.3σ, 9.8σ, 9.6σ and 9.7σ of confidence for $n = -1$, 0, 1 and 2 respectively.

In Fig. 4.6 we are showing iso-contour curves for the observable $\mathcal{R}$ in the plane Γ versus δ for four plots which corresponds to $n = -1, 0, 1$, and 2. In these plots, the maximum amplitudes are located at similar δ_{CP}, $\delta_{CP} \simeq \pi/2$ and $3\pi/2$, to those presented in Fig. 4.2. In relation to Fig. 4.2, there is a dislocation between the values of Γ at the maximum amplitudes for $\delta_{CP} \simeq \pi/2$ and $3\pi/2$. This is mainly because of the differences in the inputs used when

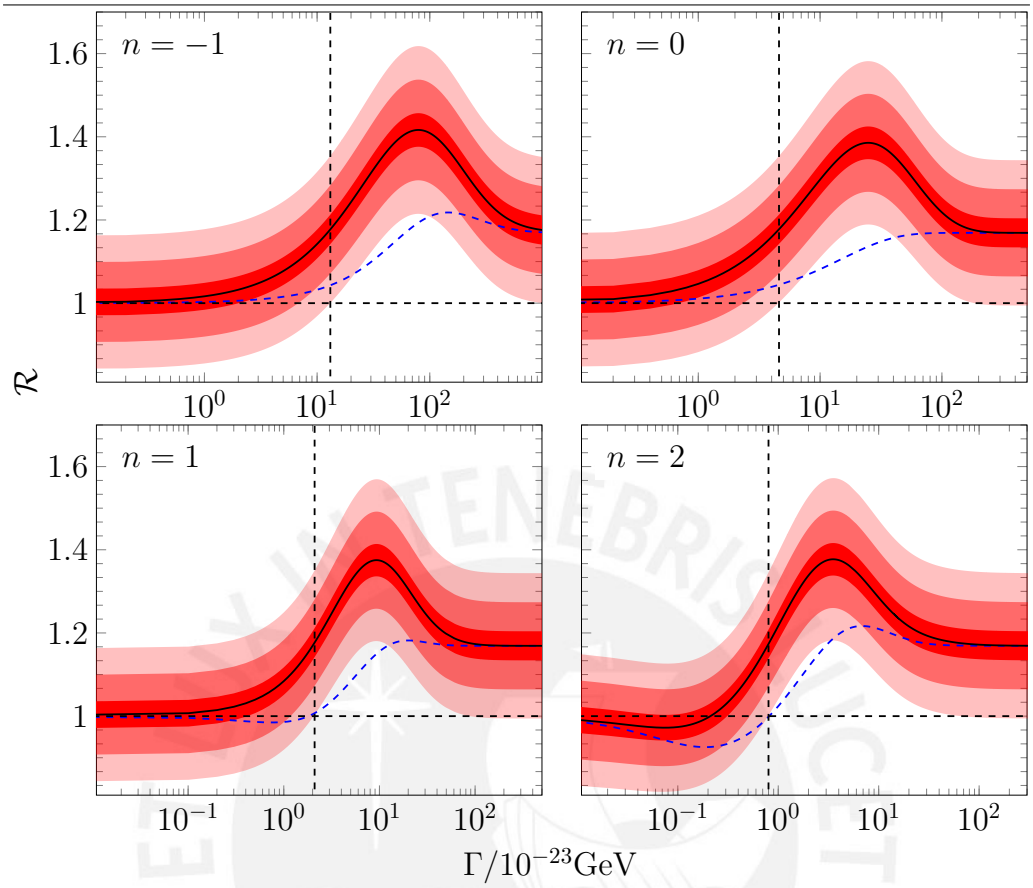

Figure 4.7: The black horizontal dashed line is the expected in the SO. The blue dashed line corresponds to the case of a DDM. Meanwhile, the solid black line corresponds to the case of a NDM both cases evaluated at $\delta_{CP} = 3\pi/2$. The red fringes (small, medium and large) represent the statistical error 1σ, 3σ and 5σ (respectively). The β's used corresponds to the ones given at section 4.2. The intersection between the black horizontal dashed line with the vertical one marks the 5σ significance of the NDM case relative to the SO case.

we convolute the probabilities for the neutrino and antineutrino mode. In addition, the Γ for $\delta_{CP} \simeq \pi/2$ and $3\pi/2$ is shifted to its lower values whenever n increases, gaining more sensitivity to lower values of Γ. The latter kind of behaviour is expected and resembles the one we have seen for $\Delta P_{\not{CPT}}$ in Fig. 4.3 (but here is a one dimensional view). Moreover, we also see the existence of degeneracies in (Γ, δ) as in [29].

In Fig. 4.7, we present the observable $\mathcal{R}$, with its corresponding error

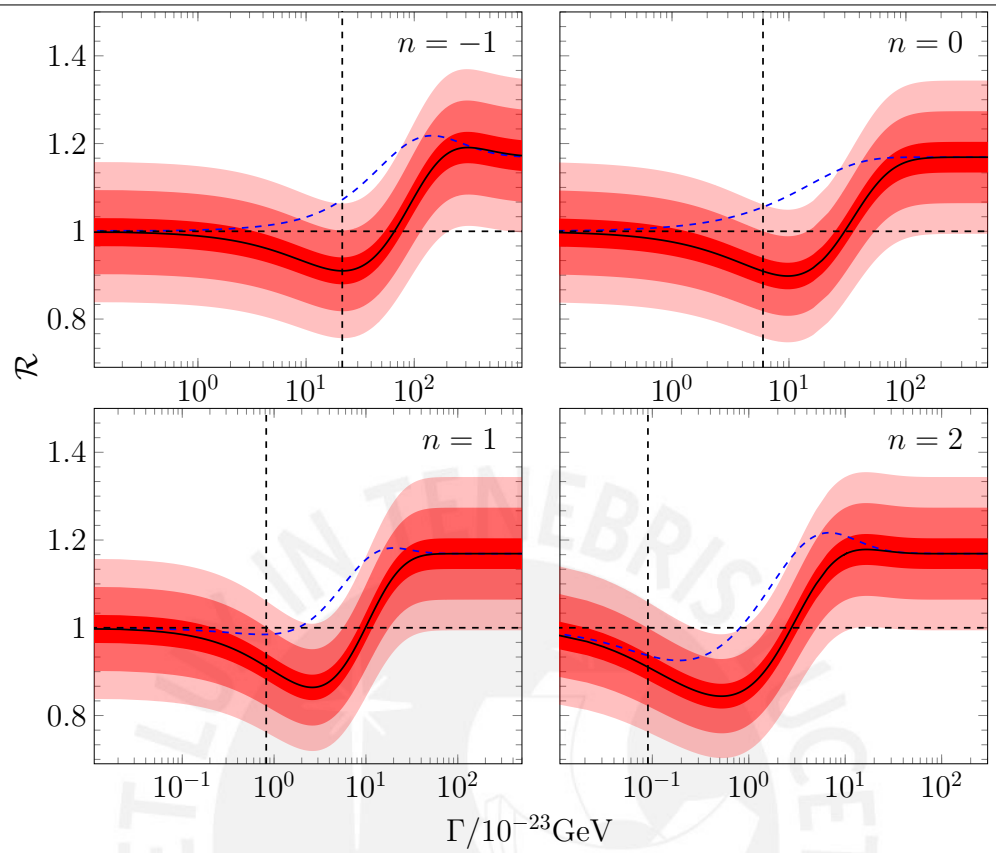

Figure 4.8: Similar to Fig. 4.7, but for $\delta_{\rm CP} = \pi/2$. Here, the intersection between the black horizontal dashed line with the vertical one marks the 3σ significance of the NDM case relative to the SO case.

bands for 1σ, 3σ and 5σ, versus Γ, for $n = -1, 0, 1$, and 2. We take $\delta_{CP} = 3\pi/2$ given that we learn from Fig. 4.6 that one of the maximum amplitude of $\Delta P_{\not{\rm CPT}}$ is obtained at this δ_{CP}. The behaviour displayed in this plot for small and medium values of Γ, at the given scale, is rather similar than that observed in Fig. 4.3. However, for large values of Γ the observable $\mathcal{R} \sim 1.17$, and not ~ 1.0, since within the signal for ν_μ ($\bar{\nu}_\mu$) we are including $\bar{\nu}_\mu(\nu_\mu)$ with their different fluxes and cross sections. Therefore, the link between these plots and those from Fig. 4.3 is not transparent straightforward. In order to make a comparison, we introduce in this plot the $\mathcal{R}$ corresponding to the single parameter DDM. We see that at small and large values of Γ, $\mathcal{R}$ tends to be $\sim 1.$ and ~ 1.17, respectively, for the DDM and NDM, irregardless the

dependency on n, as well. It is important to emphasize that for DDM, we obtain $\Delta P_{\not{CPT}} = 0$ in vaccum. As we have anticipated in section 4.2, the diagonal case also produces non-zero $\Delta P_{\not{CPT}}$ but in a lower magnitude than the NDM case. In fact, we have that for the NDM case a 5σ discrepancy, respect to the expectation value for SO ($\mathcal{R} = 1$), is reached at the following $\Gamma = \{13.1, 4.6, 2.1, 0.8\} \times 10^{-23}$GeV for $n = -1, 0, 1$ and 2, respectively. It is interesting to note that at these values of Γ the DDM is compatible with the SO prediction. Thus, here, we would be able to distinguish the NDM from the DDM.

An analogous result is shown n Fig. 4.8, but taking $\delta_{CP} = \pi/2$. In this case, the following values of Γ achieve the 3σ significance: $\{21.6, 6, 0.8, 0.09\} \times 10^{-23}$GeV for $n = -1, 0, 1$ and 2, respectively. All of them have $\mathcal{R} < 1$ For the cases $n = -1, 0$, we can discriminate between the NDM and DDM, since we have: $\mathcal{R} < 1$ and $\mathcal{R} > 1$, respectively. For $n = 1$, the DDM case is congruent with the SO, meanwhile, for $n = 2$, the DDM and NDM can be confused.

4.4 Quantum decoherence and Majorana nature

Majorana phases

In order to include the Majorana phases in Eq. (4.13), it is enough to make the replacement:

$$U_{\text{Majorana}} = U_{\text{PMNS}}.\text{diag}(1, e^{-i\phi_1}, e^{-i\phi_2}) \tag{4.42}$$

where ϕ_1 and ϕ_2 are the well-known Majorana phases. Therefore, the coefficients takes the following form:

$$\begin{aligned}
\rho_1^\alpha &\to \rho_1^\alpha \cos\phi_1 - \rho_2^\alpha \sin\phi_1 \\
\rho_2^\alpha &\to \rho_2^\alpha \cos\phi_1 + \rho_1^\alpha \sin\phi_1 \\
\rho_3^\alpha &\to \rho_3^\alpha \\
\rho_4^\alpha &\to \rho_4^\alpha \cos\phi_2 - \rho_5^\alpha \sin\phi_2 \\
\rho_5^\alpha &\to \rho_5^\alpha \cos\phi_2 + \rho_4^\alpha \sin\phi_2 \\
\rho_6^\alpha &\to \rho_6^\alpha \cos\Delta\phi - \rho_7^\alpha \sin\Delta\phi \\
\rho_7^\alpha &\to \rho_7^\alpha \cos\Delta\phi + \rho_6^\alpha \sin\Delta\phi \\
\rho_8^\alpha &\to \rho_8^\alpha,
\end{aligned} \tag{4.43}$$

where $\Delta\phi = \phi_1 - \phi_2$ and ρ_j^α are the coefficients defined in Eq. (4.13), which considers only the $U_{\rm PMNS}$ mixing elements. For other Majorana neutrino mixing matrix parametrizations, the value of the Majorana phases in the above equations can be reinterpreted as follows:

Symmetrical Parametrization of the mixing matrix

The elements of symmetric parametrization of the mixing matrix, given in Eq. (5) in [182], assuming the relation $\delta = \phi_{13} - \phi_{12} - \phi_{23}$, can be written as follows:

$$\begin{aligned}
U_{e1} &\to U_{e1} \\
U_{e2} &\to U_{e2} e^{-i\phi_{12}} \\
U_{e3} &\to U_{e3} e^{-i(\phi_{23}+\phi_{12})} \\
U_{\mu 1} &\to U_{\mu 1} e^{i\phi_{12}} \\
U_{\mu 2} &\to U_{\mu 2} \\
U_{\mu 3} &\to U_{\mu 3} e^{-i\phi_{23}} \\
U_{\tau 1} &\to U_{\tau 1} e^{i(\phi_{23}+\phi_{12})} \\
U_{\tau 2} &\to U_{\tau 2} e^{i\phi_{23}} \\
U_{\tau 3} &\to U_{\tau 3}
\end{aligned} \tag{4.44}$$

where ϕ_{13}, ϕ_{12} and ϕ_{23} are the CP phases used in [182]. The corresponding ρ_j^α are described by the following relations:

$$\begin{aligned}
\rho_1^\alpha &\to \rho_1^\alpha \cos\phi_{12} - \rho_2^\alpha \sin\phi_{12} \\
\rho_2^\alpha &= \rho_2^\alpha \cos\phi_{12} + \rho_1^\alpha \sin\phi_{12} \\
\rho_3^\alpha &\to \rho_3^\alpha \\
\rho_4^\alpha &\to \rho_4^\alpha \cos(\phi_{12}+\phi_{23}) - \rho_5^\alpha \sin(\phi_{12}+\phi_{23}) \\
\rho_5^\alpha &\to \rho_5^\alpha \cos(\phi_{12}+\phi_{23}) + \rho_4^\alpha \sin(\phi_{12}+\phi_{23}) \\
\rho_6^\alpha &\to \rho_6^\alpha \cos\phi_{23} - \rho_7^\alpha \sin\phi_{23} \\
\rho_7^\alpha &\to \rho_7^\alpha \cos\phi_{23} + \rho_7^\alpha \sin\phi_{23} \\
\rho_8^\alpha &\to \rho_8^\alpha,
\end{aligned} \tag{4.45}$$

where ρ_j^α are given in Eq. (4.13)

Particle data group parametrization type I: PDG I

Here we analyze the mixing matrix parametrization given in [120], which includes the Majorana phases ϕ_1 and ϕ_2:

$$U_{\text{Majorana}} = U_{\text{PMNS}}.\text{diag}(e^{i\phi_1}, e^{i\phi_2}, 1) \tag{4.46}$$

The corresponding ρ_j^α are described by the following equations:

$$\begin{aligned}
\rho_1^\alpha &\to \rho_1^\alpha \cos\Delta\phi + \rho_2^\alpha \sin\Delta\phi \\
\rho_2^\alpha &\to \rho_2^\alpha \cos\Delta\phi - \rho_1^\alpha \sin\Delta\phi \\
\rho_3^\alpha &\to \rho_3^\alpha \\
\rho_4^\alpha &\to \rho_4^\alpha \cos\phi_1 - \rho_5^\alpha \sin\phi_1 \\
\rho_5^\alpha &\to \rho_5^\alpha \cos\phi_1 + \rho_4^\alpha \sin\phi_1 \\
\rho_6^\alpha &\to \rho_6^\alpha \cos\phi_2 - \rho_7^\alpha \sin\phi_2 \\
\rho_7^\alpha &\to \rho_7^\alpha \cos\phi_2 + \rho_6^\alpha \sin\phi_2 \\
\rho_8^\alpha &\to \rho_8^\alpha,
\end{aligned} \tag{4.47}$$

Below, we present in Table 4.5 a summary of the equivalences between the different parameterizations.

Sym. $\leftrightarrow$ PDG I	Sym. $\leftrightarrow$ Our Work	PDG I $\leftrightarrow$ Our Work
$\phi_{12} + \phi_{23} \leftrightarrow \phi_1$	$\phi_{12} \leftrightarrow \phi_1$	$\phi_1 \leftrightarrow \Delta\phi$
$\phi_{23} \leftrightarrow \phi_2$	$\phi_{12} + \phi_{23} \leftrightarrow \phi_2$	$\phi_2 \leftrightarrow \phi_1$
$\phi_{12} \leftrightarrow \Delta\phi$	$\phi_{23} \leftrightarrow -\Delta\phi$	$\Delta\phi \leftrightarrow -\phi_2$

Table 4.5: Parameterizations comparison.

Majorana phases in neutrino oscillation probability

A very interesting scenario emerges in the neutrino oscillation phenomenon when non-zero Majorana phases and non-diagonal terms of the decoherence matrix are allowed. This is the CPV and CPTV, even when the Dirac CP-phase is zero, $\delta_{CP} = 0$.

Non-diagonal element	CPV	CPTV
$\beta_{12}, \beta_{23}, \beta_{24}, \beta_{26}, \beta_{28}$		
$\beta_{15}, \beta_{35}, \beta_{45}, \beta_{56}, \beta_{58}$	✓	✓
$\beta_{17}, \beta_{37}, \beta_{47}, \beta_{67}, \beta_{78}$		
$\beta_{13}, \beta_{14}, \beta_{16}, \beta_{18}$		
$\beta_{25}, \beta_{27}, \beta_{34}, \beta_{36}$	✓	✗
$\beta_{46}, \beta_{48}, \beta_{57}, \beta_{68}$		
β_{38}	✗	✗

Table 4.6: Violation of symmetries by the non-diagonal decoherence elements.

Assuming at least one of the Majorana phases is non-null and $\delta_{CP} = 0$, we classify in Table 4.6 which β_{ij} should be turned on in order to get either CPV, CPTV or both. The first row of β_{ij} produces both CPV and CPTV. In contrast, the second row, which has 12 elements, only produce *CP* violation, and the element β_{38} does not produce neither CPV, nor CPTV. As additional information, we must mention that Table 4.6 is almost exactly the same when $\delta_{CP} \neq 0$ and the Majorana phases are zero with the exception that β_{38} produces CPV contrary to the case when Majorana phases are switched on (and $\delta_{CP} = 0$).

We classify the correspondence between the off-diagonal terms β_{ij} and ϕ_1, ϕ_2, or $\Delta\phi$, according to the possibility of producing either CPV, CPTV or both. Since our analysis is addressed to point out the CPV cases for Majorana phases, using the vacuum oscillation probability, we performed a study in order to identify the major contributions for CPV, taking, individually, each off-diagonal elements, as shown in Table 4.7, at its maximum allowed values.

After assessing the magnitude of the CP-odd terms in the transition probability per each one of the off-diagonal elements β_{ij} (those who activate the Majorana phases), fixed at their maximum absolute allowed values, we conclude that $\beta_{28} = -\Gamma/\sqrt{3}$ gives us the most significant deviation from the standard oscillation formulae. The maximum absolute allowed values of β_{ij} are obtained, individually, through applying the complete positivity conditions [31]. Since all the diagonal elements are equal to $-\Gamma$, the aforementioned maximum values can be written in terms of this singular parameter.

CPV	CPTV	Non-null Majorana phase
$\beta_{13}, \beta_{23}, \beta_{18}, \beta_{28}, \beta_{12}$	$\beta_{23}, \beta_{28}, \beta_{12}$	ϕ_1
$\beta_{34}, \beta_{35}, \beta_{48}, \beta_{58}, \beta_{45}$	$\beta_{35}, \beta_{58}, \beta_{45}$	ϕ_2
$\beta_{37}, \beta_{36}, \beta_{68}, \beta_{67}, \beta_{78}$	$\beta_{37}, \beta_{67}, \beta_{78}$	$\Delta\phi$
$\beta_{14}, \beta_{24}, \beta_{15}, \beta_{25}$	β_{24}, β_{15}	ϕ_1, ϕ_2
$\beta_{16}, \beta_{17}, \beta_{26}, \beta_{27}$	β_{17}, β_{26}	$\phi_1, \Delta\phi$
$\beta_{46}, \beta_{47}, \beta_{56}, \beta_{57}$	β_{47}, β_{56}	$\phi_2, \Delta\phi$

Table 4.7: CP and CPT violation by non-diagonal decoherence elements and their dependence on the Majorana phases.

Therefore, taking the off-diagonal part of the decoherence matrix $\mathbf{D_{nd}}$ formed only with non-null $-\beta_{28}$ and considering $\bar{\Gamma} = \Gamma t$, the following semi-analytical perturbative $\nu_\mu \to \nu_e$ transition probability formula for SO plus decoherence (DE) is obtained:

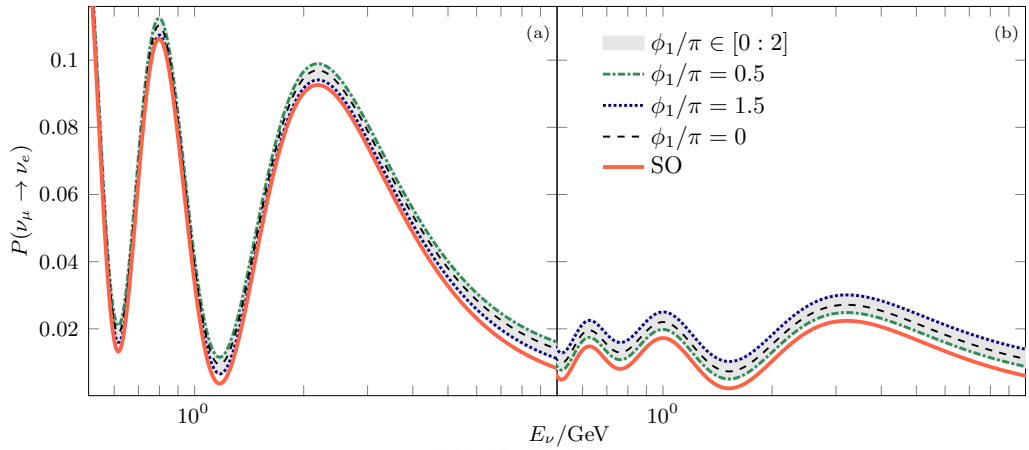

Figure 4.9: Oscillation probability depending on the neutrino energy for DUNE experiment. The figures (a) and (b) represent the $\nu_\mu \to \nu_e$ and $\bar{\nu}_\mu \to \bar{\nu}_e$ appearance channels respectively. The off-diagonal decoherence parameter is $\beta_{28} = -\Gamma/\sqrt{3}$. We consider $\delta_{\rm CP}/\pi = 1.4$, and $\Gamma = 2.5 \times 10^{-24}$GeV.

$$
\begin{aligned}
P^{\rm SO \bigoplus DE}_{\nu_\mu \to \nu_e} &= \frac{\left(1 - e^{-\bar{\Gamma}}\right)}{3} + P^{\rm SO}_{\nu_\mu \to \nu_e} e^{-\bar{\Gamma}} - \frac{\bar{\beta}_{28}}{\sqrt{3}} \sin 2\theta_{12} \sin^2\theta_{23} \times \sin\phi_1 e^{-\bar{\Gamma}} \\
&+ \bar{\beta}_{28}\theta_{13} \frac{\sin 2\theta_{23}}{2\sqrt{3}(A-1)A\Delta} \Big(\big((1-A^2)\cos\delta + A^2\cos(\delta - \Delta) - \cos(\delta - A\Delta)\big)\cos\phi_1 \\
&+ \big((1-A^2)\sin\delta + A^2\sin(\delta-\Delta) - \sin(\delta - A\Delta)\big)\cos 2\theta_{12}\sin\phi_1 \Big) e^{-\bar{\Gamma}} \\
&+ \bar{\beta}_{28}\alpha_\Delta \frac{\sin 2\theta_{12}}{\sqrt{3}A^2\Delta} \Big(2\sin^2\left(\frac{A\Delta}{2}\right)\cos 2\theta_{23}\cos\phi_1 - \cos 2\theta_{12} \\
&\times \sin^2\theta_{23}\big(\sin A\Delta - A\Delta\big)\sin\phi_1 \Big) e^{-\bar{\Gamma}} + \ldots
\end{aligned}
\tag{4.48}
$$

where $P^{\rm SO}_{\nu_\mu \to \nu_e}$ is the SO probability in matter ($t \to L$), $\Delta = (m_3^2 - m_1^2)L/(2E)$ and $A = \sqrt{2}G_F n_e L/\Delta$, where G_F is the Fermi constant, n_e is the electron number density and L is the source-detector distance. The validity of the transition probability formula relies on having the parameter-perturbative expansion $\bar{\beta}_{28}$, $\bar{\beta}_{28}\theta_{13}$ and $\bar{\beta}_{28}\alpha_\Delta$ of order: 10^{-2}, 10^{-3}, and 10^{-4}, respectively. For instance, the latter values can be attained for $|\beta_{28}| = 2 \times 10^{-24}$ GeV, and at DUNE baseline $L = 1300$ km. Furthermore, to get the antineutrino transition

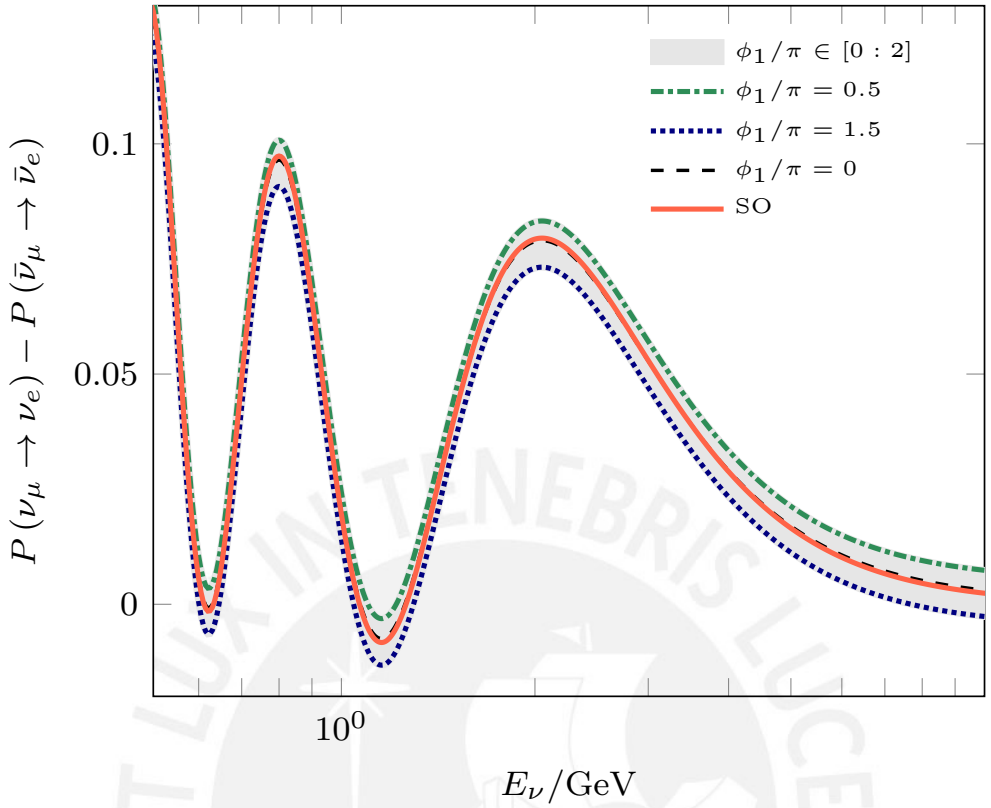

Figure 4.10: CP asymmetry depending on the neutrino energy. The off-diagonal decoherence parameter is $\beta_{28} = -\Gamma/\sqrt{3}$. We consider $\delta_{\rm CP}/\pi = 1.4$, and $\Gamma = 2.5 \times 10^{-24}$GeV.

probability is enough to: $\phi_1 \to -\phi_1$, $\delta \to -\delta$ and $A \to -A$, meanwhile, the ν_μ survival probability formula is not shown due to its negligible decoherence effect.

The $\nu_\mu \to \nu_e$ transition probability displayed in Fig. 4.9 is numerically calculated at DUNE baseline and for the maximum value of $\beta_{28} = -\beta/\sqrt{3}$, with $\Gamma = 2.5\times10^{-24}$ GeV and the following values for the SO parameters, taken from [171]: $\theta_{12} = 33.82°$, $\theta_{13} = 8.61°$, $\theta_{23} = 48.3°$, $\Delta m^2_{21} = 7.39 \times 10^{-5}\mathrm{eV}^2$, and $\Delta m^2_{31} = 2.523 \times 10^{-3}\mathrm{eV}^2$ (normal hierarchy), that are going to be fixed along this study. The Dirac CP phase is taken as: $\delta^{true}_{\rm CP}/\pi = 1.4$ inspired in the hint given by the T2K experiment [112]. From this figure it is notorious the energy-independent increase of the SO $\bigoplus$ DE probability respect to standard

one, regardless the value of ϕ_1, a feature that has been already pointed out in [29, 172], for other shape of the decoherence matrix. However, the size of this increment depends on ϕ_1, for example, in case of $\phi_1/\pi = 1.5$ ($\phi_1/\pi = 0.5$) the SO $\bigoplus$ DE neutrino (antineutrino) probability grows much less than its antineutrino (neutrino) counterpart. For $\phi_1/\pi = 0$ the gain is proportionally the same for both, neutrinos or antineutrinos.

In order to quantify the CP violating effects from the extra terms containing the Majorana phase given in our perturbatives formulae, we use the CP violation asymmetry $\Delta P = P_{\nu_\mu \to \nu_e} - P_{\bar{\nu}_\mu \to \bar{\nu}_e}$:

$$\Delta P^{\mathrm{SO} \bigoplus \mathrm{DE}} \simeq \Delta P^{\mathrm{SO}} e^{-\bar{\Gamma}} + \frac{2\bar{\Gamma}}{3} \sin 2\theta_{12} \sin^2 \theta_{23} \sin \phi_1 e^{-\bar{\Gamma}} + ... \tag{4.49}$$

here it is displayed only the leading term $\bar{\beta}_{28} \sim \mathcal{O}\ (0.01)$ taken $\beta_{28} = -\Gamma/\sqrt{3}$, which is its maximum allowed value. The predictions from Eq. (4.49) are illustrated in Fig. 4.10 where the $\nu_\mu \to \nu_e (\bar{\nu}_\mu \to \bar{\nu}_e)$ transition probability is numerically calculated at DUNE baseline for $\Gamma = 2.5 \times 10^{-24}$ GeV. In Fig. 4.10 we see how the overall negative (positive) sign of the decoherence contribution for $\phi_1/\pi = 1.5$ ($\phi_1/\pi = 0.5$) diminish (increases) the ΔP amplitude, whilst for $\phi_1/\pi = 0.0$ is, as expected, nearly equal to the SO case.

4.5 Simulation and results: Majorana nature

In the same way as with DUNE, T2HK simulated data samples are generated with GLoBES [155, 156] and nuSQuIDS [157], introducing the configuration and inputs, such as the systematic uncertainties, from [113, 161]. We consider 258-kt detector with 3 and 9 years for neutrino and antineutrino mode, respectively. For both DUNE and T2HK, the simulated samples are created for non-null values of Γ^{true} and ϕ_1^{true} and for a value of the Dirac CP violation phase set on the measurement performed by the T2K experiment: $\delta_{\mathrm{CP}}^{true}/\pi = 1.4$ [112]. At this point it is important to mention that due to the small statistics and the large size of the uncertainties, we disregard the measurement of the Dirac CP violation claimed by NOvA experiment, which is

$\delta_{\rm CP}/\pi \sim 0.82$ [183]. In this analysis, the T2K measurement is considered as the true value of the Dirac CP violation phase since it should be unaltered by any quantum decoherence effects. This is because of the small size of the higher decoherence contributions that would be $\bar{\Gamma} \sim \mathcal{O}(0.001)$, a consequence of combining the source-detector distance of the T2K experiment with the Γ elected for this study. It should be expected, that the T2HK experiment, with the same source-detector distance, would be also unaffected by the quantum decoherence effects. Within our analysis, the T2HK Dirac CP violation phase simulated measurement, which is an upgrade in the precision of the one performed at T2K, will be used as a reference point with the expectations at DUNE.

$\Gamma = 2.5 \times 10^{-24}$ GeV	$\phi_1/\pi = 0.5$	$\phi_1/\pi = 1.0$	$\phi_1/\pi = 1.5$
$\sin^2\theta_{13}^{fit}$	0.0241	0.0242	0.0247
N_σ	0.31σ	0.34σ	0.55σ
$\delta_{\rm CP}^{fit}/\pi$	1.43	1.33	1.13
N_σ	0.08σ	1.19σ	4.34σ
$\Gamma = 3.5 \times 10^{-24}$ GeV	$\phi_1/\pi = 0.5$	$\phi_1/\pi = 1.0$	$\phi_1/\pi = 1.5$
$\sin^2\theta_{13}^{fit}$	0.0247	0.0250	0.0256
N_σ	0.54σ	0.61σ	0.87σ
$\delta_{\rm CP}^{fit}/\pi$	1.44	1.28	1.06
N_σ	0.14σ	2.37σ	5.47σ

Table 4.8: Best-fit values for $\sin^2\theta_{13}$, $\delta_{\rm CP}$ and their respective shifts in terms of σ units. We consider $\delta_{\rm CP}^{true}/\pi = 1.4$

The χ^2 analysis for DUNE and T2HK relies on the comparison between the SO phenomena, adopted as theoretical hypothesis, and simulated data that incorporates the quantum decoherence effects, where the prescription given in [172] is followed. The calculation of the $\Delta\chi^2$ is described by:

$$\Delta\chi^2 = \chi^2(\theta_{13}^{test}, \delta_{\rm CP}^{test}; \theta_{13}^{true}, \delta_{\rm CP}^{true}, \Gamma^{true}, \phi_1^{true}) - \chi^2_{min}(\theta_{13}^{fit}, \delta_{\rm CP}^{fit}; \theta_{13}^{true}, \delta_{\rm CP}^{true}, \Gamma^{true}, \phi_1^{true}) \tag{4.50}$$

where θ_{13}^{fit} and $\delta_{\rm CP}^{fit}$ are the best-fit points which minimizes the χ^2, considering priors at 3σ for the rest of the oscillation parameters but $\delta_{\rm CP}$.

The DUNE and T2HK $\Delta\chi^2$ contours, projected into $\sin^2\theta_{13}$ vs $\delta_{\rm CP}$ planes and obtained after marginalizing over the rest of SO parameters, are presented in Fig. 4.11. As expected, for T2HK, the $\sin^2\theta_{13}^{fit}$ and $\delta_{\rm CP}^{fit}$ are similar to the true ones being unmodified by the parameters chosen for decoherence. Meanwhile, for DUNE there is a slight increase of $\sin^2\theta_{13}^{fit}$, respect to the $\sin^2\theta_{13}^{true}(=0.0224)$, explicitly shown in Table. 4.8. This increment is the consequence of trying to adjust the theoretical hypothesis, SO, with the energy-independent increase of the SO $\bigoplus$ DE probability amplitude embodied in the data, and modulated by the intensity of Γ (see the third term of Eq. (4.48)).

The $\delta_{\rm CP}^{fit}$ for DUNE, when $\phi_1/\pi = 1.5$, is moving away from $\delta_{\rm CP}^{true}/\pi(=1.4)$ towards $\sim\pi$, minimizing the magnitude of the CP violation asymmetry. For $\phi_1/\pi = 0.5$ the $\delta_{\rm CP}^{fit}$ takes almost exactly the value of the true one going in the direction to maximize the CP violation asymmetry. Both features, expressed numerically in Table. 4.8, can be explained from the need to accommodate the reduction (increase) of ΔP (as seen in Eq. (4.49)), when $\phi_1/\pi = 1.5(0.5)$, seen in Fig. 4.10. The quantified dislocation, in terms of σ, from $\sin^2\theta_{13}^{fit}$ and $\delta_{\rm CP}^{fit}$ (for DUNE) to the corresponding true ones (for T2HK), for $\Gamma = \{2.5, 3.5\}\times 10^{-24}$GeV and $\phi_1/\pi = \{0.0, 0.5, 1.5\}$, is depicted in Table 4.8. The aforementioned dislocations are estimated by identifying the vertical and horizontal projection of the best-fit point of DUNE on the axes. The vertical corresponds to the $\sin^2\theta_{13}^{fit}$ dislocation and the horizontal to the $\delta_{\rm CP}^{fit}$ dislocation, as shown in Fig. 4.11. For $\Gamma = 3.5(2.5)\times 10^{-24}$GeV the most prominent shift is found for $\phi_1/\pi = 1.5$ with $0.87(0.55)\sigma$ and $5.47(4.34)\sigma$ for $\sin^2\theta_{13}^{fit}$ and $\delta_{\rm CP}^{fit}$, respectively. While, for $\Gamma = 3.5\ (2.5)\times 10^{-24}$ GeV, the dislocation of $\delta_{\rm CP}^{fit}$ reaches 3σ (2σ) and 5σ (3σ) when ϕ_1/π takes values below 1.01 (1.03) and 1.30 (1.10), respectively, the $\sin^2\theta_{13}^{fit}$ is clearly stable in front of changes along the ϕ_1 interval.

The least significant distortion is for $\phi_1/\pi = 0.5$ with $0.54(0.31)\sigma$ and $0.14(0.08)\sigma$ for $\sin^2\theta_{13}^{fit}$ and $\delta_{\rm CP}^{fit}$, respectively. A way to discriminate

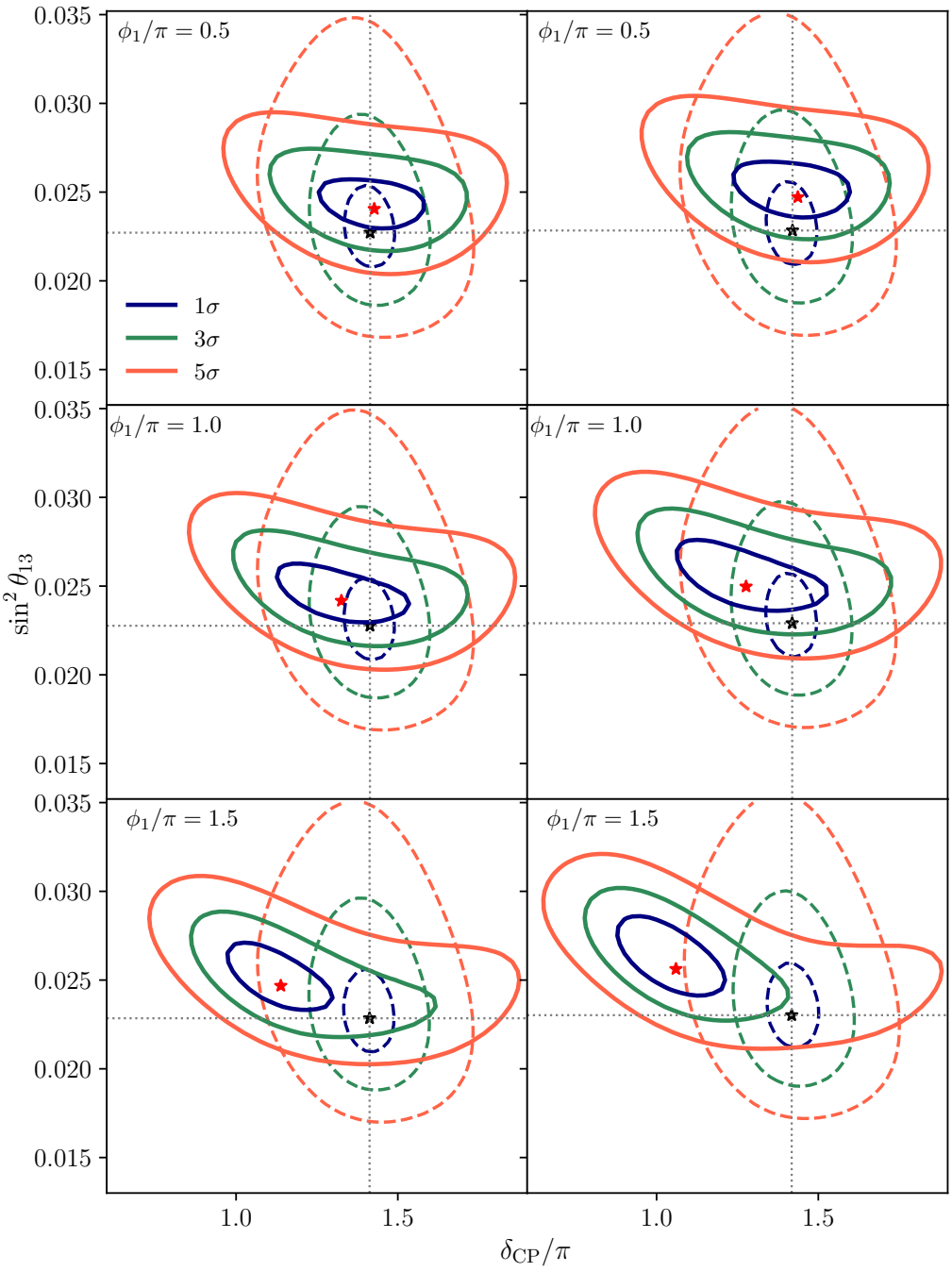

Figure 4.11: $\Delta\chi^2$ contours (2 dof) considering the effects of decoherence with Majorana phases on the standard oscillation fits. The solid and dashed lines are decoherence with $\beta_{28} = -\Gamma/\sqrt{3}$ for the DUNE and T2HK experiments, respectively. The left column is $\Gamma = 2.5 \times 10^{-24}$GeV and the right column is $\Gamma = 3.5 \times 10^{-24}$GeV. We consider $\delta_{\rm CP}^{true}/\pi = 1.4$.

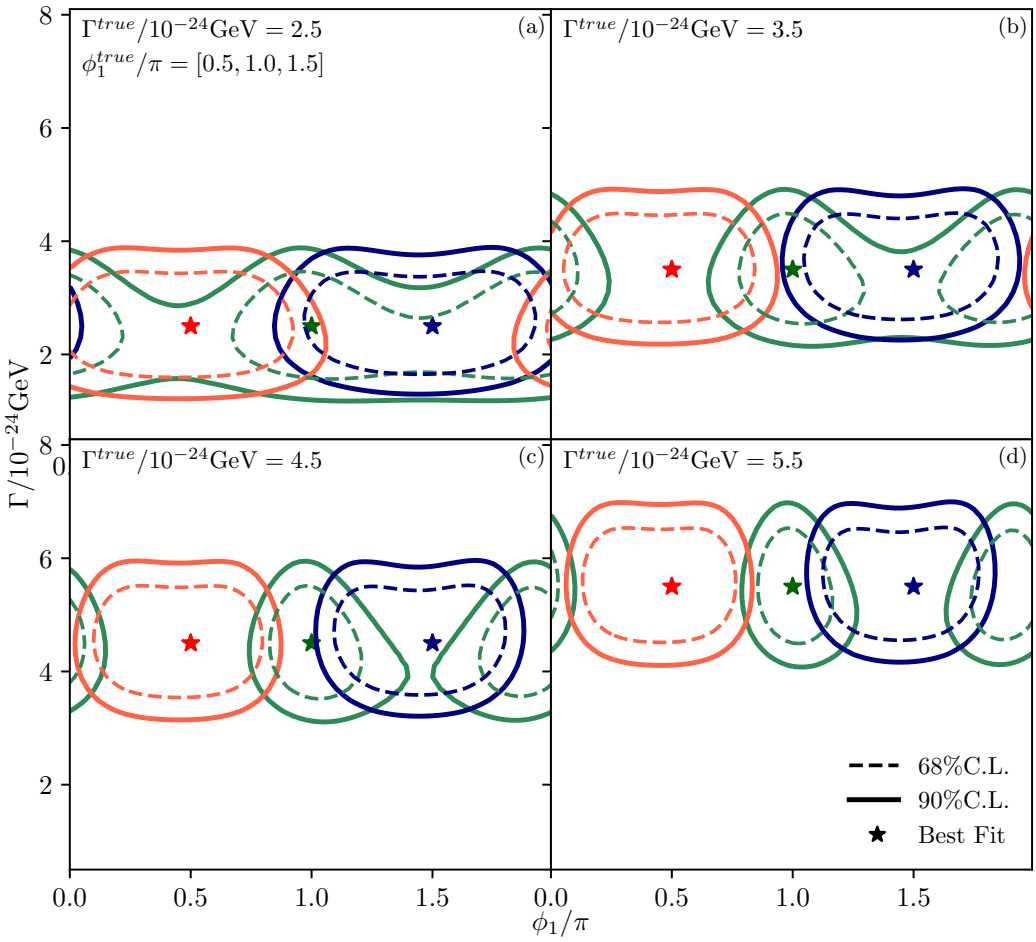

Figure 4.12: DUNE's ability to constrain (2 dof) the decoherence parameter and the Majorana phase. The red, green and blue lines represent $\phi^{true}/\pi = 0.5, 1.0, 1.5$, respectively.

between different values of ϕ_1 is through the ratio ($\mathcal{R}_\mathcal{M}$) of the number of σ deviation for $\sin^2\theta_{13}^{fit}$ to the corresponding ones for δ_{CP}^{fit}. In fact, a sort of discernment is achieved, for instance, for $\Gamma = 3.5(2.5) \times 10^{-24}$ GeV, $\mathcal{R}_\mathcal{M} \sim 0.16(0.13) - 0.26(0.29)$ for the interval $\phi_1/\pi = 1.0, 1.5$ reaching values up to $\sim 3.86(3.88)$ for $\phi_1/\pi = 0.5$. A plus that reinforces the utility of $\mathcal{R}_\mathcal{M}$ is its low variations against changes of Γ.

The aforementioned analysis had the purpose of searching for distortions in $\sin^2\theta_{13}^{fit}$ and δ_{CP}^{fit}, considering pure SO as theoretical hypothesis.

Now, the aim is to go one step further and to explore the capacity of DUNE for measuring the Majorana phase, and also Γ, under the (SO) plus decoherence (DE) as theoretical hypothesis, for $\phi_1/\pi = 0.5, 1$ and 1.5. We use for $\Gamma/10^{-24}\text{GeV} = 2.5, 3.5, 4.5$ and 5.5. In Fig. 4.12 the different allowed regions are displayed considering 68 % and 90 % C.L. for 2 dof. For $\Gamma/10^{-24}$ GeV = 2.5 and 3.5 is not possible to clearly disentangle the value of $\phi_1/\pi = 1.0$ at 90% of C.L. from $\phi_1/\pi = 0.5$ and 1.5. Meanwhile, for slightly increased values of $\Gamma/10^{-24}$ GeV = 4.5 and 5.5, the value of $\phi_1/\pi = 1.0$ is excluded at 90% either for $\phi_1/\pi = 0.5$ and 1.5, being able to separate between the chosen values of the Majorana phases ϕ_1. Thus, it is seen that DUNE is able to measure $\phi_1/\pi = 1.50 \pm 0.35(0.32)$ and $\phi_1/\pi = 0.50 \pm 0.35(0.32)$ and $\Gamma = 4.50 \pm 1.38(5.50 \pm 1.42) \times 10^{-24}$ GeV. While for $\phi_1/\pi = 1.0 \pm 0.19(0.15)$ a $\Gamma = 4.50 \pm 1.42(5.50 \pm 1.46) \times 10^{-24}$ GeV is obtained.

All the values of Γ used in our analysis are below the decoherence limits for handmade artificial sources [32] and cannot be compared with the limits imposed by Ice Cube [184] since we are considering a non-diagonal scenario for the decoherence matrix.

4.6 Summary and Conclusions

Firstly, this chapter reveals that an apparent breakdown of the fundamental CPT symmetry can occur when the environment affects the neutrino system, in the context of the DUNE experiment. This CPTV is produced by the combination of having δ_{CP} in the neutrino sector with a specific set of some non-null coherences terms in the dissipative matrix. Moreover, we have quantified a potential measurement of this CPTV employing the disappearance channels $\nu_\mu \to \nu_\mu$ and $\bar{\nu}_\mu \to \bar{\nu}_\mu$, their corresponding backgrounds, and an observable $\mathcal{R}$.

We perform the simulated $\mathcal{R}$ measurements assuming four hypotheses of energy dependence on the decoherence parameters: $n = -1, 0, 1$, and 2,

where $\Gamma_{E_\nu} = \Gamma(E_\nu/\text{GeV})^n$. Considering the following values of Γ: $\{13.1, 4.6, 2.1, 0.8\} \times 10^{-23}$GeV, for $n = -1, 0, 1$ and 2, respectively, and $\delta_{CP} = 3\pi/2$, which is relatively close to the current value of δ_{CP} given by the global fit [171] and the T2K measurement, we achieve a 5σ for $\mathcal{R}$ concerning its expectation value at the SO case, $\mathcal{R} = 1$. At all these points, the DDM is consistent with the SO case. Meanwhile, for $\delta_{CP} = \pi/2$, we get discrepancies of the order of 3σ. Additionally, in our best case, with an energy dependency $n = 2$, we have $\Gamma \simeq 10^{-24}$GeV, but with the incapacity to discriminate from the DDM case.

We also show the strong displacement displayed by the measured value of δ_{CP} at DUNE induced by decoherence and the Majorana phases, compared with the one measured at T2HK, where the decoherence effects would not influence. For a decoherence parameter $\Gamma = 3.5 \times 10^{-24}$ GeV, the aforementioned displacement can be as large as 5.47 σ for a Majorana phase $\phi_1 = 1.5\pi$. Additionally, we estimated the power of the DUNE experiment in constraining the Majorana phase, achieving a precision of 23% (21%) for $\phi_1/\pi = 1.5$ with $\Gamma = 4.5(5.5)\times10^{-24}$GeV. These precision values are consistent with the recent results on the Dirac CP phase reached by the T2K experiment [112].

CHAPTER 5

CONCLUSIONS

We analyzed the potential of long baseline neutrino oscillation experiments, DUNE and T2HK, to detect manifestations of new physics. Among the physics scenarios studied beyond the standard model is the violation of the equivalence principle and within the framework of quantum decoherence, the CPT violation, and the emergence of the Majorana nature via the neutrino in the oscillation phenomenon.

First, we study the possible manifestations of the VEP in the DUNE experiment. Among the findings, we have the distortion of the measurements of the parameters Δm^2_{31}, $\sin^2\theta_{13}$ and $\delta_{\rm CP}$ when we consider the VEP in nature but not in our hypothesis. In addition, the VEP affects the DUNE CP sensitivity, causing the manifestation of a fake CP violation. Similarly, the different VEP scenarios alter the sensitivity of the DUNE experiment for the mass hierarchy. We find the sensitivity limits of the DUNE experiment for the

VEP and LV with different energy dependencies.

Second, it is essential to note that the observations indicated in chapter 4 about CPTV emerge when we treat the neutrino system as an open system. The latter means that it is possible that if we had access to the information of the environment, i.e., to the entire system, the general CPT symmetry would be preserved. Consequently, it deserves a more profound study to ascertain if this CPTV is breaking at the fundamental level or if it is only an apparent one because of our lack of information from the environment.

Finally, within the context of quantum decoherence, we demonstrated the possibility of revealing the Majorana nature of neutrinos through the oscillation phenomenon in the DUNE experiment. Therefore, we can infer that if decoherence exists in the mode indicated in chapter 4 , DUNE would be an exciting opportunity to perform a first-time measurement of the Majorana CP phase with some reasonable uncertainties.

APPENDIX A

CONSTRAINTS FOR THE DECOHERENCE MATRIX ELEMENTS

For the two-flavor and three-flavor case, the conditions for the decoherence entries can be found in [61] and [185], respectively. Here we display the latter:

$$
\begin{aligned}
0 \leq |\vec{a}_1| &= -\gamma_1 + \gamma_2 + \gamma_3 - \frac{1}{3}\gamma_8, \\
0 \leq |\vec{a}_2| &= \gamma_1 - \gamma_2 + \gamma_3 - \frac{1}{3}\gamma_8, \\
0 \leq |\vec{a}_3| &= \gamma_1 + \gamma_2 - \gamma_3 - \frac{1}{3}\gamma_8, \\
0 \leq |\vec{a}_4| &= -\gamma_4 + \gamma_5 + \frac{2}{3}\gamma_8 - \frac{2}{\sqrt{3}}\beta_{38}, \\
0 \leq |\vec{a}_5| &= \gamma_4 - \gamma_5 + \frac{2}{3}\gamma_8 - \frac{2}{\sqrt{3}}\beta_{38}, \\
0 \leq |\vec{a}_6| &= -\gamma_6 + \gamma_7 + \frac{2}{3}\gamma_8 + \frac{2}{\sqrt{3}}\beta_{38},
\end{aligned}
$$

$$
\begin{aligned}
0 \leq |\vec{a}_7| &= \gamma_6 - \gamma_7 + \frac{2}{3}\gamma_8 + \frac{2}{\sqrt{3}}\beta_{38}, \\
0 \leq |\vec{a}_8| &= -\frac{1}{3}\gamma_1 - \frac{1}{3}\gamma_2 - \frac{1}{3}\gamma_3 \\
&\quad + \frac{2}{3}\gamma_4 + \frac{2}{3}\gamma_5 + \frac{2}{3}\gamma_6 + \frac{2}{3}\gamma_7 - \gamma_8.
\end{aligned} \tag{A.1}
$$

Being their Schwartz inequalities:

$$
\begin{aligned}
4{\beta_{12}}^2 &\leq \left(\gamma_3 - \frac{\gamma_8}{3}\right)^2 - \left(\gamma_1 - \gamma_2\right)^2, \\
4{\beta_{13}}^2 &\leq \left(\gamma_2 - \frac{\gamma_8}{3}\right)^2 - \left(\gamma_1 - \gamma_3\right)^2, \\
4{\beta_{23}}^2 &\leq \left(\gamma_1 - \frac{\gamma_8}{3}\right)^2 - \left(\gamma_2 - \gamma_3\right)^2, \\
4{\beta_{45}}^2 &\leq \left(\frac{2\gamma_8}{3} - \frac{2\beta_{38}}{\sqrt{3}}\right)^2 - \left(\gamma_4 - \gamma_5\right)^2, \\
4{\beta_{67}}^2 &\leq \left(\frac{2\gamma_8}{3} + \frac{2\beta_{38}}{\sqrt{3}}\right)^2 - \left(\gamma_6 - \gamma_7\right)^2,
\end{aligned}
$$

$$
\begin{aligned}
\left(\frac{2}{3}\beta_{38} + \frac{1}{\sqrt{3}}\gamma_4 + \frac{1}{\sqrt{3}}\gamma_5 - \frac{1}{\sqrt{3}}\gamma_6 - \frac{1}{\sqrt{3}}\gamma_7\right)^2 &\leq |\vec{a}_3||\vec{a}_8|, \\
\left(\frac{1}{\sqrt{3}}\beta_{16} - \frac{1}{\sqrt{3}}\beta_{27} + \frac{1}{\sqrt{3}}\beta_{34} + \frac{5}{3}\beta_{48}\right)^2 &\leq |\vec{a}_4||\vec{a}_8|, \\
\left(\frac{1}{\sqrt{3}}\beta_{17} + \frac{1}{\sqrt{3}}\beta_{26} + \frac{1}{\sqrt{3}}\beta_{35} + \frac{5}{3}\beta_{58}\right)^2 &\leq |\vec{a}_5||\vec{a}_8|, \\
\left(\frac{1}{\sqrt{3}}\beta_{14} + \frac{1}{\sqrt{3}}\beta_{25} - \frac{1}{\sqrt{3}}\beta_{36} + \frac{5}{3}\beta_{68}\right)^2 &\leq |\vec{a}_6||\vec{a}_8|, \\
\left(\frac{1}{\sqrt{3}}\beta_{15} - \frac{1}{\sqrt{3}}\beta_{24} - \frac{1}{\sqrt{3}}\beta_{37} + \frac{5}{3}\beta_{78}\right)^2 &\leq |\vec{a}_7||\vec{a}_8|, \\
\left(\beta_{14} - \beta_{25} + \beta_{36} + \frac{1}{\sqrt{3}}\beta_{68}\right)^2 &\leq |\vec{a}_1||\vec{a}_4|, \\
\left(\beta_{15} + \beta_{24} + \beta_{37} + \frac{1}{\sqrt{3}}\beta_{78}\right)^2 &\leq |\vec{a}_1||\vec{a}_5|, \\
\left(\beta_{16} + \beta_{27} - \beta_{34} + \frac{1}{\sqrt{3}}\beta_{48}\right)^2 &\leq |\vec{a}_1||\vec{a}_6|, \\
\left(\beta_{17} - \beta_{26} - \beta_{35} + \frac{1}{\sqrt{3}}\beta_{58}\right)^2 &\leq |\vec{a}_1||\vec{a}_7|, \\
\left(\frac{2}{3}\beta_{18} - \frac{2}{\sqrt{3}}\beta_{46} - \frac{2}{\sqrt{3}}\beta_{57}\right)^2 &\leq |\vec{a}_1||\vec{a}_8|, \\
\left(\beta_{15} + \beta_{24} - \beta_{37} - \frac{1}{\sqrt{3}}\beta_{78}\right)^2 &\leq |\vec{a}_2||\vec{a}_4|, \\
\left(\beta_{14} - \beta_{25} - \beta_{36} - \frac{1}{\sqrt{3}}\beta_{68}\right)^2 &\leq |\vec{a}_2||\vec{a}_5|, \\
\left(\beta_{17} - \beta_{26} + \beta_{35} - \frac{1}{\sqrt{3}}\beta_{58}\right)^2 &\leq |\vec{a}_2||\vec{a}_6|,
\end{aligned}
$$

$$
\begin{aligned}
\left(\beta_{16}+\beta_{27}+\beta_{34}-\frac{1}{\sqrt{3}}\beta_{48}\right)^2 &\leq |\vec{a}_2||\vec{a}_7|,\\
\left(\frac{2}{3}\beta_{28}+\frac{2}{\sqrt{3}}\beta_{47}-\frac{2}{\sqrt{3}}\beta_{56}\right)^2 &\leq |\vec{a}_2||\vec{a}_8|,\\
\left(\beta_{16}-\beta_{27}-\beta_{34}-\frac{1}{\sqrt{3}}\beta_{48}\right)^2 &\leq |\vec{a}_3||\vec{a}_4|,\\
\left(\beta_{17}+\beta_{26}-\beta_{35}-\frac{1}{\sqrt{3}}\beta_{58}\right)^2 &\leq |\vec{a}_3||\vec{a}_5|,\\
\left(\beta_{14}+\beta_{25}+\beta_{36}-\frac{1}{\sqrt{3}}\beta_{68}\right)^2 &\leq |\vec{a}_3||\vec{a}_6|,\\
\left(\beta_{15}-\beta_{24}+\beta_{37}-\frac{1}{\sqrt{3}}\beta_{78}\right)^2 &\leq |\vec{a}_3||\vec{a}_7|,\\
\left(\beta_{46}-\beta_{57}-\frac{2}{\sqrt{3}}\beta_{18}\right)^2 &\leq |\vec{a}_4||\vec{a}_6|,\\
\left(\beta_{47}+\beta_{56}+\frac{2}{\sqrt{3}}\beta_{28}\right)^2 &\leq |\vec{a}_4||\vec{a}_7|,\\
\left(\beta_{47}+\beta_{56}-\frac{2}{\sqrt{3}}\beta_{28}\right)^2 &\leq |\vec{a}_5||\vec{a}_6|,\\
\left(\beta_{46}-\beta_{57}+\frac{2}{\sqrt{3}}\beta_{18}\right)^2 &\leq |\vec{a}_5||\vec{a}_7|.
\end{aligned}
\tag{A.2}
$$

Moreover, in order to analyze the positivity for the matrix $\mathbf{A}$, we use for simplicity our optimal case composed by β_{12}, β_{28}, β_{56} and β_{47},

$$
\mathbf{D}=\begin{pmatrix}
-\Gamma & \beta_{12} & 0 & 0 & 0 & 0 & 0 & 0\\
\beta_{12} & -\Gamma & 0 & 0 & 0 & 0 & 0 & \beta_{28}\\
0 & 0 & -\Gamma & 0 & 0 & 0 & 0 & 0\\
0 & 0 & 0 & -\Gamma & 0 & 0 & \beta_{47} & 0\\
0 & 0 & 0 & 0 & -\Gamma & \beta_{56} & 0 & 0\\
0 & 0 & 0 & 0 & \beta_{56} & -\Gamma & 0 & 0\\
0 & 0 & 0 & \beta_{47} & 0 & 0 & -\Gamma & 0\\
0 & \beta_{28} & 0 & 0 & 0 & 0 & 0 & -\Gamma
\end{pmatrix},
\tag{A.3}
$$

then, the matrix $\mathbf{A} \equiv [a_{kj}]$ is

$$\mathbf{A} = \begin{pmatrix} -\Gamma' & \beta'_{12} & 0 & 0 & 0 & 0 & 0 & 0 \\ \beta'_{12} & -\Gamma' & 0 & 0 & 0 & 0 & 0 & \beta'_{28} \\ 0 & 0 & -\Gamma' & 0 & 0 & 0 & 0 & 0 \\ 0 & 0 & 0 & -\Gamma' & 0 & 0 & \beta'_{47} & 0 \\ 0 & 0 & 0 & 0 & -\Gamma' & \beta'_{56} & 0 & 0 \\ 0 & 0 & 0 & 0 & \beta'_{56} & -\Gamma' & 0 & 0 \\ 0 & 0 & 0 & \beta'_{47} & 0 & 0 & -\Gamma' & 0 \\ 0 & \beta'_{28} & 0 & 0 & 0 & 0 & 0 & -\Gamma' \end{pmatrix}, \tag{A.4}$$

with

$$\begin{aligned} \Gamma' = -\frac{2}{3}\Gamma, \quad \beta'_{12} = 2\beta_{12}, \\ \beta'_{28} = \frac{2}{3}\left(\beta_{28} + \sqrt{3}(\beta_{47} - \beta_{56})\right), \\ \beta'_{56} = \beta_{47} + \beta_{56} - \frac{2}{\sqrt{3}}\beta_{28}, \\ \beta'_{47} = \beta_{47} + \beta_{56} + \frac{2}{\sqrt{3}}\beta_{28}. \end{aligned} \tag{A.5}$$

We get its corresponding eigenvalues:

$$\begin{aligned} \lambda_{1,2} = \frac{2}{3}\Gamma \geq 0, \\ \lambda_{3,4} = \frac{1}{3}\left(2\Gamma - 3(\beta_{47} + \beta_{56}) \mp 2\sqrt{3}\beta_{28}\right) \geq 0, \\ \lambda_{5,6} = \frac{1}{3}\left(2\Gamma + 3(\beta_{47} + \beta_{56}) \mp 2\sqrt{3}\beta_{28}\right) \geq 0, \\ \lambda_{7,8} = \frac{2}{3}\Big(\Gamma \mp \big(9\beta_{12}^2 + \beta_{28}^2 + 3(\beta_{47}^2 + \beta_{56}^2) \\ + 2\sqrt{3}\beta_{28}(\beta_{47} - \beta_{56}) - 6\beta_{47}\beta_{56}\big)^{1/2}\Big) \geq 0. \end{aligned} \tag{A.6}$$

Thus, using Eqs. (A.6) and (A.2), we can obtain the following individual maximum values for the said β's: $|\beta_{28}| = 1/\sqrt{3}$, $|\beta_{12}| = 1/3$, $|\beta_{56}| = 1/\sqrt{3}$ and $|\beta_{47}| = 1/\sqrt{3}$.

While, when we set on all the aforementioned β's together, and following the procedure described in section 4.2, we get afterwards: $\beta_{28} = \Gamma/\sqrt{3}$, $\beta_{12} = (\sqrt{2/3})\Gamma/3$ and $\beta_{56} = -\beta_{47} = \Gamma/3$.

BIBLIOGRAPHY

[1] S. Fukuda *et al.*, "Solar B-8 and hep neutrino measurements from 1258 days of Super-Kamiokande data," *Phys. Rev. Lett.*, vol. 86, pp. 5651–5655, 2001. DOI: 10.1103/PhysRevLett.86.5651. arXiv: hep-ex/0103032.

[2] A. B. McDonald, "Sudbury neutrino observatory results," *Phys. Scripta T*, vol. 121, L. Bergström, O. Botner, P. Carlson, P. O. Hulth, and T. Ohlsson, Eds., pp. 29–32, 2005. DOI: 10.1088/0031-8949/2005/T121/003. arXiv: hep-ex/0412060.

[3] Q. R. Ahmad *et al.*, "Measurement of day and night neutrino energy spectra at SNO and constraints on neutrino mixing parameters," *Phys. Rev. Lett.*, vol. 89, p. 011 302, 2002. DOI: 10.1103/PhysRevLett.89.011302. arXiv: nucl-ex/0204009.

[4] Y. Fukuda *et al.*, "Evidence for oscillation of atmospheric neutrinos," *Phys. Rev. Lett.*, vol. 81, pp. 1562–1567, 1998. DOI: 10.1103/PhysRevLett.81.1562. arXiv: hep-ex/9807003.

[5] T. Kajita, E. Kearns, and M. Shiozawa, "Establishing atmospheric neutrino oscillations with Super-Kamiokande," *Nucl. Phys. B*, vol. 908, pp. 14–29, 2016. DOI: 10.1016/j.nuclphysb.2016.04.017.

[6] T. Araki *et al.*, "Measurement of neutrino oscillation with KamLAND: Evidence of spectral distortion," *Phys. Rev. Lett.*, vol. 94, p. 081 801, 2005. DOI: 10.1103/PhysRevLett.94.081801. arXiv: hep-ex/0406035.

[7] F. P. An *et al.*, "Observation of electron-antineutrino disappearance at Daya Bay," *Phys. Rev. Lett.*, vol. 108, p. 171 803, 2012. DOI: 10.1103/PhysRevLett.108.171803. arXiv: 1203.1669 [hep-ex].

[8] P. Adamson *et al.*, "A Study of Muon Neutrino Disappearance Using the Fermilab Main Injector Neutrino Beam," *Phys. Rev. D*, vol. 77, p. 072 002, 2008. DOI: 10.1103/PhysRevD.77.072002. arXiv: 0711.0769 [hep-ex].

[9] J. K. Ahn *et al.*, "Observation of Reactor Electron Antineutrino Disappearance in the RENO Experiment," *Phys. Rev. Lett.*, vol. 108, p. 191 802, 2012. DOI: 10.1103/PhysRevLett.108.191802. arXiv: 1204.0626 [hep-ex].

[10] Y. Abe *et al.*, "Indication of Reactor $\bar{\nu}_e$ Disappearance in the Double Chooz Experiment," *Phys. Rev. Lett.*, vol. 108, p. 131 801, 2012. DOI: 10.1103/PhysRevLett.108.131801. arXiv: 1112.6353 [hep-ex].

[11] A. M. Gago, M. M. Guzzo, H. Nunokawa, W. J. C. Teves, and R. Zukanovich Funchal, "Probing flavor changing neutrino interactions using neutrino beams from a muon storage ring," *Phys. Rev. D*, vol. 64, p. 073 003, 2001. DOI: 10.1103/PhysRevD.64.073003. arXiv: hep-ph/0105196.

[12] M. M. Guzzo, P. C. de Holanda, and O. L. G. Peres, "Effects of non-standard neutrino interactions on MSW - LMA solution to the solar neutrino problems," *Phys. Lett. B*, vol. 591, pp. 1–6, 2004. DOI: 10.1016/j.physletb.2004.04.035. arXiv: hep-ph/0403134.

[13] A. de Gouvêa and K. J. Kelly, "Non-standard neutrino interactions at dune," *Nucl. Phys. B*, vol. 908, pp. 318–335, 2016. DOI: 10.1016/j.nuclphysb.2016.03.013. arXiv: 1511.05562 [hep-ph].

[14] M. Masud and P. Mehta, "Nonstandard interactions and resolving the ordering of neutrino masses at DUNE and other long baseline experiments," *Phys. Rev. D*, vol. 94, no. 5, p. 053 007, 2016. DOI: 10.1103/PhysRevD.94.053007. arXiv: 1606.05662 [hep-ph].

[15] J. Liao, D. Marfatia, and K. Whisnant, "Nonstandard neutrino interactions at DUNE, T2HK and T2HKK," *JHEP*, vol. 01, p. 071, 2017. DOI: 10.1007/JHEP01(2017)071. arXiv: 1612.01443 [hep-ph].

[16] J. A. Frieman, H. E. Haber, and K. Freese, "Neutrino Mixing, Decays and Supernova Sn1987a," *Phys. Lett. B*, vol. 200, pp. 115–121, 1988. DOI: 10.1016/0370-2693(88)91120-3.

[17] P. F. de Salas, S. Pastor, C. A. Ternes, T. Thakore, and M. Tórtola, "Constraining the invisible neutrino decay with KM3NeT-ORCA," *Phys. Lett. B*, vol. 789, pp. 472–479, 2019. DOI: 10.1016/j.physletb.2018.12.066. arXiv: 1810.10916 [hep-ph].

[18] V. D. Barger, J. G. Learned, P. Lipari, M. Lusignoli, S. Pakvasa, and T. J. Weiler, "Neutrino decay and atmospheric neutrinos," *Phys. Lett. B*, vol. 462, pp. 109–114, 1999. DOI: 10.1016/S0370-2693(99)00887-4. arXiv: hep-ph/9907421.

[19] A. Bandyopadhyay, S. Choubey, and S. Goswami, "Neutrino decay confronts the SNO data," *Phys. Lett. B*, vol. 555, pp. 33–42, 2003. DOI: 10.1016/S0370-2693(03)00044-3. arXiv: hep-ph/0204173.

[20] G. L. Fogli, E. Lisi, A. Mirizzi, and D. Montanino, "Three generation flavor transitions and decays of supernova relic neutrinos," *Phys. Rev. D*, vol. 70, p. 013 001, 2004. DOI: 10.1103/PhysRevD.70.013001. arXiv: hep-ph/0401227.

[21] J. M. Berryman, A. de Gouvêa, D. Hernández, and R. L. N. Oliveira, "Non-Unitary Neutrino Propagation From Neutrino Decay," *Phys. Lett. B*, vol. 742, pp. 74–79, 2015. DOI: 10.1016/j.physletb.2015.01.002. arXiv: 1407.6631 [hep-ph].

[22] R. Picoreti, M. M. Guzzo, P. C. de Holanda, and O. L. G. Peres, "Neutrino Decay and Solar Neutrino Seasonal Effect," *Phys. Lett. B*, vol. 761, pp. 70–73, 2016. DOI: 10.1016/j.physletb.2016.08.007. arXiv: 1506.08158 [hep-ph].

[23] M. Bustamante, J. F. Beacom, and K. Murase, "Testing decay of astrophysical neutrinos with incomplete information," *Phys. Rev. D*, vol. 95, no. 6, p. 063 013, 2017. DOI: 10.1103/PhysRevD.95.063013. arXiv: 1610.02096 [astro-ph.HE].

[24] A. M. Gago, R. A. Gomes, A. L. G. Gomes, J. Jones-Perez, and O. L. G. Peres, "Visible neutrino decay in the light of appearance and disappearance long baseline experiments," *JHEP*, vol. 11, p. 022, 2017. DOI: 10.1007/JHEP11(2017)022. arXiv: 1705.03074 [hep-ph].

[25] M. V. Ascencio-Sosa, A. M. Calatayud-Cadenillas, A. M. Gago, and J. Jones-Pérez, "Matter effects in neutrino visible decay at future long-baseline experiments," *Eur. Phys. J. C*, vol. 78, no. 10, p. 809, 2018. DOI: 10.1140/epjc/s10052-018-6276-0. arXiv: 1805.03279 [hep-ph].

[26] E. Lisi, A. Marrone, and D. Montanino, "Probing possible decoherence effects in atmospheric neutrino oscillations," *Phys. Rev. Lett.*, vol. 85,

pp. 1166–1169, 2000. DOI: 10.1103/PhysRevLett.85.1166. arXiv: hep-ph/0002053.

[27] G. Barenboim, N. E. Mavromatos, S. Sarkar, and A. Waldron-Lauda, "Quantum decoherence and neutrino data," *Nucl. Phys. B*, vol. 758, pp. 90–111, 2006. DOI: 10.1016/j.nuclphysb.2006.09.012. arXiv: hep-ph/0603028.

[28] P. Bakhti, Y. Farzan, and T. Schwetz, "Revisiting the quantum decoherence scenario as an explanation for the LSND anomaly," *JHEP*, vol. 05, p. 007, 2015. DOI: 10.1007/JHEP05(2015)007. arXiv: 1503.05374 [hep-ph].

[29] J. Carpio, E. Massoni, and A. M. Gago, "Revisiting quantum decoherence for neutrino oscillations in matter with constant density," *Phys. Rev. D*, vol. 97, no. 11, p. 115 017, 2018. DOI: 10.1103/PhysRevD.97.115017. arXiv: 1711.03680 [hep-ph].

[30] A. Capolupo, S. M. Giampaolo, and G. Lambiase, "Decoherence in neutrino oscillations, neutrino nature and CPT violation," *Phys. Lett. B*, vol. 792, pp. 298–303, 2019. DOI: 10.1016/j.physletb.2019.03.062. arXiv: 1807.07823 [hep-ph].

[31] J. C. Carrasco, F. N. Díaz, and A. M. Gago, "Probing CPT breaking induced by quantum decoherence at DUNE," *Phys. Rev. D*, vol. 99, no. 7, p. 075 022, 2019. DOI: 10.1103/PhysRevD.99.075022. arXiv: 1811.04982 [hep-ph].

[32] A. L. G. Gomes, R. A. Gomes, and O. L. G. Peres, "Quantum decoherence and relaxation in neutrinos using long-baseline data," Jan. 2020. arXiv: 2001.09250 [hep-ph].

[33] O. Yasuda, "A Test of a kind of the equivalence principle by long baseline neutrino oscillation experiments," in *3rd Workshop on General Relativity and Gravitation*, Mar. 1994, pp. 0510–516. arXiv: gr-qc/9403023.

[34] A. Datta, "Probing the violation of equivalence principle at a muon storage ring via neutrino oscillation," *Phys. Lett. B*, vol. 504, pp. 247–253, 2001. DOI: 10.1016/S0370-2693(01)00299-4. arXiv: hep-ph/0011240.

[35] G. Valdiviesso, "Novos limites para violação do princípio da equivalência em neutrinos solares," Ph.D. dissertation, University of Campinas, Brazil, 2008.

[36] G. A. Valdiviesso, M. M. Guzzo, and P. C. Holanda, "Equivalence Principle from the Solar and Reactor Neutrino Observations," *Nucl. Phys. B Proc. Suppl.*, vol. 229-232, G. S. Tzanakos, Ed., p. 452, 2012. DOI: 10.1016/j.nuclphysbps.2012.09.089.

[37] A. Esmaili, D. R. Gratieri, M. M. Guzzo, P. C. de Holanda, O. L. G. Peres, and G. A. Valdiviesso, "Constraining the violation of the equivalence principle with IceCube atmospheric neutrino data," *Phys. Rev. D*, vol. 89, no. 11, p. 113 003, 2014. DOI: 10.1103/PhysRevD.89.113003. arXiv: 1404.3608 [hep-ph].

[38] P. Adamson *et al.*, "Testing Lorentz Invariance and CPT Conservation with NuMI Neutrinos in the MINOS Near Detector," *Phys. Rev. Lett.*, vol. 101, p. 151 601, 2008. DOI: 10.1103/PhysRevLett.101.151601. arXiv: 0806.4945 [hep-ex].

[39] A. A. Aguilar-Arevalo *et al.*, "Test of Lorentz and CPT violation with Short Baseline Neutrino Oscillation Excesses," *Phys. Lett. B*, vol. 718, pp. 1303–1308, 2013. DOI: 10.1016/j.physletb.2012.12.020. arXiv: 1109.3480 [hep-ex].

[40] Y.-F. Li and Z.-h. Zhao, "Tests of Lorentz and CPT Violation in the Medium Baseline Reactor Antineutrino Experiment," *Phys. Rev. D*, vol. 90, no. 11, p. 113 014, 2014. DOI: 10.1103/PhysRevD.90.113014. arXiv: 1409.6970 [hep-ph].

[41] D. Colladay and V. A. Kostelecky, "CPT violation and the standard model," *Phys. Rev. D*, vol. 55, pp. 6760–6774, 1997. DOI: 10.1103/PhysRevD.55.6760. arXiv: hep-ph/9703464.

[42] S. R. Coleman and S. L. Glashow, "High-energy tests of Lorentz invariance," *Phys. Rev. D*, vol. 59, p. 116 008, 1999. DOI: 10.1103/PhysRevD.59.116008. arXiv: hep-ph/9812418.

[43] S. R. Coleman and S. L. Glashow, "Cosmic ray and neutrino tests of special relativity," *Phys. Lett. B*, vol. 405, pp. 249–252, 1997. DOI: 10.1016/S0370-2693(97)00638-2. arXiv: hep-ph/9703240.

[44] M. Gasperini, "Testing the Principle of Equivalence with Neutrino Oscillations," *Phys. Rev. D*, vol. 38, pp. 2635–2637, 1988. DOI: 10.1103/PhysRevD.38.2635.

[45] M. Gasperini, "Experimental Constraints on a Minimal and Nonminimal Violation of the Equivalence Principle in the Oscillations of Massive Neutrinos," *Phys. Rev. D*, vol. 39, pp. 3606–3611, 1989. DOI: 10.1103/PhysRevD.39.3606.

[46] A. Halprin and C. N. Leung, "Can the sun shed light on neutrino gravitational interactions?" *Phys. Rev. Lett.*, vol. 67, pp. 1833–1835, 1991. DOI: 10.1103/PhysRevLett.67.1833.

[47] J. T. Pantaleone, A. Halprin, and C. N. Leung, "Neutrino mixing due to a violation of the equivalence principle," *Phys. Rev. D*, vol. 47, R4199–R4202, 1993. DOI: 10.1103/PhysRevD.47.R4199. arXiv: hep-ph/9211214.

[48] M. N. Butler, S. Nozawa, R. A. Malaney, and A. I. Boothroyd, "Gravitationally induced neutrino oscillations," *Phys. Rev. D*, vol. 47, pp. 2615–2618, 1993. DOI: 10.1103/PhysRevD.47.2615.

[49] J. N. Bahcall, P. I. Krastev, and C. N. Leung, "Solar neutrinos and the principle of equivalence," *Phys. Rev. D*, vol. 52, pp. 1770–1779, 1995. DOI: 10.1103/PhysRevD.52.1770. arXiv: hep-ph/9410353.

[50] S. W. Mansour and T.-K. Kuo, "Solar neutrinos and the violation of equivalence principle," *Phys. Rev. D*, vol. 60, p. 097 301, 1999. DOI: 10.1103/PhysRevD.60.097301. arXiv: hep-ph/9810510.

[51] A. M. Gago, H. Nunokawa, and R. Zukanovich Funchal, "The Solar neutrino problem and gravitationally induced long wavelength neutrino oscillation," *Phys. Rev. Lett.*, vol. 84, pp. 4035–4038, 2000. DOI: 10.1103/PhysRevLett.84.4035. arXiv: hep-ph/9909250.

[52] T. Alion *et al.*, "Experiment Simulation Configurations Used in DUNE CDR," Jun. 2016. arXiv: 1606.09550 [physics.ins-det].

[53] R. Acciarri *et al.*, "Long-Baseline Neutrino Facility (LBNF) and Deep Underground Neutrino Experiment (DUNE): Conceptual Design Report, Volume 2: The Physics Program for DUNE at LBNF," Dec. 2015. arXiv: 1512.06148 [physics.ins-det].

[54] D. Colladay and V. A. Kostelecky, "Lorentz violating extension of the standard model," *Phys. Rev. D*, vol. 58, p. 116 002, 1998. DOI: 10.1103/PhysRevD.58.116002. arXiv: hep-ph/9809521.

[55] V. A. Kostelecky and S. Samuel, "Spontaneous Breaking of Lorentz Symmetry in String Theory," *Phys. Rev. D*, vol. 39, p. 683, 1989. DOI: 10.1103/PhysRevD.39.683.

[56] M. Bustamante, A. M. Gago, and C. Pena-Garay, "Energy-Independent New Physics in the Flavour Ratios of High-Energy Astrophysical Neutrinos," *JHEP*, vol. 04, p. 066, 2010. DOI: 10.1007/JHEP04(2010)066. arXiv: 1001.4878 [hep-ph].

[57] J. S. Diaz, A. Kostelecky, and M. Mewes, "Testing Relativity with High-Energy Astrophysical Neutrinos," *Phys. Rev. D*, vol. 89, no. 4, p. 043 005, 2014. DOI: 10.1103/PhysRevD.89.043005. arXiv: 1308.6344 [astro-ph.HE].

[58] C. A. Argüelles, T. Katori, and J. Salvado, "New Physics in Astrophysical Neutrino Flavor," *Phys. Rev. Lett.*, vol. 115, p. 161 303, 2015. DOI: 10.1103/PhysRevLett.115.161303. arXiv: 1506.02043 [hep-ph].

[59] P. Adamson *et al.*, "A Search for Lorentz Invariance and CPT Violation with the MINOS Far Detector," *Phys. Rev. Lett.*, vol. 105, p. 151 601, 2010. DOI: 10.1103/PhysRevLett.105.151601. arXiv: 1007.2791 [hep-ex].

[60] F. Benatti and R. Floreanini, "Open system approach to neutrino oscillations," *JHEP*, vol. 02, p. 032, 2000. DOI: 10.1088/1126-6708/2000/02/032. arXiv: hep-ph/0002221.

[61] F. Benatti and R. Floreanini, "Massless neutrino oscillations," *Phys. Rev. D*, vol. 64, p. 085 015, 2001. DOI: 10.1103/PhysRevD.64.085015. arXiv: hep-ph/0105303.

[62] J. R. Ellis, N. E. Mavromatos, and D. V. Nanopoulos, "String theory modifies quantum mechanics," *Phys. Lett. B*, vol. 293, pp. 37–48, 1992. DOI: 10.1016/0370-2693(92)91478-R. arXiv: hep-th/9207103.

[63] J. R. Ellis, N. E. Mavromatos, and D. V. Nanopoulos, "CPT violation in string modified quantum mechanics and the neutral kaon system," *Int. J. Mod. Phys. A*, vol. 11, pp. 1489–1508, 1996. DOI: 10.1142/S0217751X96000687. arXiv: hep-th/9212057.

[64] F. Benatti and R. Floreanini, "Non-standard Neutral Kaon Dynamics from Infinite Statistics," *Annals Phys.*, vol. 273, pp. 58–71, 1999. DOI: 10.1006/aphy.1998.5896. arXiv: hep-th/9811196.

[65] S. W. Hawking, "The Unpredictability of Quantum Gravity," *Commun. Math. Phys.*, vol. 87, pp. 395–415, 1982. DOI: 10.1007/BF01206031.

[66] S. W. Hawking, "Wormholes in Space-Time," *Phys. Rev. D*, vol. 37, G. W. Gibbons and S. W. Hawking, Eds., pp. 904–910, 1988. DOI: 10.1103/PhysRevD.37.904.

[67] S. W. Hawking, "Virtual black holes," *Phys. Rev. D*, vol. 53, pp. 3099–3107, 1996. DOI: 10.1103/PhysRevD.53.3099. arXiv: hep-th/9510029.

[68] S. W. Hawking and C. J. Hunter, "Gravitational entropy and global structure," *Phys. Rev. D*, vol. 59, p. 044 025, 1999. DOI: 10.1103/PhysRevD.59.044025. arXiv: hep-th/9808085.

[69] A. M. Gago, E. M. Santos, W. J. C. Teves, and R. Zukanovich Funchal, "Quantum dissipative effects and neutrinos: Current constraints and future perspectives," *Phys. Rev. D*, vol. 63, p. 073 001, 2001. DOI: 10.1103/PhysRevD.63.073001. arXiv: hep-ph/0009222.

[70] A. M. Gago, E. M. Santos, W. J. C. Teves, and R. Zukanovich Funchal, "A Study on quantum decoherence phenomena with three generations of neutrinos," Aug. 2002. arXiv: hep-ph/0208166.

[71] G. Barenboim and N. E. Mavromatos, "CPT violating decoherence and LSND: A Possible window to Planck scale physics," *JHEP*, vol. 01, p. 034, 2005. DOI: 10.1088/1126-6708/2005/01/034. arXiv: hep-ph/0404014.

[72] G. L. Fogli, E. Lisi, A. Marrone, D. Montanino, and A. Palazzo, "Probing non-standard decoherence effects with solar and KamLAND neutrinos," *Phys. Rev. D*, vol. 76, p. 033 006, 2007. DOI: 10.1103/PhysRevD.76.033006. arXiv: 0704.2568 [hep-ph].

[73] Y. Farzan, T. Schwetz, and A. Y. Smirnov, "Reconciling results of LSND, MiniBooNE and other experiments with soft decoherence," *JHEP*, vol. 07, p. 067, 2008. DOI: 10.1088/1126-6708/2008/07/067. arXiv: 0805.2098 [hep-ph].

[74] R. L. N. Oliveira and M. M. Guzzo, "Dissipation and θ_{13} in neutrino oscillations," *Eur. Phys. J. C*, vol. 73, p. 2434, 2013. DOI: 10.1140/epjc/s10052-013-2434-6.

[75] R. M. Wald, "QUANTUM GRAVITY AND TIME REVERSIBILITY," *Phys. Rev. D*, vol. 21, pp. 2742–2755, 1980. DOI: 10.1103/PhysRevD.21.2742.

[76] N. E. Mavromatos, "CPT Violation and Decoherence in Quantum Gravity," *J. Phys. Conf. Ser.*, vol. 171, J. Bernabeu, F. J. Botella, N. E. Mavromatos, and V. A. Mitsou, Eds., p. 012 007, 2009. DOI: 10.1088/1742-6596/171/1/012007. arXiv: 0904.0606 [hep-ph].

[77] Y. Liu, L.-z. Hu, and M.-L. Ge, "The Effect of quantum mechanics violation on neutrino oscillation," *Phys. Rev. D*, vol. 56, pp. 6648–6652, 1997. DOI: 10.1103/PhysRevD.56.6648.

[78] J. R. Ellis, J. L. Lopez, N. E. Mavromatos, and D. V. Nanopoulos, "Precision tests of CPT symmetry and quantum mechanics in the neutral kaon system," *Phys. Rev. D*, vol. 53, pp. 3846–3870, 1996. DOI: 10.1103/PhysRevD.53.3846. arXiv: hep-ph/9505340.

[79] J. R. Ellis, N. E. Mavromatos, and D. V. Nanopoulos, "How large are dissipative effects in noncritical Liouville string theory?" *Phys. Rev. D*, vol. 63, p. 024 024, 2001. DOI: 10.1103/PhysRevD.63.024024. arXiv: gr-qc/0007044.

[80] H. Murayama, "Origin of neutrino mass," *Prog. Part. Nucl. Phys.*, vol. 57, A. Faessler, Ed., pp. 3–21, 2006. DOI: 10.1016/j.ppnp.2006.02.001.

[81] J. W. F. Valle, "Status and implications of neutrino masses: a brief panorama," *Int. J. Mod. Phys. A*, vol. 30, no. 13, H. Fritzsch, Ed., p. 1 530 034, 2015. DOI: 10.1142/S0217751X15300343. arXiv: 1504.01913 [hep-ph].

[82] F. Englert and R. Brout, "Broken Symmetry and the Mass of Gauge Vector Mesons," *Phys. Rev. Lett.*, vol. 13, J. C. Taylor, Ed., pp. 321–323, 1964. DOI: 10.1103/PhysRevLett.13.321.

[83] P. W. Higgs, "Broken Symmetries and the Masses of Gauge Bosons," *Phys. Rev. Lett.*, vol. 13, J. C. Taylor, Ed., pp. 508–509, 1964. DOI: 10.1103/PhysRevLett.13.508.

[84] T. Yanagida, "Horizontal gauge symmetry and masses of neutrinos," *Conf. Proc. C*, vol. 7902131, O. Sawada and A. Sugamoto, Eds., pp. 95–99, 1979.

[85] R. E. Shrock, "General Theory of Weak Leptonic and Semileptonic Decays. 1. Leptonic Pseudoscalar Meson Decays, with Associated Tests For, and Bounds on, Neutrino Masses and Lepton Mixing," *Phys. Rev. D*, vol. 24, p. 1232, 1981. DOI: 10.1103/PhysRevD.24.1232.

[86] W. Konetschny and W. Kummer, "Nonconservation of Total Lepton Number with Scalar Bosons," *Phys. Lett. B*, vol. 70, pp. 433–435, 1977. DOI: 10.1016/0370-2693(77)90407-5.

[87] T. P. Cheng and L.-F. Li, "Neutrino Masses, Mixings and Oscillations in SU(2) x U(1) Models of Electroweak Interactions," *Phys. Rev. D*, vol. 22, p. 2860, 1980. DOI: 10.1103/PhysRevD.22.2860.

[88] G. Lazarides, Q. Shafi, and C. Wetterich, "Proton Lifetime and Fermion Masses in an SO(10) Model," *Nucl. Phys. B*, vol. 181, pp. 287–300, 1981. DOI: 10.1016/0550-3213(81)90354-0.

[89] M. Gell-Mann, P. Ramond, and R. Slansky, "Complex Spinors and Unified Theories," *Conf. Proc. C*, vol. 790927, pp. 315–321, 1979. arXiv: 1306.4669 [hep-th].

[90] S. L. Glashow, "The Future of Elementary Particle Physics," *NATO Sci. Ser. B*, vol. 61, p. 687, 1980. DOI: 10.1007/978-1-4684-7197-7_15.

[91] P. Minkowski, "$\mu \to e\gamma$ at a Rate of One Out of 10^9 Muon Decays?" *Phys. Lett. B*, vol. 67, pp. 421–428, 1977. DOI: 10.1016/0370-2693(77)90435-X.

[92] R. N. Mohapatra and G. Senjanovic, "Neutrino Mass and Spontaneous Parity Nonconservation," *Phys. Rev. Lett.*, vol. 44, p. 912, 1980. DOI: 10.1103/PhysRevLett.44.912.

[93] M. Magg and C. Wetterich, "Neutrino Mass Problem and Gauge Hierarchy," *Phys. Lett. B*, vol. 94, pp. 61–64, 1980. DOI: 10.1016/0370-2693(80)90825-4.

[94] J. Schechter and J. W. F. Valle, "Neutrino Masses in SU(2) x U(1) Theories," *Phys. Rev. D*, vol. 22, p. 2227, 1980. DOI: 10.1103/PhysRevD.22.2227.

[95] R. N. Mohapatra and G. Senjanovic, "Neutrino Masses and Mixings in Gauge Models with Spontaneous Parity Violation," *Phys. Rev. D*, vol. 23, p. 165, 1981. DOI: 10.1103/PhysRevD.23.165.

[96] R. Foot, H. Lew, X. G. He, and G. C. Joshi, "Seesaw Neutrino Masses Induced by a Triplet of Leptons," *Z. Phys. C*, vol. 44, p. 441, 1989. DOI: 10.1007/BF01415558.

[97] A. Atre, T. Han, S. Pascoli, and B. Zhang, "The Search for Heavy Majorana Neutrinos," *JHEP*, vol. 05, p. 030, 2009. DOI: 10.1088/1126-6708/2009/05/030. arXiv: 0901.3589 [hep-ph].

[98] A. Zee, "Quantum Numbers of Majorana Neutrino Masses," *Nucl. Phys. B*, vol. 264, pp. 99–110, 1986. DOI: 10.1016/0550-3213(86)90475-X.

[99] A. Faessler and F. Simkovic, "Double beta decay," *J. Phys. G*, vol. 24, pp. 2139–2178, 1998. DOI: 10.1088/0954-3899/24/12/001. arXiv: hep-ph/9901215.

[100] F. T. Avignone III, S. R. Elliott, and J. Engel, "Double Beta Decay, Majorana Neutrinos, and Neutrino Mass," *Rev. Mod. Phys.*, vol. 80, pp. 481–516, 2008. DOI: 10.1103/RevModPhys.80.481. arXiv: 0708.1033 [nucl-ex].

[101] J. D. Vergados, H. Ejiri, and F. Simkovic, "Theory of Neutrinoless Double Beta Decay," *Rept. Prog. Phys.*, vol. 75, p. 106 301, 2012. DOI: 10.1088/0034-4885/75/10/106301. arXiv: 1205.0649 [hep-ph].

[102] S. M. Bilenky and C. Giunti, "Neutrinoless double-beta decay: A brief review," *Mod. Phys. Lett. A*, vol. 27, p. 1 230 015, 2012. DOI: 10.1142/S0217732312300157. arXiv: 1203.5250 [hep-ph].

[103] M. Agostini *et al.*, "Probing Majorana neutrinos with double-β decay," *Science*, vol. 365, p. 1445, 2019. DOI: 10.1126/science.aav8613. arXiv: 1909.02726 [hep-ex].

[104] G. Anton *et al.*, "Search for Neutrinoless Double-β Decay with the Complete EXO-200 Dataset," *Phys. Rev. Lett.*, vol. 123, no. 16, p. 161 802, 2019. DOI: 10.1103/PhysRevLett.123.161802. arXiv: 1906.02723 [hep-ex].

[105] D. Q. Adams *et al.*, "Improved Limit on Neutrinoless Double-Beta Decay in ^{130}Te with CUORE," *Phys. Rev. Lett.*, vol. 124, no. 12, p. 122 501, 2020. DOI: 10.1103/PhysRevLett.124.122501. arXiv: 1912.10966 [nucl-ex].

[106] A. Gando *et al.*, "Search for Majorana Neutrinos near the Inverted Mass Hierarchy Region with KamLAND-Zen," *Phys. Rev. Lett.*, vol. 117, no. 8, p. 082 503, 2016, [Addendum: Phys.Rev.Lett. 117, 109903 (2016)]. DOI: 10.1103/PhysRevLett.117.082503. arXiv: 1605.02889 [hep-ex].

[107] A. M. Sirunyan *et al.*, "Search for heavy Majorana neutrinos in same-sign dilepton channels in proton-proton collisions at $\sqrt{s} = 13$ TeV," *JHEP*, vol. 01, p. 122, 2019. DOI: 10.1007/JHEP01(2019)122. arXiv: 1806.10905 [hep-ex].

[108] R. Aaij *et al.*, "Search for Majorana neutrinos in $B^- \to \pi^+\mu^-\mu^-$ decays," *Phys. Rev. Lett.*, vol. 112, no. 13, p. 131 802, 2014. DOI: 10.1103/PhysRevLett.112.131802. arXiv: 1401.5361 [hep-ex].

[109] A. B. Balantekin, A. de Gouvêa, and B. Kayser, "Addressing the Majorana vs. Dirac Question with Neutrino Decays," *Phys. Lett. B*, vol. 789, pp. 488–495, 2019. DOI: 10.1016/j.physletb.2018.11.068. arXiv: 1808.10518 [hep-ph].

[110] K. Bora, D. Borah, and D. Dutta, "Probing Majorana Neutrino Textures at DUNE," *Phys. Rev. D*, vol. 96, no. 7, p. 075 006, 2017. DOI: 10.1103/PhysRevD.96.075006. arXiv: 1611.01097 [hep-ph].

[111] C. Giunti, "No Effect of Majorana Phases in Neutrino Oscillations," *Phys. Lett. B*, vol. 686, pp. 41–43, 2010. DOI: 10.1016/j.physletb.2010.02.020. arXiv: 1001.0760 [hep-ph].

[112] K. Abe *et al.*, "Constraint on the matter–antimatter symmetry-violating phase in neutrino oscillations," *Nature*, vol. 580, no. 7803, pp. 339–344, 2020, [Erratum: Nature 583, E16 (2020)]. DOI: 10.1038/s41586-020-2177-0. arXiv: 1910.03887 [hep-ex].

[113] K. Abe *et al.*, "Hyper-Kamiokande Design Report," May 2018. arXiv: 1805.04163 [physics.ins-det].

[114] J. Chadwick, "The intensity distribution in the magnetic spectrum of beta particles from radium (B + C)," *Verh. Phys. Gesell.*, vol. 16, pp. 383–391, 1914.

[115] C. L. Cowan, F. Reines, F. B. Harrison, H. W. Kruse, and A. D. McGuire, "Detection of the free neutrino: A Confirmation," *Science*, vol. 124, pp. 103–104, 1956. DOI: 10.1126/science.124.3212.103.

[116] G. Danby *et al.*, "Observation of High-Energy Neutrino Reactions and the Existence of Two Kinds of Neutrinos," *Phys. Rev. Lett.*, vol. 9, pp. 36–44, 1962. DOI: 10.1103/PhysRevLett.9.36.

[117] M. Kobayashi and T. Maskawa, "CP Violation in the Renormalizable Theory of Weak Interaction," *Prog. Theor. Phys.*, vol. 49, pp. 652–657, 1973. DOI: 10.1143/PTP.49.652.

[118] M. L. Perl *et al.*, "Evidence for Anomalous Lepton Production in e+ - e- Annihilation," *Phys. Rev. Lett.*, vol. 35, pp. 1489–1492, 1975. DOI: 10.1103/PhysRevLett.35.1489.

[119] Q. R. Ahmad *et al.*, "Direct evidence for neutrino flavor transformation from neutral current interactions in the Sudbury Neutrino Observatory," *Phys. Rev. Lett.*, vol. 89, p. 011 301, 2002. DOI: 10.1103/PhysRevLett.89.011301. arXiv: nucl-ex/0204008.

[120] M. Tanabashi *et al.*, "Review of Particle Physics," *Phys. Rev. D*, vol. 98, no. 3, p. 030 001, 2018. DOI: 10.1103/PhysRevD.98.030001.

[121] M. Fukugita and T. Yanagida, *Physics of neutrinos and applications to astrophysics* (Theoretical and Mathematical Physics). Berlin, Germany:

Springer-Verlag, 2003, ISBN: 978-3-662-05119-1, 978-3-540-43800-7, 978-3-642-07851-4. DOI: 10.1007/978-3-662-05119-1.

[122] S. M. Bilenky and S. T. Petcov, "Massive Neutrinos and Neutrino Oscillations," *Rev. Mod. Phys.*, vol. 59, p. 671, 1987, [Erratum: Rev.Mod.Phys. 61, 169 (1989), Erratum: Rev.Mod.Phys. 60, 575–575 (1988)]. DOI: 10.1103/RevModPhys.59.671.

[123] T.-K. Kuo and J. T. Pantaleone, "Neutrino Oscillations in Matter," *Rev. Mod. Phys.*, vol. 61, p. 937, 1989. DOI: 10.1103/RevModPhys.61.937.

[124] T. D. Lee and C.-N. Yang, "Question of Parity Conservation in Weak Interactions," *Phys. Rev.*, vol. 104, pp. 254–258, 1956. DOI: 10.1103/PhysRev.104.254.

[125] C. S. Wu, E. Ambler, R. W. Hayward, D. D. Hoppes, and R. P. Hudson, "Experimental Test of Parity Conservation in β Decay," *Phys. Rev.*, vol. 105, pp. 1413–1414, 1957. DOI: 10.1103/PhysRev.105.1413.

[126] L. D. Landau, "On the conservation laws for weak interactions," *Nucl. Phys.*, vol. 3, pp. 127–131, 1957. DOI: 10.1016/0029-5582(57)90061-5.

[127] J. H. Christenson, J. W. Cronin, V. L. Fitch, and R. Turlay, "Evidence for the 2π Decay of the K_2^0 Meson," *Phys. Rev. Lett.*, vol. 13, pp. 138–140, 1964. DOI: 10.1103/PhysRevLett.13.138.

[128] J.-P. Luminet, "Editorial note to "A Homogeneous Universe of Constant Mass and Increasing Radius accounting for the Radial Velocity of Extra–Galactic Nebulae" by Georges Lema\^itre (1927)," *Gen. Rel. Grav.*, vol. 45, pp. 1619–1633, 2013. DOI: 10.1007/s10714-013-1547-4. arXiv: 1305.6470 [physics.hist-ph].

[129] E. Hubble, "A relation between distance and radial velocity among extra-galactic nebulae," *Proceedings of the National Academy of Sciences*, vol. 15, no. 3, pp. 168–173, 1929. DOI: 10.1073/pnas.15.3.168. eprint: https://www.pnas.org/doi/pdf/10.1073/pnas.15.3.168. [Online]. Available: https://www.pnas.org/doi/abs/10.1073/pnas.15.3.168.

[130] R. J. Defouw, "Separation of matter and antimatter," *Nature*, vol. 228, pp. 1068–1069, 1970. DOI: 10.1038/2281068a0.

[131] G. Steigman, "Observational tests of antimatter cosmologies," *Ann. Rev. Astron. Astrophys.*, vol. 14, pp. 339–372, 1976. DOI: 10.1146/annurev.aa.14.090176.002011.

[132] F. W. Stecker, "Baryon Symmetric Big Bang Cosmology," *Nature*, vol. 273, pp. 493–497, 1978. DOI: 10.1038/273493a0.

[133] A. G. Cohen, A. D. Rújula, and S. L. Glashow, "A matter-antimatter universe?" *The Astrophysical Journal*, vol. 495, no. 2, pp. 539–549, Mar. 1998. DOI: 10.1086/305328. [Online]. Available: https://doi.org/10.1086/305328.

[134] A. D. Sakharov, "Violation of CP Invariance, C asymmetry, and baryon asymmetry of the universe," *Pisma Zh. Eksp. Teor. Fiz.*, vol. 5, pp. 32–35, 1967. DOI: 10.1070/PU1991v034n05ABEH002497.

[135] V. Kuzmin, V. Rubakov, and M. Shaposhnikov, "On anomalous electroweak baryon-number non-conservation in the early universe," *Physics Letters B*, vol. 155, no. 1, pp. 36–42, 1985, ISSN: 0370-2693. DOI: https://doi.org/10.1016/0370-2693(85)91028-7. [Online]. Available: https://www.sciencedirect.com/science/article/pii/0370269385910287.

[136] M. Fukugita and T. Yanagida, "Barygenesis without grand unification," *Physics Letters B*, vol. 174, no. 1, pp. 45–47, 1986, ISSN: 0370-2693. DOI: https://doi.org/10.1016/0370-2693(86)91126-3. [Online]. Available: https://www.sciencedirect.com/science/article/pii/0370269386911263.

[137] W. Buchmuller, R. D. Peccei, and T. Yanagida, "Leptogenesis as the origin of matter," *Ann. Rev. Nucl. Part. Sci.*, vol. 55, pp. 311–355, 2005. DOI: 10.1146/annurev.nucl.55.090704.151558. arXiv: hep-ph/0502169.

[138] S. Antusch, S. F. King, and A. Riotto, "Flavour-Dependent Leptogenesis with Sequential Dominance," *JCAP*, vol. 11, p. 011, 2006. DOI: 10.1088/1475-7516/2006/11/011. arXiv: hep-ph/0609038.

[139] S. Davidson, E. Nardi, and Y. Nir, "Leptogenesis," *Physics Reports*, vol. 466, no. 4, pp. 105–177, 2008, ISSN: 0370-1573. DOI: https://doi.org/10.1016/j.physrep.2008.06.002. [Online]. Available: https://www.sciencedirect.com/science/article/pii/S0370157308001889.

[140] P. Di Bari, "An introduction to leptogenesis and neutrino properties," *Contemp. Phys.*, vol. 53, no. 4, pp. 315–338, 2012. DOI: 10.1080/00107514.2012.701096. arXiv: 1206.3168 [hep-ph].

[141] J. S. Schwinger, "The Theory of quantized fields. 1.," *Phys. Rev.*, vol. 82, K. A. Milton, Ed., pp. 914–927, 1951. DOI: 10.1103/PhysRev.82.914.

[142] R. Jost, "A remark on the c.t.p. theorem," *Helv. Phys. Acta*, vol. 30, pp. 409–416, 1957.

[143] R. B. Patterson, "Prospects for Measurement of the Neutrino Mass Hierarchy," *Ann. Rev. Nucl. Part. Sci.*, vol. 65, pp. 177–192, 2015. DOI: 10.1146/annurev-nucl-102014-021916. arXiv: 1506.07917 [hep-ex].

[144] P. F. de Salas, D. V. Forero, C. A. Ternes, M. Tortola, and J. W. F. Valle, "Status of neutrino oscillations 2018: 3σ hint for normal mass ordering and improved CP sensitivity," *Phys. Lett. B*, vol. 782, pp. 633–640, 2018. DOI: 10.1016/j.physletb.2018.06.019. arXiv: 1708.01186 [hep-ph].

[145] M. Bass *et al.*, "Baseline Optimization for the Measurement of CP Violation, Mass Hierarchy, and θ_{23} Octant in a Long-Baseline Neutrino Oscillation Experiment," *Phys. Rev. D*, vol. 91, no. 5, p. 052 015, 2015. DOI: 10.1103/PhysRevD.91.052015. arXiv: 1311.0212 [hep-ex].

[146] C. R. Das, J. Pulido, J. Maalampi, and S. Vihonen, "Determination of the θ_{23} octant in long baseline neutrino experiments within and beyond the standard model," *Phys. Rev. D*, vol. 97, no. 3, p. 035 023, 2018. DOI: 10.1103/PhysRevD.97.035023. arXiv: 1708.05182 [hep-ph].

[147] S. K. Agarwalla, S. S. Chatterjee, and A. Palazzo, "Octant of θ_{23} in danger with a light sterile neutrino," *Phys. Rev. Lett.*, vol. 118, no. 3, p. 031 804, 2017. DOI: 10.1103/PhysRevLett.118.031804. arXiv: 1605.04299 [hep-ph].

[148] M. Masud, M. Bishai, and P. Mehta, "Extricating New Physics Scenarios at DUNE with Higher Energy Beams," *Sci. Rep.*, vol. 9, no. 1, p. 352, 2019. DOI: 10.1038/s41598-018-36790-6. arXiv: 1704.08650 [hep-ph].

[149] J. M. Berryman, A. de Gouvêa, K. J. Kelly, and A. Kobach, "Sterile neutrino at the Deep Underground Neutrino Experiment," *Phys. Rev. D*, vol. 92, no. 7, p. 073 012, 2015. DOI: 10.1103/PhysRevD.92.073012. arXiv: 1507.03986 [hep-ph].

[150] P. Coloma, J. López-Pavón, S. Rosauro-Alcaraz, and S. Urrea, "New physics from oscillations at the DUNE near detector, and the role of systematic uncertainties," *JHEP*, vol. 08, p. 065, 2021. DOI: 10.1007/JHEP08(2021)065. arXiv: 2105.11466 [hep-ph].

[151] T. Han, J. Liao, H. Liu, and D. Marfatia, "Nonstandard neutrino interactions at COHERENT, DUNE, T2HK and LHC," *JHEP*, vol. 11,

p. 028, 2019. DOI: 10.1007/JHEP11(2019)028. arXiv: 1910.03272 [hep-ph].

[152] B. Abi *et al.*, "Deep Underground Neutrino Experiment (DUNE), Far Detector Technical Design Report, Volume III: DUNE Far Detector Technical Coordination," *JINST*, vol. 15, no. 08, T08009, 2020. DOI: 10.1088/1748-0221/15/08/T08009. arXiv: 2002.03008 [physics.ins-det].

[153] A. Abed Abud *et al.*, "Deep Underground Neutrino Experiment (DUNE) Near Detector Conceptual Design Report," *Instruments*, vol. 5, no. 4, p. 31, 2021. DOI: 10.3390/instruments5040031. arXiv: 2103.13910 [physics.ins-det].

[154] B. Abi *et al.*, "Deep Underground Neutrino Experiment (DUNE), Far Detector Technical Design Report, Volume I Introduction to DUNE," *JINST*, vol. 15, no. 08, T08008, 2020. DOI: 10.1088/1748-0221/15/08/T08008. arXiv: 2002.02967 [physics.ins-det].

[155] P. Huber, M. Lindner, and W. Winter, "Simulation of long-baseline neutrino oscillation experiments with GLoBES (General Long Baseline Experiment Simulator)," *Comput. Phys. Commun.*, vol. 167, p. 195, 2005. DOI: 10.1016/j.cpc.2005.01.003. arXiv: hep-ph/0407333.

[156] P. Huber, J. Kopp, M. Lindner, M. Rolinec, and W. Winter, "New features in the simulation of neutrino oscillation experiments with GLoBES 3.0: General Long Baseline Experiment Simulator," *Comput. Phys. Commun.*, vol. 177, pp. 432–438, 2007. DOI: 10.1016/j.cpc.2007.05.004. arXiv: hep-ph/0701187.

[157] C. A. Argüelles Delgado, J. Salvado, and C. N. Weaver, "A Simple Quantum Integro-Differential Solver (SQuIDS)," *Comput. Phys. Commun.*, vol. 196, pp. 569–591, 2015. DOI: 10.1016/j.cpc.2015.06.022. arXiv: 1412.3832 [hep-ph].

[158] K. Abe *et al.*, "The T2K Experiment," *Nucl. Instrum. Meth. A*, vol. 659, pp. 106–135, 2011. DOI: 10.1016/j.nima.2011.06.067. arXiv: 1106.1238 [physics.ins-det].

[159] K. Abe *et al.*, "Physics potential of a long-baseline neutrino oscillation experiment using a J-PARC neutrino beam and Hyper-Kamiokande," *PTEP*, vol. 2015, p. 053C02, 2015. DOI: 10.1093/ptep/ptv061. arXiv: 1502.05199 [hep-ex].

[160] K. Abe *et al.*, "Physics potentials with the second Hyper-Kamiokande detector in Korea," *PTEP*, vol. 2018, no. 6, p. 063C01, 2018. DOI: 10.1093/ptep/pty044. arXiv: 1611.06118 [hep-ex].

[161] P. Huber, M. Mezzetto, and T. Schwetz, "On the impact of systematical uncertainties for the CP violation measurement in superbeam experiments," *JHEP*, vol. 03, p. 021, 2008. DOI: 10.1088/1126-6708/2008/03/021. arXiv: 0711.2950 [hep-ph].

[162] H. Minakata and H. Nunokawa, "Testing the principle of equivalence by solar neutrinos," *Phys. Rev. D*, vol. 51, pp. 6625–6634, 1995. DOI: 10.1103/PhysRevD.51.6625. arXiv: hep-ph/9405239.

[163] H. Minakata and A. Y. Smirnov, "High-energy cosmic neutrinos and the equivalence principle," *Phys. Rev. D*, vol. 54, pp. 3698–3705, 1996. DOI: 10.1103/PhysRevD.54.3698. arXiv: hep-ph/9601311.

[164] A. Halprin, C. N. Leung, and J. T. Pantaleone, "A Possible violation of the equivalence principle by neutrinos," *Phys. Rev. D*, vol. 53, pp. 5365–5376, 1996. DOI: 10.1103/PhysRevD.53.5365. arXiv: hep-ph/9512220.

[165] G. Lambiase, "Neutrino oscillations in non-inertial frames and the violation of the equivalence principle. Neutrino mixing induced by the equivalence principle violation," *Eur. Phys. J. C*, vol. 19, pp. 553–560, 2001. DOI: 10.1007/s100520100599.

[166] M. M. Guzzo, H. Nunokawa, and R. Tomas, "Testing the principle of equivalence by supernova neutrinos," *Astropart. Phys.*, vol. 18, pp. 277–286, 2002. DOI: 10.1016/S0927-6505(02)00149-4. arXiv: hep-ph/0104054.

[167] J. Liao, D. Marfatia, and K. Whisnant, "Degeneracies in long-baseline neutrino experiments from nonstandard interactions," *Phys. Rev. D*, vol. 93, no. 9, p. 093 016, 2016. DOI: 10.1103/PhysRevD.93.093016. arXiv: 1601.00927 [hep-ph].

[168] R. Majhi, S. Chembra, and R. Mohanta, "Exploring the effect of Lorentz invariance violation with the currently running long-baseline experiments," *Eur. Phys. J. C*, vol. 80, no. 5, p. 364, 2020. DOI: 10.1140/epjc/s10052-020-7963-1. arXiv: 1907.09145 [hep-ph].

[169] A. Kostelecky and M. Mewes, "Neutrinos with Lorentz-violating operators of arbitrary dimension," *Phys. Rev. D*, vol. 85, p. 096 005, 2012. DOI: 10.1103/PhysRevD.85.096005. arXiv: 1112.6395 [hep-ph].

[170] M. G. Aartsen *et al.*, "Neutrino Interferometry for High-Precision Tests of Lorentz Symmetry with IceCube," *Nature Phys.*, vol. 14, no. 9, pp. 961–966, 2018. DOI: 10.1038/s41567-018-0172-2. arXiv: 1709.03434 [hep-ex].

[171] I. Esteban, M. C. Gonzalez-Garcia, M. Maltoni, I. Martinez-Soler, and T. Schwetz, "Updated fit to three neutrino mixing: exploring the accelerator-reactor complementarity," *JHEP*, vol. 01, p. 087, 2017. DOI: 10.1007/JHEP01(2017)087. arXiv: 1611.01514 [hep-ph].

[172] J. A. Carpio, E. Massoni, and A. M. Gago, "Testing quantum decoherence at DUNE," *Phys. Rev. D*, vol. 100, no. 1, p. 015 035, 2019. DOI: 10.1103/PhysRevD.100.015035. arXiv: 1811.07923 [hep-ph].

[173] H. Jurkovich, C. P. Ferreira, and P. Pasquini, "Shadowing Neutrino Mass Hierarchy with Lorentz Invariance Violation," Jun. 2018. arXiv: 1806.08752 [hep-ph].

[174] G. Barenboim, M. Masud, C. A. Ternes, and M. Tórtola, "Exploring the intrinsic Lorentz-violating parameters at DUNE," *Phys. Lett. B*, vol. 788, pp. 308–315, 2019. DOI: 10.1016/j.physletb.2018.11.040. arXiv: 1805.11094 [hep-ph].

[175] V. A. Kostelecky and N. Russell, "Data Tables for Lorentz and CPT Violation," *Rev. Mod. Phys.*, vol. 83, pp. 11–31, 2011. DOI: 10.1103/RevModPhys.83.11.

[176] K. Abe *et al.*, "Test of Lorentz invariance with atmospheric neutrinos," *Phys. Rev. D*, vol. 91, no. 5, p. 052 003, 2015. DOI: 10.1103/PhysRevD.91.052003. arXiv: 1410.4267 [hep-ex].

[177] B. Aharmim *et al.*, "Tests of Lorentz invariance at the Sudbury Neutrino Observatory," *Phys. Rev. D*, vol. 98, no. 11, p. 112 013, 2018. DOI: 10.1103/PhysRevD.98.112013. arXiv: 1811.00166 [hep-ex].

[178] B. Pontecorvo, "Mesonium and anti-mesonium," *Sov. Phys. JETP*, vol. 6, p. 429, 1957.

[179] Z. Maki, M. Nakagawa, and S. Sakata, "Remarks on the unified model of elementary particles," *Prog. Theor. Phys.*, vol. 28, pp. 870–880, 1962. DOI: 10.1143/PTP.28.870.

[180] D. Indumathi and N. Sinha, "Effect of tau neutrino contribution to muon signals at neutrino factories," *Phys. Rev. D*, vol. 80, p. 113 012, 2009. DOI: 10.1103/PhysRevD.80.113012. arXiv: 0910.2020 [hep-ph].

[181] A. Donini, J. J. Gomez Cadenas, and D. Meloni, "The τ-contamination of the golden muon sample at the Neutrino Factory," *JHEP*, vol. 02, p. 095, 2011. DOI: 10.1007/JHEP02(2011)095. arXiv: 1005.2275 [hep-ph].

[182] W. Rodejohann and J. W. F. Valle, "Symmetrical Parametrizations of the Lepton Mixing Matrix," *Phys. Rev. D*, vol. 84, p. 073 011, 2011. DOI: 10.1103/PhysRevD.84.073011. arXiv: 1108.3484 [hep-ph].

[183] A. Himmel, *New oscillation results from the nova experiment*, Jul. 2020. DOI: 10.5281/zenodo.3959581. [Online]. Available: https://doi.org/10.5281/zenodo.3959581.

[184] P. Coloma, J. Lopez-Pavon, I. Martinez-Soler, and H. Nunokawa, "Decoherence in Neutrino Propagation Through Matter, and Bounds from IceCube/DeepCore," *Eur. Phys. J. C*, vol. 78, no. 8, p. 614, 2018. DOI: 10.1140/epjc/s10052-018-6092-6. arXiv: 1803.04438 [hep-ph].

[185] S. Hernandez, "Revisitando efectos de decoherencia en las oscilaciones de neutrinos," M.S. thesis, Pontificia Universidad Católica del Perú, Perú, 2016.